Supplementary Information

Diagnosing the Role of Hydrogen Bonding in the Organization, Aggregation, and Optical Properties of Phthalhydrazide-Functionalized Molecules in Solution and Solid State

Cheng-Yen Pan,[a] Nathan J. Grinalds,[b] Ion Ghiviriga,[a] Khalil A. Abboud,[a] Jiangeng Xue,[b*] Ronald K. Castellano[a*]

[a]Department of Chemistry, University of Florida, PO Box 117200, Gainesville, FL, 32611, USA

Email: castellano@chem.ufl.edu

[b]Department of Materials Science and Engineering, University of Florida, PO Box 116400, Gainesville, FL, 32611, USA

Email: jxue@ufl.edu

*indicates corresponding author

Table of Contents

Experimental Details

General

Reagents and solvents were purchased from commercial sources and used without further purification unless otherwise specified. THF and DMF were degassed in 20 L drums and passed through two sequential purification columns (activated alumina; molecular sieves for DMF) under a positive argon atmosphere. Thin layer chromatography (TLC) was performed on SiO_2-60 F_{254} aluminum plates with visualization by UV light. Flash column chromatography was performed using Silica gel technical grade, pore size 60 Å, 230 – 400 mesh particle size, 40 – 63 μm particle size from Sigma-Aldrich. ^1H (^{13}C) NMR were recorded on INOVA-500 (^1H at 500 MHz; ^{13}C at 125 MHz) spectrometer, Bruker 600 MHz spectrometer (^1H at 600 MHz; ^{13}C at 150 MHz) and Bruker 400 MHz spectrometer (^1H at 400 MHz; ^{13}C at 100 MHz). Chemical shifts (δ) are given in parts per million (ppm) referenced to residual deuterated solvent purchased from Cambridge Isotope Laboratories, Inc. ($CDCl_3$: δ H 7.26 ppm, δ C 77.16 ppm; DMSO-d_6: δ H 2.50 ppm, δ C 39.52 ppm; DMF-d_7: δ H 8.03 ppm, δ C 163.15 ppm; TCE-d_2: δ H 6.00 ppm: δ C 73.78 ppm; Acetone-d_6: δ H 2.05 ppm, δ C 29.92 ppm). Spin multiplicities are presented by the following abbreviations: s (singlet), d (doublet), t (triplet), q (quartet), quin (quintet), sext, b (broad) and m (multiplet). Electrospray ionization (ESI) high resolution mass spectra (HRMS) were recorded on an Agilent 6210 TOF spectrometer with MassHunter software.

Synthesis

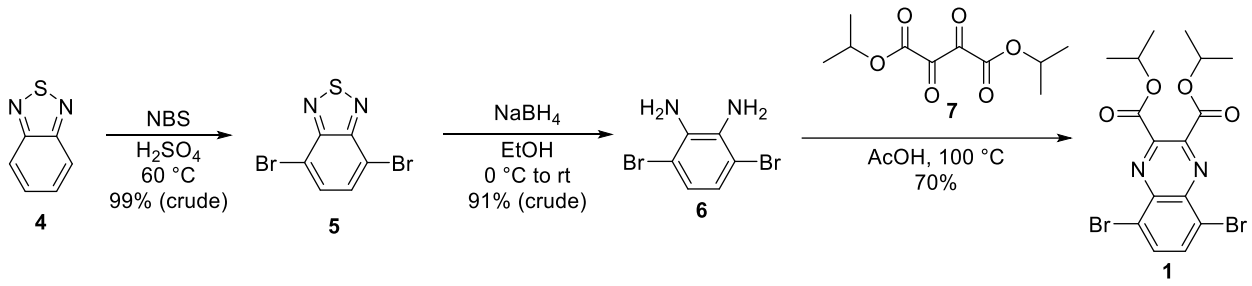

Fig. S1 Synthesis of compound **1**.

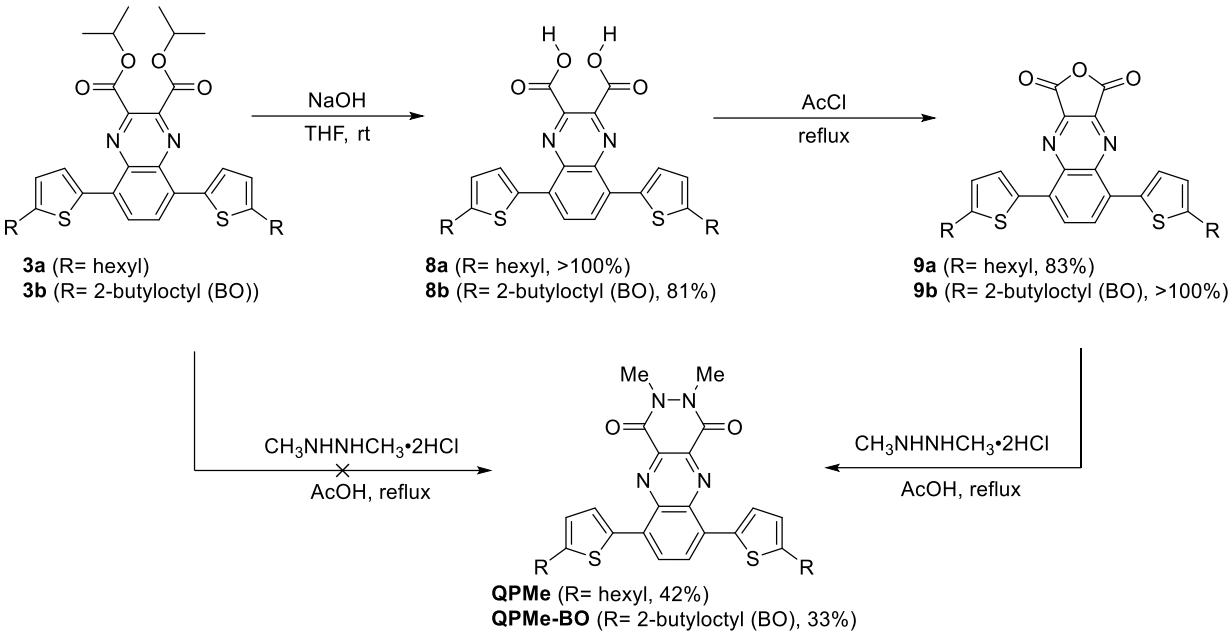

Fig. S2 Syntheses of H-bonding incapable compounds **QPMe** and **QPMe-BO**.

The syntheses of the target molecules where R is either a hexyl chain or a 2-butyloctyl chain are shown in Fig. S2. Compound **2a**, **4**, **5**, **6**, and **7** were synthesized following the existing literature with modifications and optimizations.[1–5]

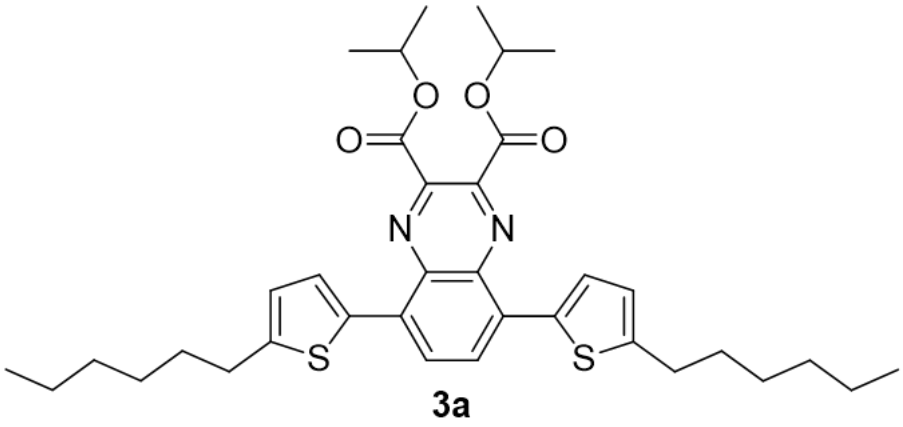

Diisopropyl 5,8-bis(5-hexylthiophen-2-yl)quinoxaline-2,3-dicarboxylate (3a). Compound **1** (0.46 g, 1.00 mmol), compound **2a** (3.01 mmol), and $Pd(PPh_3)_4$ (57.9 mg, 0.050 mmol) were added into a 100 mL three-neck round bottom flask with a stir bar, two septa, and a reflux condenser. After the flask was flushed with argon three times, degassed toluene (57 mL) was added to the flask. The reaction mixture was heated to reflux and was allowed to stir for 23 hours. Upon cooling to room temperature, the mixture was transferred to a separatory funnel. After the mixture was extracted with DCM and brine, the organic layers were combined and dried over anhydrous $MgSO_4$. After filtration and evaporation, the residue was purified with silica gel chromatography (DCM:hexanes = 1:1) to give a dark red solid (0.54 g, 0.85 mmol, 86%).

^{1}H NMR (600 MHz, $CDCl_3$) δ 8.16 (s, 2H), 7.79 (d, *J* = 3.7 Hz, 2H), 6.85 (d, *J* = 3.7 Hz, 2H), 5.43 (hept, *J* = 6.3 Hz, 2H), 2.88 (t, *J* = 7.7 Hz, 4H), 1.75 (p, *J* = 7.6 Hz, 4H), 1.50 (d, *J* = 6.3 Hz, 12H), 1.46 – 1.38 (m, 4H), 1.37 – 1.30 (m, 8H), 0.91 (t, *J* = 7.1 Hz, 6H) ppm. ^{13}C NMR (150 MHz, $CDCl_3$): δ 164.34, 150.21, 142.70, 137.78, 135.56, 131.86, 128.71, 127.70, 124.52, 70.56, 31.83, 31.77, 30.45, 29.04, 22.73, 22.00, 14.24 ppm. HRMS-ESI: m/z $[M+H]^+$ calcd for $[C_{36}H_{46}N_2O_4S_2+H]^+$: 635.2972, found: 635.2984 (1.9 ppm); m/z $[M+Na]^+$ calcd for $[C_{36}H_{46}N_2O_4S_2+Na]^+$: 657.2791, found: 657.2805 (2.1 ppm).

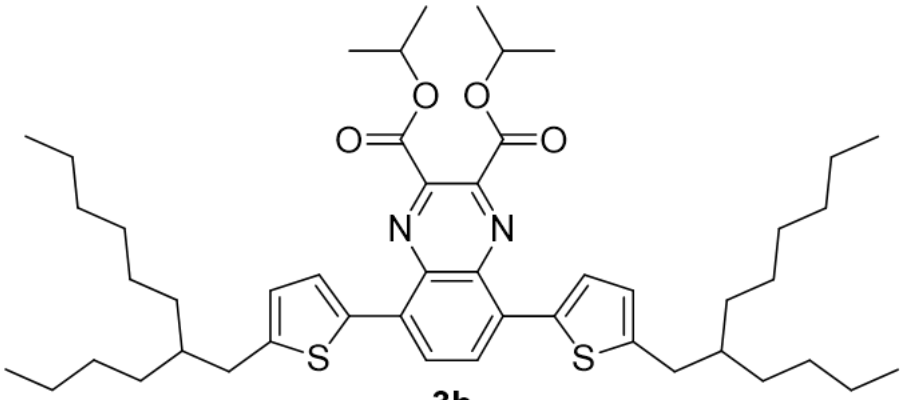

3b

Diisopropyl 5,8-bis(5-(2-butyloctyl)thiophen-2-yl)quinoxaline-2,3-dicarboxylate (3b). Compound **1** (0.97 g, 2.11 mmol), compound **2b** (6.32 mmol), and $Pd(PPh_3)_4$ (0.18 g, 0.16 mmol) were added into a 250 mL three-neck round bottom flask with a stir bar, two septa, and a reflux condenser. After the flask was flushed with argon three times, degassed toluene (120 mL) was added to the flask. The reaction mixture was heated to reflux and was allowed to stir for 23 hours. Upon cooling to room temperature, the mixture was transferred to a separatory funnel. After the mixture was extracted with DCM and brine, the organic layers were combined and dried over anhydrous $MgSO_4$. After filtration and evaporation, the residue was purified with silica gel chromatography (DCM:hexanes = 1:1) to give a dark red solid (1.50 g, 2.11 mmol, 89%). ^{1}H NMR (600 MHz, $CDCl_3$): δ 8.17 (s, 2H), 7.82 (d, *J* = 3.7 Hz, 2H), 6.83 (d, *J* = 3.8 Hz, 2H), 5.43 (hept, *J* = 6.3 Hz, 2H), 2.81 (d, *J* = 6.8 Hz, 4H), 1.76 – 1.66 (m, 2H), 1.50 (d, *J* = 6.3 Hz, 12H), 1.40 – 1.21 (m, 32H), 0.92 – 0.85 (m, 6H) ppm.^{13}C NMR (100 MHz, $CDCl_3$): δ 164.34, 148.84, 142.67, 137.78, 135.81, 131.79, 128.67, 127.69, 125.62, 70.53, 40.35, 34.92, 33.44, 33.10, 32.07, 29.83, 29.03, 26.78, 23.19, 22.83, 22.03, 14.32, 14.26 ppm. HRMS-ESI: m/z $[M+H]^+$ calcd for $[C_{48}H_{70}N_2O_4S_2+H]^+$: 803.4850, found: 803.4838 (1.5 ppm); m/z $[M+Na]^+$ calcd for $[C_{48}H_{70}N_2O_4S_2+Na]^+$: 825.4669, found 825.4665: (0.9 ppm).

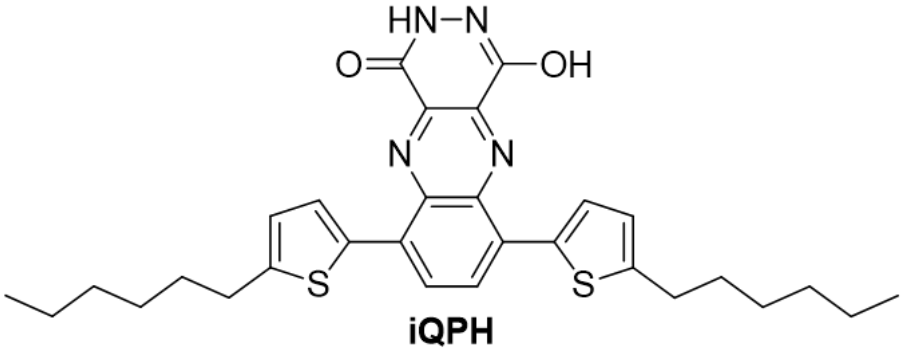

iQPH

6,9-Bis(5-hexylthiophen-2-yl)-2,3-dihydropyridazino[4,5-*b*]quinoxaline-1,4-dione (QPH) / 6,9-Bis(5-hexylthiophen-2-yl)-4-hydroxypyridazino[4,5-b]quinoxalin-1(2*H*)-one (iQPH). Compound **3a** (0.82 mg, 1.29 mmol) and 20 mL ethanol were added into a 50 mL three-neck round bottom flask with a stir bar, two septa, and a reflux condenser. Hydrazine monohydrate (3.00 mL, 61.7 mmol) was added portionwise

to the flask under argon. The mixture was heated to reflux overnight. After the reaction, the mixture was cooled to room temperature and the solvent was removed under vacuum. The resulting concentrate was purified with silica gel chromatography (chloroform:methanol = 95:5), followed by precipitation in methanol to give a purple solid (0.56 g, 1.02 mmol, 79%). ^{1}H NMR (600 MHz, $CDCl_3$): δ 8.30 (s, 2H), 7.82 (b, 2H), 6.91 (d, *J* = 3.7 Hz, 2H), 2.92 (t, *J* = 7.7 Hz, 4H), 1.77 (p, *J* = 7.7 Hz, 4H), 1.48 – 1.40 (m, 4H), 1.40 – 1.29 (m, 8H), 0.91 (t, *J* = 7.1 Hz, 6H) ppm. ^{1}H NMR (600 MHz, DMSO-d_6): δ 12.03 (b, 1H), 11.66 (b, 1H), 8.41 (s, 2H), 8.06 (d, *J* = 3.6 Hz, 2H), 6.98 (d, *J* = 3.6 Hz, 2H), 2.88 (t, *J* = 7.6 Hz, 4H), 1.74 – 1.66 (m, 4H), 1.43 – 1.36 (m, 4H), 1.36 – 1.25 (m, 8H), 0.88 (t, *J* = 6.8 Hz, 6H) ppm. ^{1}H NMR (600 MHz, DMF-d_7): δ 11.93 (b, 1H), 8.50 (s, 2H), 8.21 (d, *J* = 3.7 Hz, 2H), 7.03 (d, *J* = 3.7 Hz, 2H), 2.94 (t, *J* = 7.7 Hz, 4H), 1.77 (p, *J* = 7.6 Hz, 4H), 1.49 – 1.41 (m, 4H), 1.40 – 1.29 (m, 8H), 0.90 (t, *J* = 7.2 Hz, 6H) ppm. ^{13}C NMR (150 MHz, TCE-d_2, 80 °C): δ 154.73, 150.17, 141.07, 135.71, 134.74, 132.09, 129.89, 128.60, 124.83, 31.36, 31.17, 30.03, 28.71, 22.36, 13.82 ppm. HRMS-ESI: m/z $[M+H]^+$ calcd for $[C_{30}H_{34}N_4O_2S_2+H]^+$: 547.2196, found: 547.2206 (2.2 ppm); m/z $[M+Na]^+$ calcd for $[C_{30}H_{34}N_4O_2S_2+Na]^+$: 569.2015, found 569.2025: (2.4 ppm).

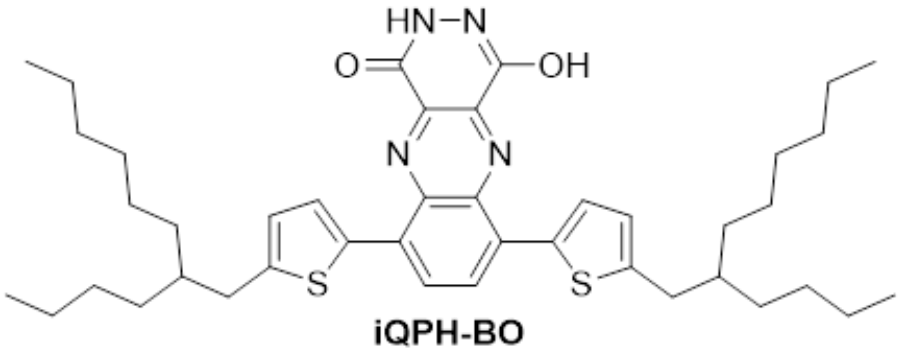

iQPH-BO

6,9-Bis(5-(2-butyloctyl)thiophen-2-yl)-2,3-dihydropyridazino[4,5-*b*]quinoxaline-1,4-dione (QPH-BO) / 6,9-Bis(5-(2-butyloctyl)thiophen-2-yl)-4-hydroxypyridazino[4,5-*b*]quinoxalin-1(2*H*)-one (iQPH-BO). Compound **3b** (0.42 mg, 0.52 mmol) and 26 mL ethanol were added into a 50 mL three-neck round bottom flask with a stir bar, two septa, and a reflux condenser. Hydrazine monohydrate (0.70 mL, 14.6 mmol) was added to the flask under argon. The mixture was heated to reflux overnight. After the reaction, the mixture was cooled to room temperature and the solvent was removed under vacuum. The resulting concentrate was purified with silica gel chromatography (DCM:methanol = 98:2), followed by precipitation in methanol to give a purple solid (0.13 g, 0.18 mmol, 34%). ^{1}H NMR (400 MHz, $CDCl_3$): δ 9.35 (b, 1H), 8.31 (s, 2H), 7.91 (b, 3H), 6.90 (d, *J* = 3.7 Hz, 2H), 2.86 (d, *J* = 6.7 Hz, 4H), 1.80 – 1.68 (m, 2H), 1.43 – 1.23 (m, 32H), 0.95 – 0.84 (m, 12H) ppm. ^{1}H NMR (400 MHz, DMSO-d_6): δ 12.05 (b, 1H), 11.76 (b, 1H), 8.41 (s, 2H), 8.10 (d, *J* = 3.7 Hz, 2H), 6.96 (d, *J* = 3.7 Hz, 2H), 2.82 (d, *J* = 6.6 Hz, 4H), 1.75 – 1.60 (m, 2H), 1.38 – 1.20 (m, 32H), 0.91 – 0.80 (m, 12H) ppm. ^{13}C NMR (150 MHz, TCE-d_2): δ 155.94, 148.13, 141.29, 135.72, 135.29, 131.82, 130.18, 129.21, 126.45, 39.65, 34.39, 33.12, 32.75, 31.81, 29.61, 28.67, 26.47, 22.99, 22.63, 14.20, 14.15 ppm. HRMS-ESI: m/z $[M+H]^+$ calcd for $[C_{42}H_{58}N_4O_2S_2+H]^+$: 715.4074, found: 715.4055 (2.7 ppm); m/z $[M+Na]^+$ calcd for $[C_{42}H_{58}N_4O_2S_2+Na]^+$: 737.3893, found: 737.3873 (2.7 ppm).

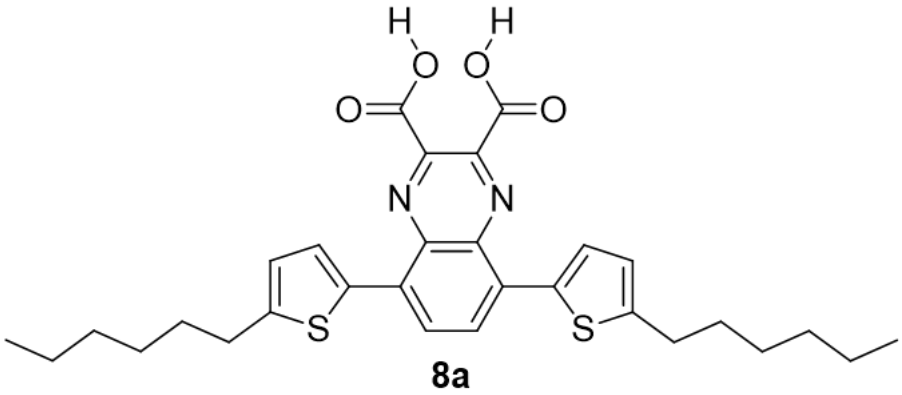

8a

5,8-Bis(5-hexylthiophen-2-yl)quinoxaline-2,3-dicarboxylic acid (8a). Compound **3a** (0.84 g, 1.32 mmol) was added into 5 mL THF, in a 15 mL round bottom flask with a stir bar. 2M NaOH (21 mL, 27.8 mmol) was added portionwise to the flask. The reaction mixture was allowed to stir at room temperature for 30 hours under argon. After the reaction, the mixture was acidified with 1M HCl to pH = 1. Then, the mixture was transferred into a separatory funnel, and the organic layer was extracted with DCM, washed with brine, and dried over anhydrous $MgSO_4$. The solvent was removed under vacuum to give an orange solid (0.73 g, 1.32 mmol, >100%). The product was used in the next step without further purification. ^{1}H NMR (600 MHz, Acetone-d_6): δ 8.37 (s, 2H), 7.94 (d, J = 3.7 Hz, 2H), 6.94 (d, J = 3.8 Hz, 2H), 2.91 (t, J = 7.5 Hz, 4H), 2.82 (b, 2H), 1.75 (p, J = 7.6 Hz, 4H), 1.50 – 1.41 (m, 2H), 1.39 – 1.32 (m, 8H), 0.90 (t, J = 7.2 Hz, 6H) ppm. ^{13}C NMR (100 MHz, Acetone-d_6): δ 166.03, 150.54, 143.80, 138.48, 136.28, 132.67, 130.03, 129.04, 125.65, 32.54, 32.42, 30.75, 23.35, 14.43, 0.08 ppm. HRMS-ESI: m/z $[M+H]^+$ calcd for $[C_{30}H_{34}N_2O_4S_2+H]^+$: 551.2033, found: 551.2046 (2.5 ppm); m/z $[M+Na]^+$ calcd for $[C_{30}H_{34}N_2O_4S_2+Na]^+$: 573.1852, found: 573.1863 (1.9 ppm).

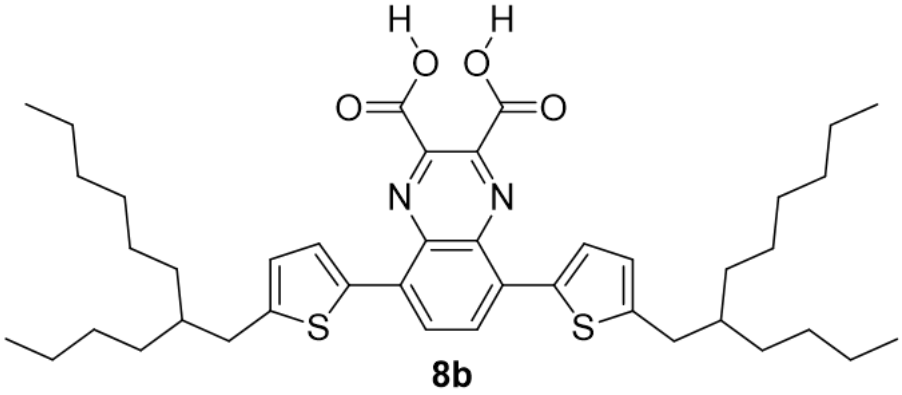

8b

5,8-Bis(5-(2-butyloctyl)thiophen-2-yl)quinoxaline-2,3-dicarboxylic acid (8b). Compound **3b** (0.91 g, 1.13 mmol) was added into 15 mL THF, in a 25 mL round bottom flask with a stir bar. 2M NaOH (37.5 mL, 75.0 mmol) was added portionwise to the flask. The reaction mixture was allowed to stir at room temperature for 45 hours under argon. After the reaction, the mixture was acidified with 1M HCl to pH = 1. Then, the mixture was transferred into separatory funnel, and the organic layer was extracted with DCM, washed with brine, and dried over anhydrous $MgSO_4$. The solvent was removed under reduced pressure and washed with hexanes to give an orange solid (0.66 g, 0.92 mmol, 81%). The product was used in the next step without further purification. ^{1}H NMR (500 MHz, $CDCl_3$): δ 8.25 (s, 2H), 7.73 (d, J = 3.7 Hz, 2H), 6.88 (d, J = 3.7 Hz, 2H), 2.85 (d, J = 6.6 Hz, 4H), 2.64 (b, 2H), 1.79 – 1.66 (m, 2H), 1.40 – 1.19 (m, 32H), 0.94 – 0.84 (m, 12H) ppm. ^{13}C NMR (100 MHz, $CDCl_3$): δ 164.75, 149.12, 139.89, 137.83, 134.81, 131.88,

130.20, 128.34, 126.07, 40.08, 34.69, 33.41, 33.06, 32.04, 29.80, 29.00, 26.76, 23.17, 22.82, 14.30, 14.26 ppm. HRMS-ESI: m/z $[M+H]^+$ calcd for $[C_{42}H_{58}N_2O_4S_2+H]^+$: 717.3765, found: 717.3771 (0.8 ppm).

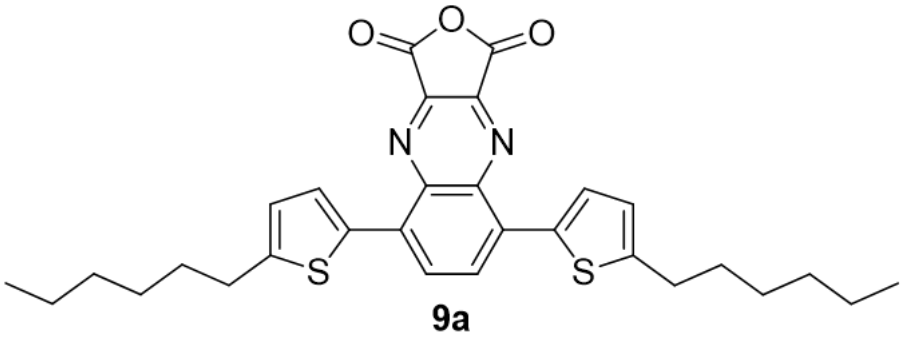

9a

5,8-Bis(5-hexylthiophen-2-yl)furo[3,4-*b*]quinoxaline-1,3-dione (9a). Compound **8a** (0.73 g, 1.32 mmol) and 20 mL acetyl chloride were added into a 50 mL three-neck round bottom flask with a stir bar, two septa, and a reflux condenser. The mixture was heated to 50 °C for 22 hours. After the reaction, the mixture was cooled to room temperature and the solvent was removed under vacuum. The resulting concentrate was washed with hexanes to give a dark red solid (0.68 g, 1.27 mmol, 96%). The product was used in the next step without further purification. ^{1}H NMR (500 MHz, $CDCl_3$): δ 8.34 (s, 2H), 7.81 (d, *J* = 3.8 Hz, 2H), 6.91 (d, *J* = 4.0 Hz, 2H), 2.91 (t, *J* = 7.7 Hz, 4H), 1.84 – 1.69 (m, 4H), 1.47 – 1.39 (m, 4H), 1.39 – 1.25 (m, 8H), 0.91 (t, *J* = 7.0 Hz, 6H) ppm. Attempts to obtain ^{13}C NMR were not successful. HRMS-DART: m/z $[M+H]^+$ calcd for $[C_{30}H_{32}N_2O_3S_2+H]^+$: 533.1927, found: 533.1930 (0.6 ppm); m/z $[M+NH_4]^+$ calcd for $[C_{30}H_{32}N_2O_3S_2+Na]^+$: 550.2193, found: 550.2167 (4.7 ppm).

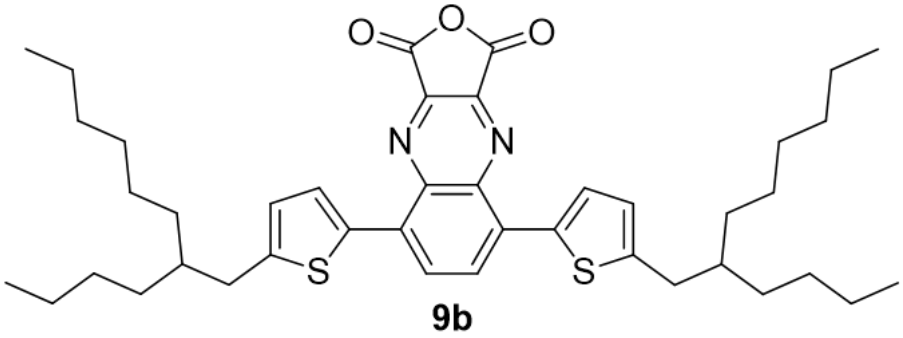

9b

5,8-Bis(5-(2-butyloctyl)thiophen-2-yl)furo[3,4-*b*]quinoxaline-1,3-dione (9b). Compound **8b** (0.66 g, 0.92 mmol) and 15 mL acetyl chloride were added into a 25 mL three-neck round bottom flask with a stir bar, two septa, and a reflux condenser. The mixture was heated to 50 °C for 24 hours. After the reaction, the mixture was cooled to room temperature and the solvent was removed under vacuum. The resulting concentrate was washed with hexanes to give a dark red solid (0.72 g, 1.02 mmol, >100%). The product was used in the next step without further purification. ^{1}H NMR (500 MHz, $CDCl_3$): δ 8.33 (s, 2H), 7.84 (d, *J* = 3.7 Hz, 2H), 6.89 (d, *J* = 3.7 Hz, 2H), 2.86 (d, *J* = 6.7 Hz, 4H), 1.78 – 1.68 (m, 2H), 1.37 – 1.26 (m, 32H), 0.94 – 0.85 (m, 12H) ppm. ^{13}C NMR (100 MHz, $CDCl_3$): δ 158.64, 150.01, 142.08, 141.48, 134.85, 133.72, 131.73, 129.30, 126.29, 40.10, 34.77, 33.41, 33.07, 32.05, 29.82, 28.99, 26.74, 23.19, 22.83, 14.31, 14.27 ppm.

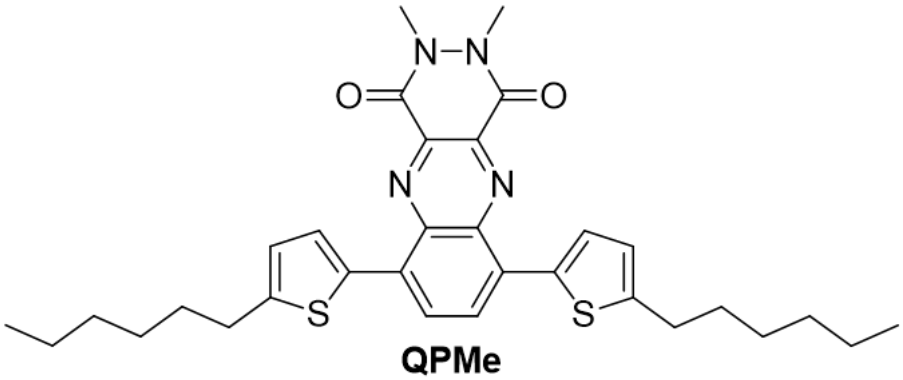

QPMe

6,9-Bis(5-hexylthiophen-2-yl)-2,3-dimethyl-2,3-dihydropyridazino[4,5-*b*]quinoxaline-1,4-dione (QPMe). Compound **9a** (0.14 mg, 0.27 mmol) and 10 mL acetic acid were added into a 25 mL three-neck round bottom flask with a stir bar, two septa, and a reflux condenser. 1,2-Dimethylhydrazine dihydrochloride (77.6 mg, 0.58 mmol) was added into the flask under argon. The mixture was heated to reflux for 17 hours. Upon cooling to room temperature, the mixture was transferred to a separatory funnel. After the mixture was extracted with DCM and brine, the organic layers were combined and dried over anhydrous $MgSO_4$. After filtration and evaporation, the residue was purified by silica gel chromatography (DCM: ethyl acetate = 15:1), followed by precipitation in methanol to give a dark red solid (63.2 mg, 0.11 mmol, 42%). ^{1}H NMR (600 MHz, $CDCl_3$): δ 8.26 (s, 2H), 7.95 (d, *J* = 3.7 Hz, 2H), 6.89 (d, *J* = 3.7 Hz,2), 3.87 (s, 6H), 2.91 (t, *J* = 7.7 Hz, 4H), 1.76 (p, *J* = 7.5 Hz, 4H), 1.46 – 1.38 (m, 4H), 1.38 – 1.28 (m, 8H), 0.90 (t, *J* = 7.1 Hz, 6H) ppm. ^{13}C NMR (150 MHz, $CDCl_3$): δ 156.72, 150.64, 141.27, 138.20, 135.43, 132.45, 129.82, 128.59, 124.96, 33.98, 31.83, 31.76, 30.44, 29.07, 22.76, 14.25 ppm. HRMS-ESI: m/z $[M+H]^+$ calcd for $[C_{32}H_{38}N_4O_2S_2+H]^+$: 575.2509, found: 575.2480 (5.0 ppm); m/z $[M+Na]^+$ calcd for $[C_{32}H_{38}N_4O_2S_2+Na]^+$: 597.2328, found: 597.2299 (4.9 ppm).

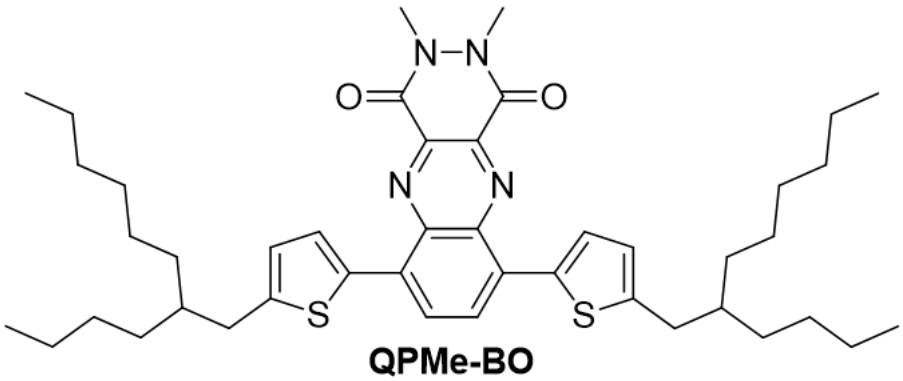

QPMe-BO

6,9-Bis(5-(2-butyloctyl)thiophen-2-yl)-2,3-dimethyl-2,3-dihydropyridazino[4,5-*b*]quinoxaline-1,4-dione (QPMe-BO). Compound **9b** (0.72 mg, 1.03 mmol) and 45 mL acetic acid were added into a 100 mL three-neck round bottom flask with a stir bar, two septa, and a reflux condenser. 1,2-Dimethylhydrazine dihydrochloride (0.40 g, 3.01 mmol) was added into the flask under argon. The mixture was heated to reflux for 22 hours. Upon cooling to room temperature, the mixture was transferred to a separatory funnel. After the mixture was extracted with DCM and brine, the organic layers were combined and dried over anhydrous $MgSO_4$. After filtration and evaporation, the residue was purified with silica gel chromatography (DCM: ethyl acetate = 98:2), followed by precipitation in methanol to give a dark red solid (0.25 g, 0.34 mmol, 33%). ^{1}H NMR (500 MHz, $CDCl_3$): δ 8.25 (s, 2H), 8.05 (d, *J* = 3.7 Hz, 2H), 6.88 (d, *J* = 3.8 Hz, 2H), 3.87 (s, 6H), 2.84 (d, *J* = 6.8 Hz, 4H), 1.81 – 1.69 (m, 2H), 1.36 – 1.26 (m, 32H), 0.93 – 0.85 (m, 12H) ppm. ^{13}C NMR (100 MHz, $CDCl_3$): δ 156.78, 148.85, 141.43, 138.22, 135.83, 132.43, 129.99, 128.98, 126.25, 40.07, 34.85, 34.00, 33.35, 33.02, 32.07, 29.85, 28.96, 26.71, 23.22, 22.84, 14.33, 14.27 ppm. HRMS-ESI: m/z

$[M+H]^+$ calcd for $[C_{44}H_{62}N_4O_2S_2+H]^+$: 743.4387, found: 743.4365 (3.0 ppm); m/z $[M+Na]^+$ calcd for $[C_{44}H_{62}N_4O_2S_2+Na]^+$: 765.4206, found: 765.4183 (3.0 ppm).

Table S1 Summary for solubility test of **iQPH**, **QPMe**, **iQPH-BO** and **QPMe-BO** in different deuterated solvents.

	iQPH	**QPMe**	**iQPH-BO**	**QPMe-BO**
$CDCl_3$	1.5 mM	15 mM	30 mM	134 mM
Toluene-d_8	0.14 mM	1.5 mM	29 mM	134 mM
DMSO-d_6	6 mM	0.49 mM	0.83 mM	0.62 mM
DMF-d_7	12 mM	0.49 mM	6 mM	0.62 mM

Compounds were dissolved in the deuterated solvent and the suspended solid was filtered off to prepare concentrated samples. 0.05% of 1,2-dichloroethane was added in the samples as an internal reference for calculating solubility.

^{1}H NMR Characterization

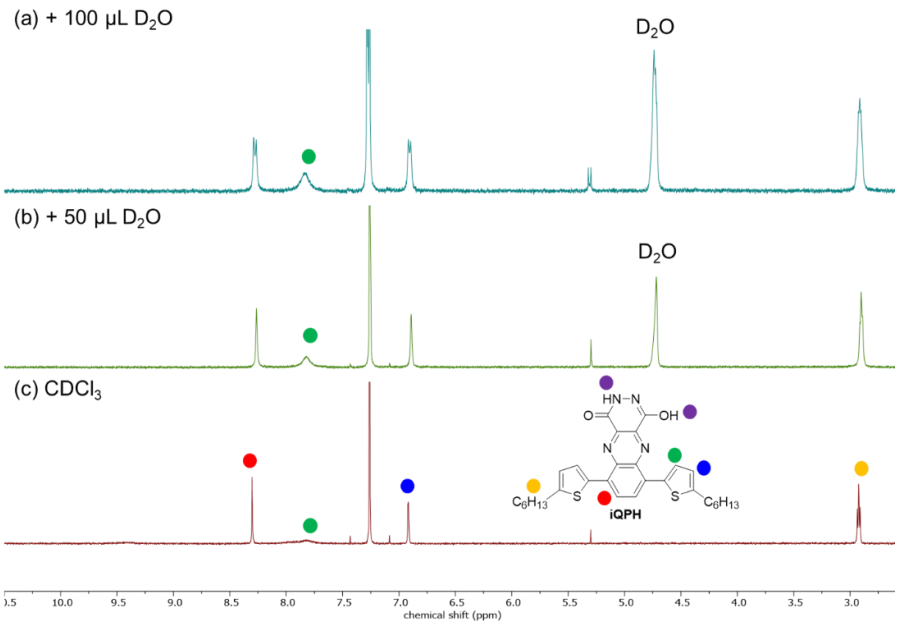

Fig. S3 Stacked ^{1}H NMR spectra of hydrogen-deuterium exchange experiment of **iQPH** in $CDCl_3$ with (a) 0 µL, (b) 50 µL, and (c) 100 µL D_2O added in the sample.

From an H/D exchange experiment, the broad peak at 7.8 ppm was still present after adding 100 µL D_2O to the sample, indicating that the broad peak is an aromatic proton on thiophene because this proton

did not undergo proton-deuterium exchange with D_2O (Fig. S3). In the variable-temperature NMR (VT-NMR) experiment, this peak demonstrates a significant change in chemical shift as the temperature increases in the opposite direction compared to the other protons (Fig. S4).

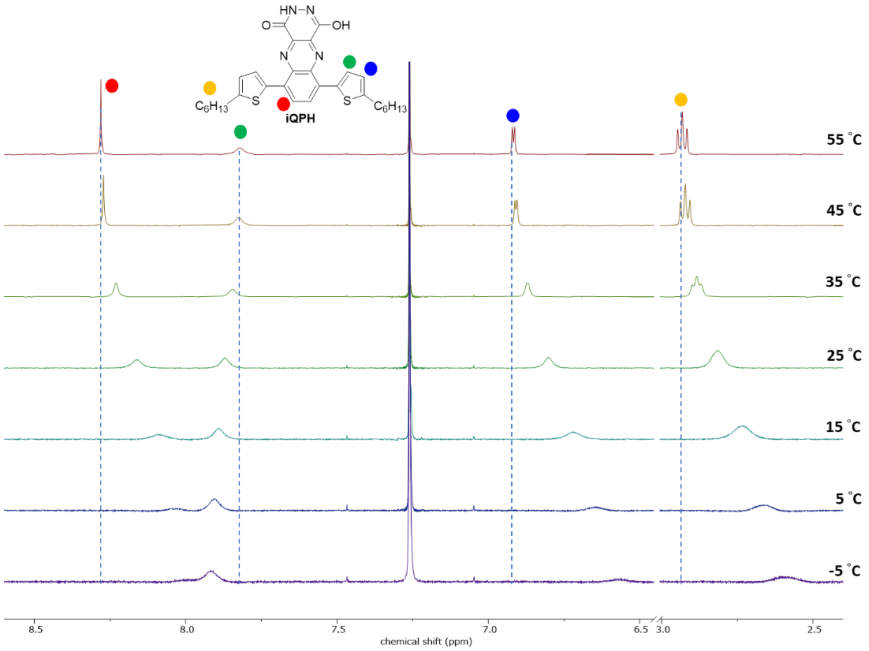

Fig. S4 Stacked VT ^{1}H NMR spectra of **iQPH** in $CDCl_3$ from -5 to 55 °C.

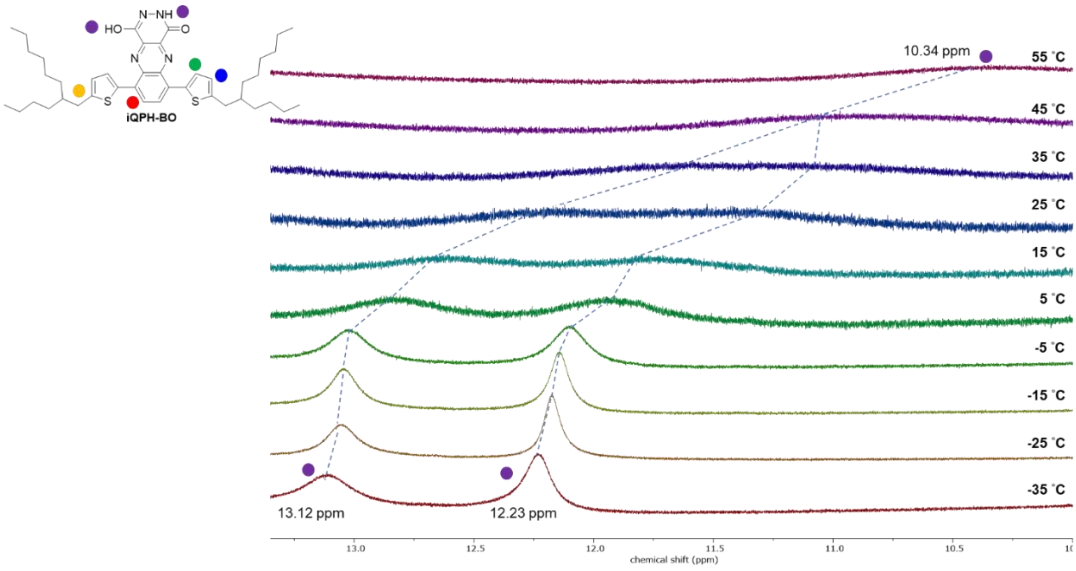

Fig. S5 VT ^{1}H NMR of concentrated **iQPH-BO** (27 mM) in $CDCl_3$. (NH/OH region) from -35 °C to 55 °C.

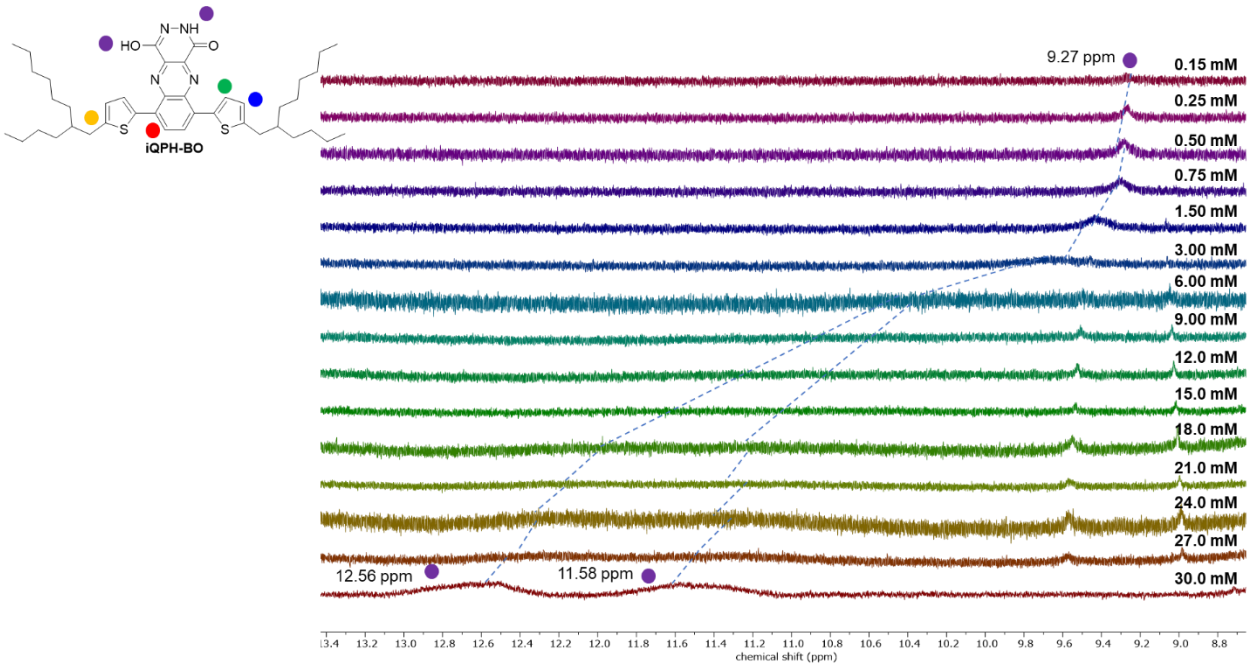

Fig. S6 Concentration-dependent ^{1}H NMR of **iQPH-BO** in $CDCl_3$. (NH/OH region)

^{13}C and HMBC Characterization

Proton exchange between NH and OH protons on the PH unit makes the proton signals appear broad in the ^{1}H NMR spectrum, and the nearby carbon peaks also become too broad to be detected in the ^{13}C NMR spectrum. When **iQPH** was prepared in DMSO-d_6 and taken at room temperature, only 7 carbons were observed in the downfield region (Fig. S7). (**iQPH** didn't have enough solubility in $CDCl_3$ for ^{13}C spectrum) Theoretically, there should be 9 carbons from aromatic and carbonyl carbons visible for the molecule considering the remote isochronous site has little change on the carbons. Different solvents and temperatures were employed to achieve sharp NH/OH resonances in ^{1}H spectra, to observe missing carbons in ^{13}C spectra. Fortunately, the ^{13}C spectrum of **iQPH** with the correct carbon number was found in TCE-d_2 at 80 °C (Fig. S8), which provided the suitable solubility to observe the missing carbons. The same trends were observed for the BO-version. The ^{13}C spectrum of **iQPH-BO** with correct carbon number was taken at room temperature in TCE-d_2 (Fig. S9), which was not observed in the $CDCl_3$. It was theorized that the single NH/OH peak indicates fast proton exchange. The nearby carbons also switch fast resulting in broad carbon signals that are difficult to observe in the ^{13}C spectrum. On the contrary, at lower temperatures, the rate of proton exchange between NH and OH is decreased, but the low solubility of **iQPH** at low temperatures limits the signal in the ^{13}C spectrum. By utilizing heteronuclear multiple bond correlation (HMBC), the correlations from the NH and OH in the spectrum were observed in the DMF-d_7 at -50 °C

(Fig. S10). Although the correlation signals are weak, the information gives further confirmation for the **iQPH** structure.

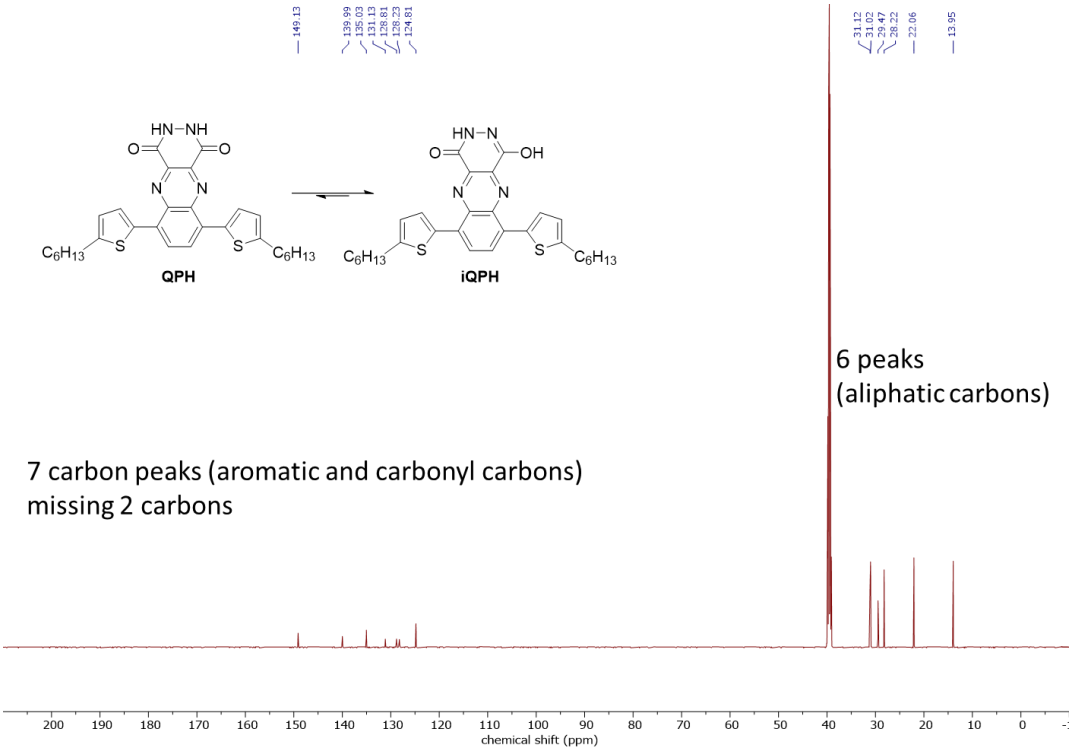

Fig. S7 ^{13}C NMR spectrum of **iQPH** in DMSO-d_6 at 25°C.

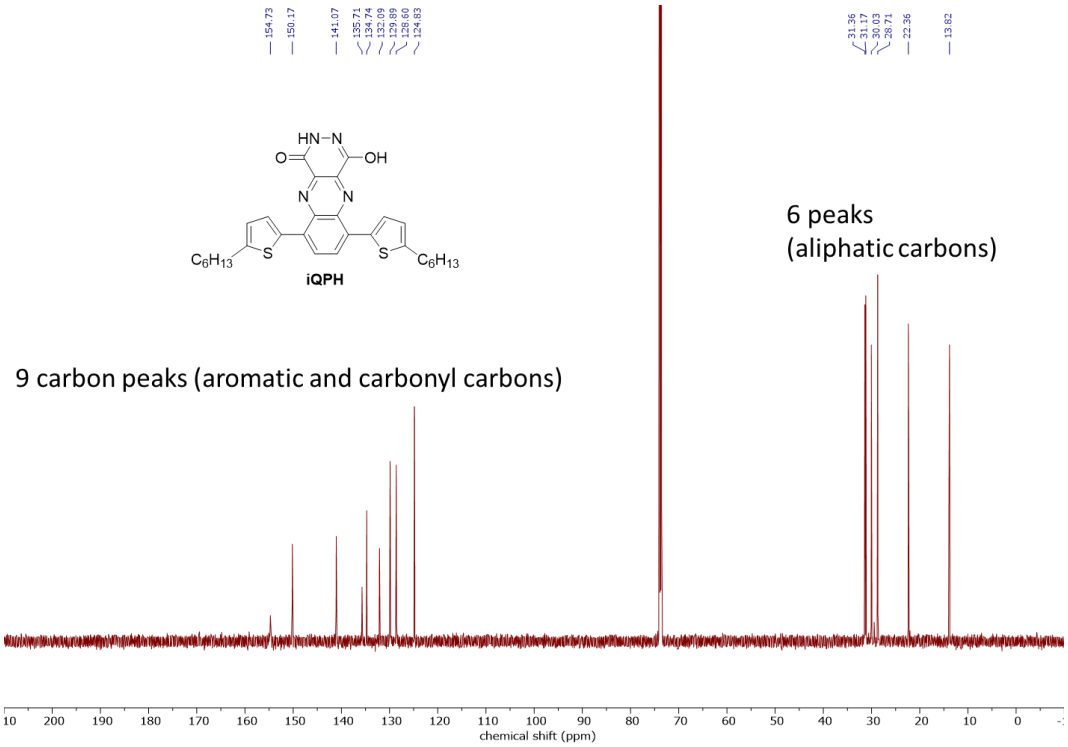

Fig. S8 ^{13}C NMR spectrum of **iQPH** in TCE-d_2 at 80 °C.

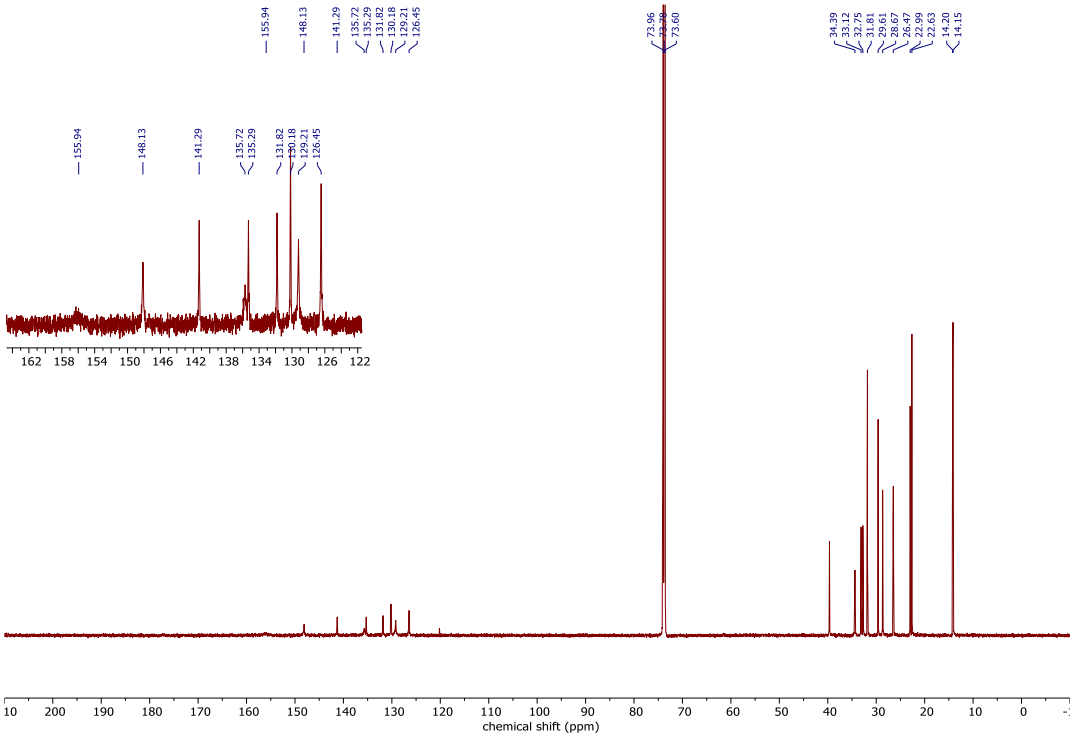

Fig. S9 ^{13}C NMR spectrum of **iQPH-BO** in TCE-d_2 at 25 °C. (full)

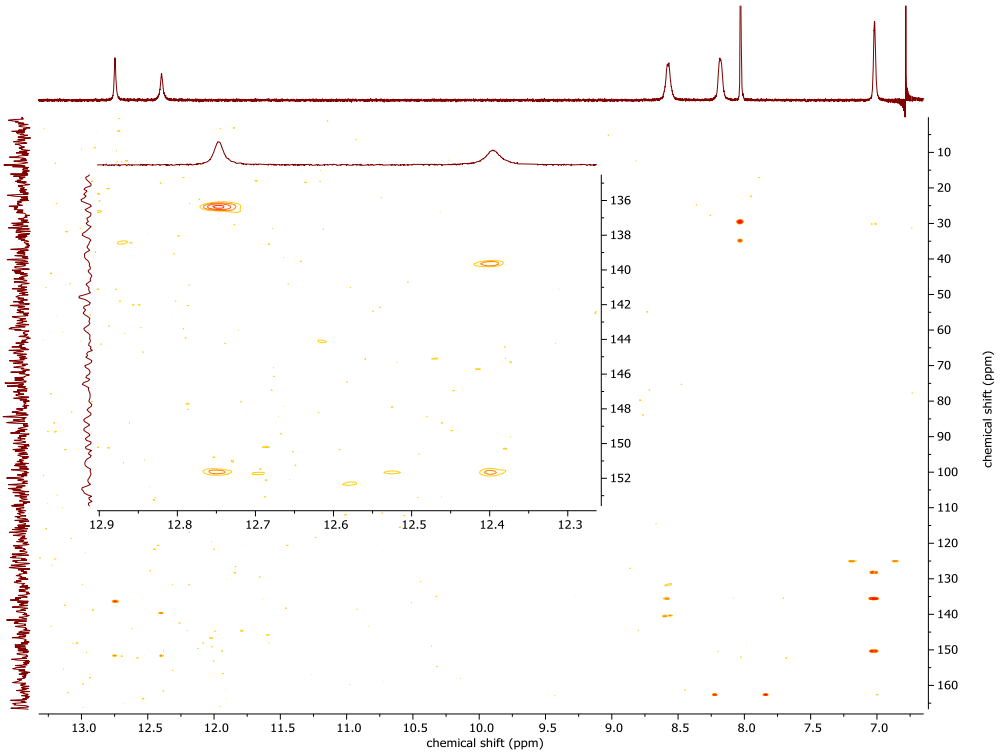

Fig. S10 HMBC spectrum of **iQPH** in DMF-d_7 at -50 °C. (expanded)

DFT structural analysis of compound iQPH

All calculations were performed using Gaussian 09, accessed through the UF High Performance Computing Center. The optimized geometries and orbital energies of ground state were calculated using ab initio DFT with the B3LYP functional and the 6-31+G(d) basis set in gas phase. Excited-state calculations were performed at the for TD-DFT calculations (TD (singlets, N States = 10)) using Gaussian 09 to determine the S0 to S1 electronic transition energies. Molecular orbital plots were made using VMD from the Gaussian output files or using Avogadro visualization software. Frontier molecular orbital shapes were visualized using Avogadro molecular editor and visualization software. The ground-state structural (NH/OH positions on the PH unit) and conformational (the direction of hydrogen on OH and the direction of attached thiophenes) preferences for **iQPH** were investigated with ground-state DFT at the B3LYP/6-31+G(d) level of theory in the gas phase. To simplify the calculations, all the alkyl chains were replaced by CH_3 groups to reduce computational cost. All optimized geometries were confirmed to be at true local minima via frequency calculations to ensure the existence of no imaginary frequencies. According to the tautomeric structures of the PH unit, the structural isomers can be categorized as the series with two NH groups (NHNH) (Fig. S11), the series of one NH and OH groups (NHOH) (Fig. S12), and the series of two OH groups (OHOH) (Fig. S13). Each series also has the conformers with different arrangements in the direction of two thiophene spacers. In addition, for the NHOH and OHOH series, the hydrogen on the OH

group also exists in the inward and outward direction. Overall, these structures were scanned to find the most favorable structure. The structural and conformational scan was in gas phase, so not all the conformational preferences may be present in solution.

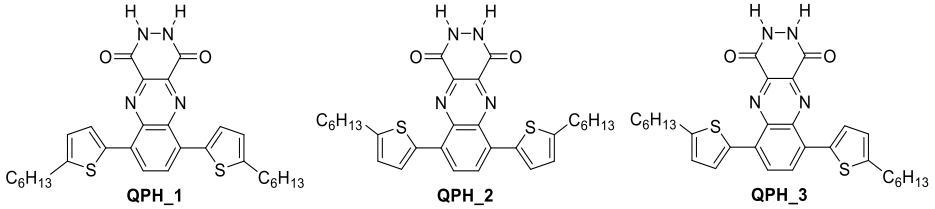

Fig. S11 List of **QPH** conformers in the series of structures with two NH groups (NHNH).

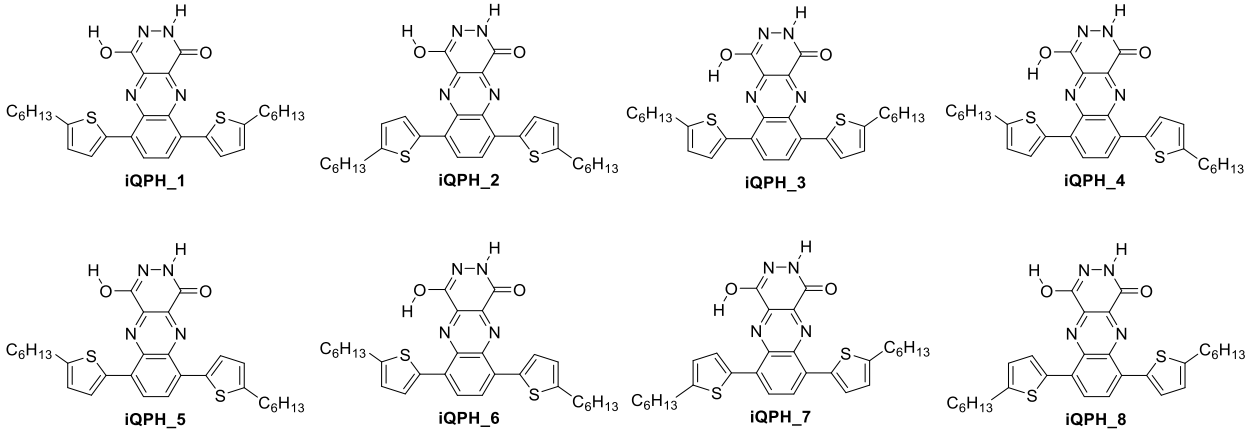

Fig. S12 List of **iQPH** conformers in the series of structures with one NH and one OH group (NHOH).

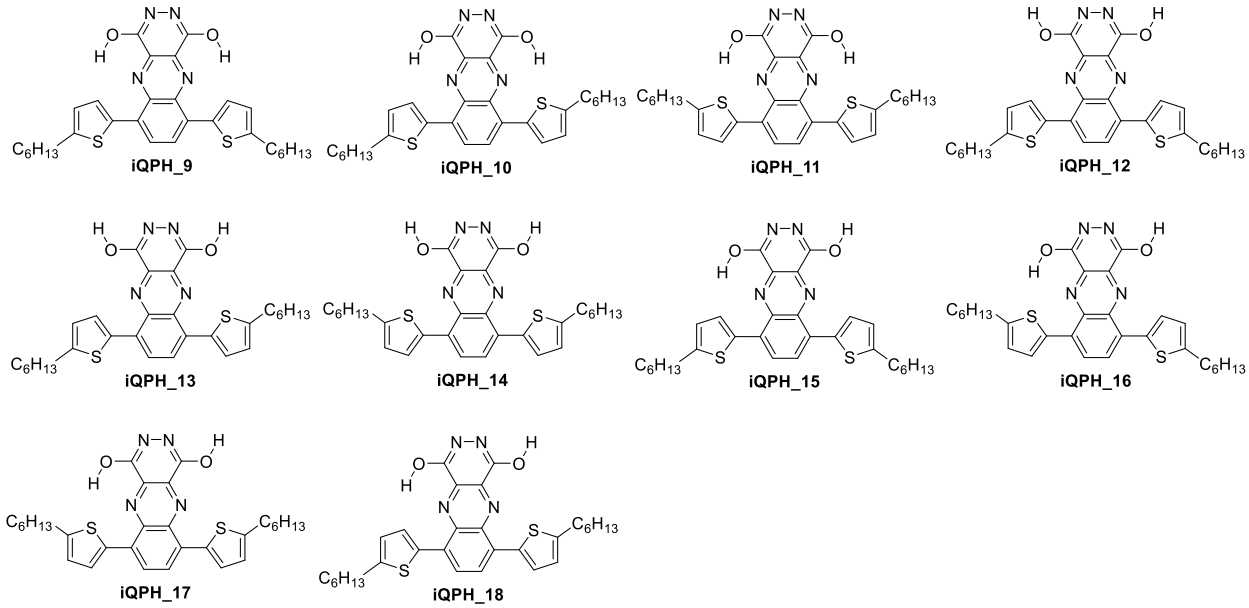

Fig. S13 List of **iQPH** conformers in the series of structures with two OH groups. (OHOH).

Table S2 DFT data summary for structural and conformational analysis of **iQPH**.

NHNH	Relative energy (kcal/mol)[a]	NHOH	Relative energy (kcal/mol) [a]	OHOH	Relative energy (kcal/mol)[a]
QPH_1	4.59	**iQPH_1**	2.57	**iQPH_9**	17.28
QPH_2	5.76	**iQPH_2**	1.74	**iQPH_10**	16.56
QPH_3	5.12	**iQPH_3**	0.60	**iQPH_11**	16.03
		iQPH_4	0.68	**iQPH_12**	13.83
		iQPH_5	1.97	**iQPH_13**	14.11
		iQPH_6	0.00	**iQPH_14**	14.35
		iQPH_7	1.22	**iQPH_15**	14.97
		iQPH_8	2.29	**iQPH_16**	14.29
				iQPH_17	14.58
				iQPH_18	15.19

[a]The relative energy is the difference between the calculated most stable structure, **iQPH_6**. [b] DFT calculation level is B3LYP/6-31+G(d) in gas phase.

In Table S2, **iQPH_6** has the lowest energy among all the possible structures, so this structure was used as reference to calculate the relative energies for the other structures. As expected, the structures with two OH groups are not thermodynamically favorable compared with the other two series, and display energy differences more than 9 kcal/mol. The structures with two NH groups are the second most-stable series, and the **QPH_1** is most stable structure in this series. The two downward thiophene spacers in the **QPH_1** allow the inner protons on the thiophene spacers to form an intramolecular H-bonding interaction with the nitrogen atoms on the quinoxaline to stabilize molecule. The NHOH series has significantly lower energy, and this matches with the molecular structure characterized by NMR techniques. In this series, structures with lower energies possess a downward facing proton on the OH group, followed by the structures with upward facing OH group which indicates the downward proton on the OH group participates

in the intramolecular H-bonding interaction with the nitrogen on quinoxaline. Thus, structure **iQPH_6** with one downward thiophene and one downward OH has the lowest energy, while **iQPH_1** is the most unstable structure in this series because no intramolecular H-bonding interaction is present for this structure.

Binding energy calculation

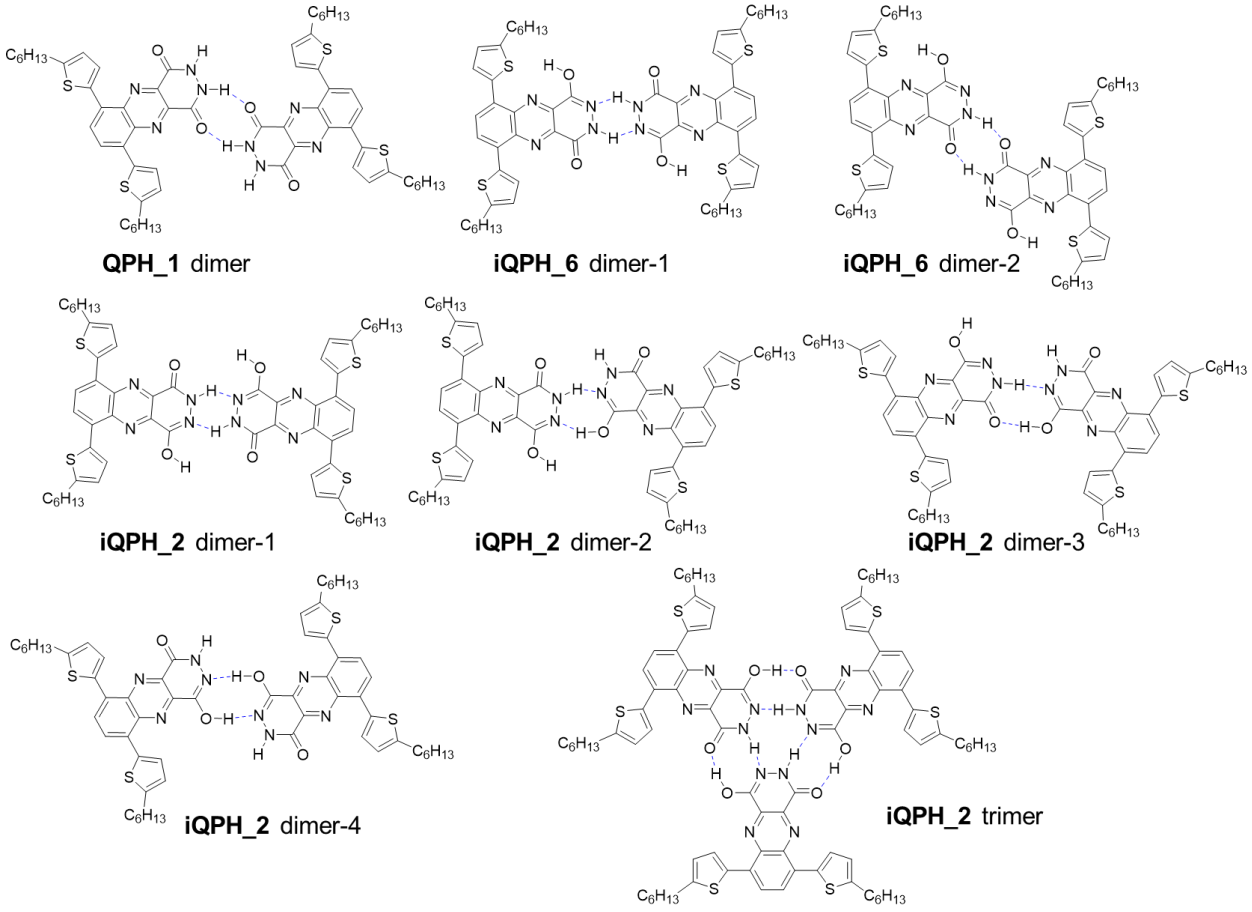

Fig. S14 Possible arrangements from the structures **QPH_1**, **iQPH_2**, and **iQPH_6**.

The first four structures with lowest energies possess the downward OH group (**iQPH_3**, **iQPH_4**, **iQPH_6**, and **iQPH_7**), which are not able to form trimers. Only the upward OH group are possible to lead the molecules to form trimers, while the downward OH group would form an alternative arrangement, like ribbon-type assemblies. Accordingly, the direction of the OH group on the PH unit is significant in deciding the mode of self-assembly, and the calculated binding energy was useful to understand the structural preference. The structures **iQPH_6** (the lowest energy with downward OH group in the NHOH series), **iQPH_2** (the lowest energy with upward OH group in the NHOH series), and **QPH_1** (the lowest energy in the NHNH series) were selected to calculate the binding energy in different arrangements. In Fig. S14, the intermolecular H-bonding arrangements are the possible combinations of electronegative carbonyl and

imine group, along with the acidic hydrogens from amide and enol group. Structures **QPH_1** and **iQPH_6** only can form dimers while **iQPH_2** can form four types of dimers and trimers. The electrostatic potential (ESP) calculation was performed to understand the electron-rich and electron-deficient sites on the molecules in each arrangement, and to observe the electron distribution before and after H-bonding (Fig. S15). In Table S3, despite **QPH_1** having the strongest binding energy among the dimer arrangements, structure **iQPH_2** is able to generate the most stable trimer arrangement with 40 kcal/mol of binding energy (Fig. S16). The ESP map of the trimer also demonstrates the well-matched electron-rich and electron-deficient sites from the monomer compared with the other arrangements (Fig. S17, Fig. S18, and Fig. S19).

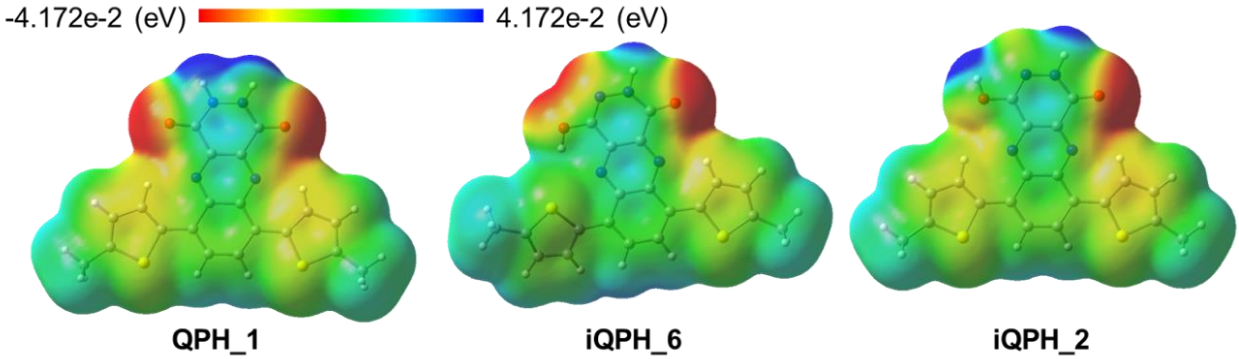

Fig. S15 ESP maps for the structures **QPH_1**, **iQPH_6**, **iQPH_2**.

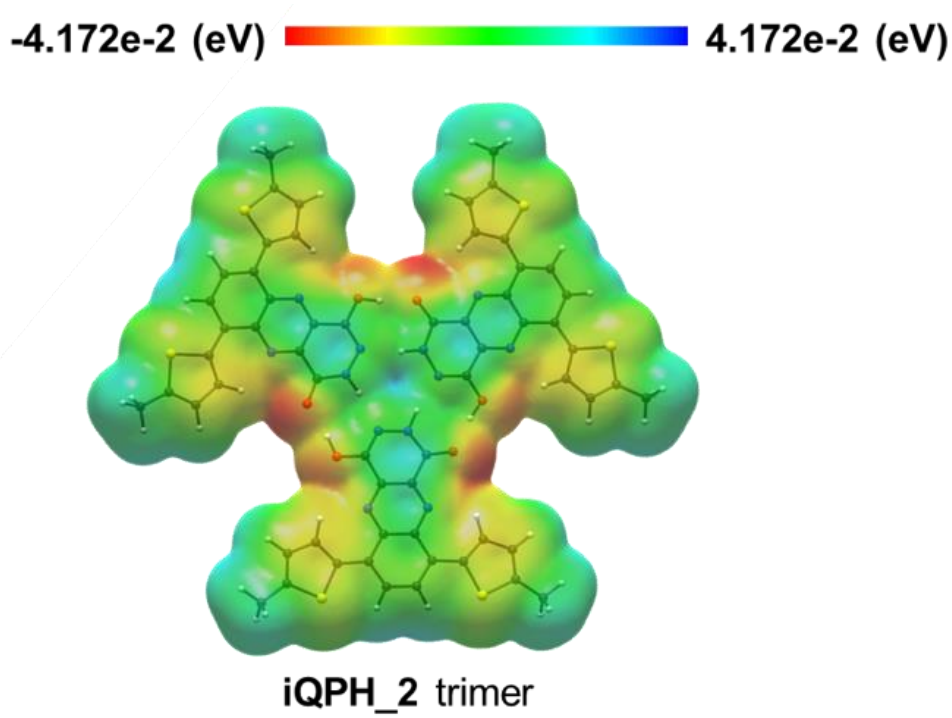

Fig. S16 ESP map for trimer arrangement from structure **iQPH_2**.

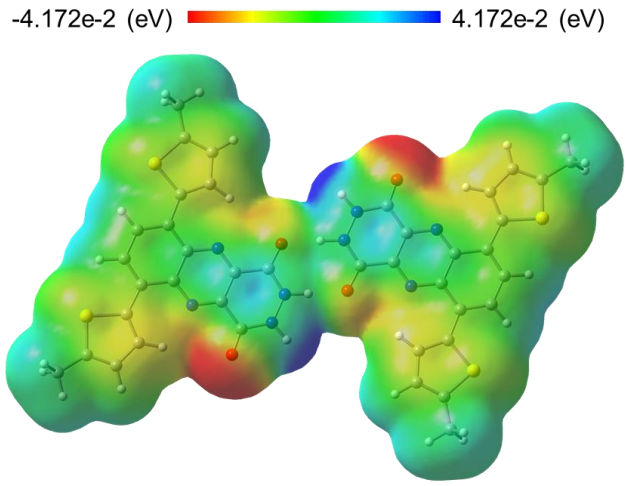

Fig. S17 ESP maps of possible arrangement with structure **QPH_1**.

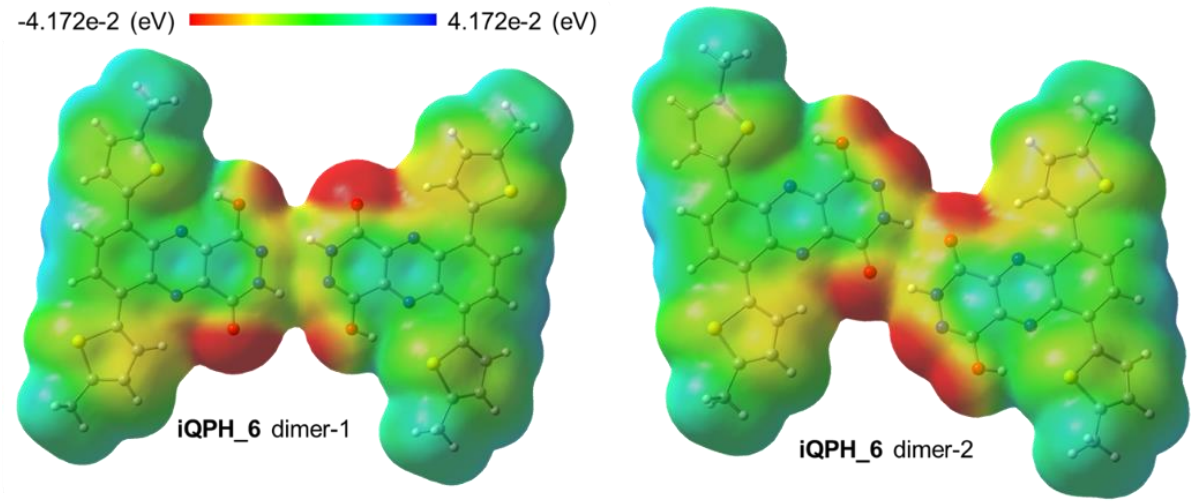

Fig. S18 ESP maps of possible arrangements with structure **iQPH_6**.

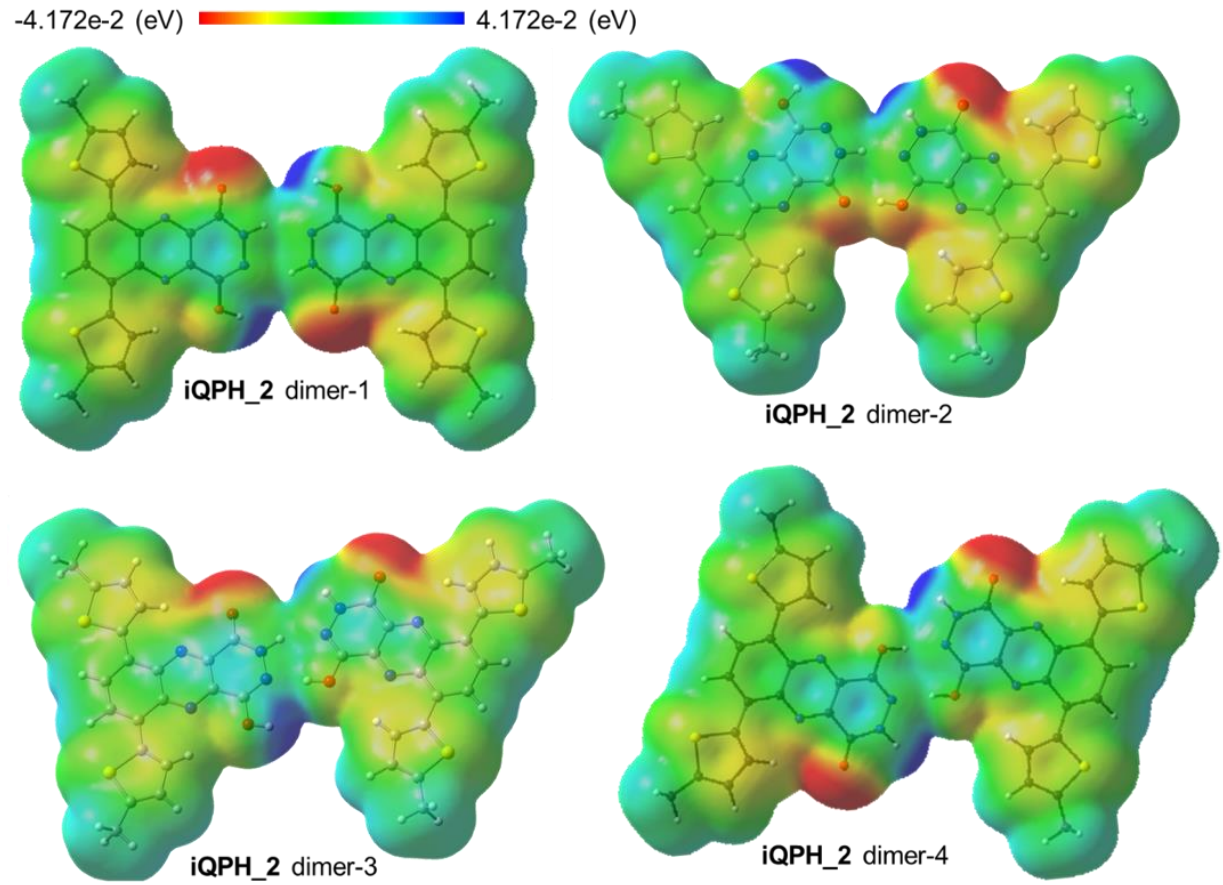

Fig. S19 ESP maps of possible dimer arrangements with structure **iQPH_2**.

Table S3 DFT data summary of possible arrangements in Fig. S14 and their calculated binding energies.

	Binding energy (kcal/mol)[a]	Binding energy per molecule (kcal/mol)
QPH_1 dimer	18.8	9.40
iQPH_6 dimer-1	7.3	3.65
iQPH_6 dimer-2	12.3	6.15
iQPH_2 dimer-1	6.5	3.25
iQPH_2 dimer-2	9.3	4.65
iQPH_2 dimer-3	13.3	6.65
iQPH_2 dimer-4	12.8	6.40
iQPH_2 trimer	40.0	13.3

[a] Binding energy = Energy (nA) - n Energy (A), n = 2 for dimer; n = 3 for trimer. [b] DFT calculation level is B3LYP/6-31+G(d) in gas phase.

DFT and TD-DFT optoelectronic analysis of target molecules

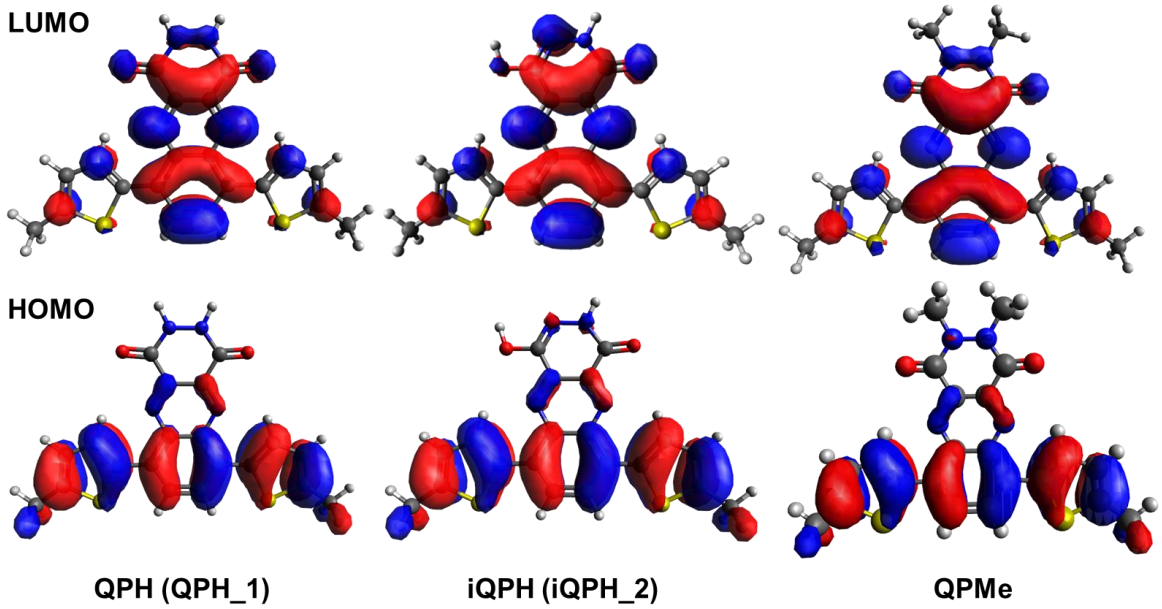

Fig. S20 LUMO and HOMO frontier molecular orbital plots of **QPH**, **iQPH** and **QPMe**.

Table S4 DFT data summary for optoelectronic properties of target molecule conformers and comparators.

	HOMO (eV)	LUMO (eV)	E_g (eV)	$\lambda_{max,vis}$ (nm)[a]
QPH	-5.47	-3.10	2.37	649
iQPH	-5.48	-3.15	2.33	662
QPMe	-5.42	-3.01	2.41	637

[a] $\lambda_{max,vis}$ was the maximum absorption in the low-energy region calculated by TD-DFT. [b] DFT and TD-DFT calculation levels are B3LYP/6-31+G(d) in gas phase.

Cartesian coordinates of all molecules for theoretical calculations

iQPH_2:

C	0.724438	-2.62431	-0.00049
C	-0.67898	-2.62829	-0.00079
C	-1.45677	-1.47333	-0.00089
C	-0.71735	-0.23325	-0.00069
C	0.740693	-0.22909	-0.00038
C	1.491956	-1.46246	-0.00028
N	-1.38838	0.934133	-0.00078
C	-0.69843	2.065295	-0.00058
C	0.721386	2.069887	-0.00028
N	1.40551	0.941051	-0.00019
C	2.953973	-1.52043	9.1E-06
C	-2.91886	-1.54793	-0.00119
C	3.910504	-0.52089	0.000237
C	5.247466	-1.0076	0.000478
C	5.34807	-2.3762	0.000441
S	3.760854	-3.09732	0.000106
S	-3.70889	-3.13286	-0.0012
C	-5.30453	-2.43014	-0.00164
C	-5.21891	-1.06086	-0.00174
C	-3.88655	-0.56004	-0.00148
C	-1.37524	3.355274	-0.00068
N	-0.74938	4.485397	-0.00048
N	0.619081	4.458117	-0.00011
C	1.463943	3.361501	-7.7E-05
O	2.682083	3.489009	0.000142
O	-2.72743	3.348826	-0.00103
C	-6.53226	-3.29158	-0.00186
C	6.585684	-3.22331	0.000654
H	1.218538	-3.59117	-0.00043

H	-1.16621	-3.59876	-0.00094
H	3.656202	0.529567	0.000226
H	6.115875	-0.35555	0.000672
H	-6.09527	-0.41929	-0.00199
H	-3.64129	0.491961	-0.00151
H	1.052076	5.373803	-3.4E-05
H	-3.02401	4.276935	-0.00104
H	-6.57788	-3.9394	0.882692
H	-7.42611	-2.65917	-0.00198
H	-6.5776	-3.93934	-0.88646
H	7.471955	-2.5804	0.000803
H	6.638727	-3.87048	-0.88397
H	6.638425	-3.87047	0.885297

iQPH_6:

C	0.757921	-2.65734	0.060243
C	-0.6468	-2.67517	0.046072
C	-1.42083	-1.52173	-0.0208
C	-0.69711	-0.28236	-0.04318
C	0.757703	-0.25641	-0.01193
C	1.515017	-1.48714	0.033282
N	-1.38564	0.875549	-0.1009
C	-0.70672	2.013721	-0.1165
C	0.709214	2.040845	-0.07376
N	1.40962	0.922328	-0.02599
C	2.976617	-1.53377	0.0599
C	-2.88157	-1.61551	-0.07947
C	3.923077	-0.52508	0.098094
C	5.264019	-0.99871	0.119178
C	5.377257	-2.36645	0.095572
S	3.798513	-3.10256	0.045953
S	-3.9843	-0.40065	0.557759
C	-5.39024	-1.36893	0.193598
C	-5.01717	-2.54856	-0.40166
C	-3.60959	-2.68938	-0.55309
C	-1.43532	3.27271	-0.1838
N	-0.84694	4.422081	-0.20021
N	0.522146	4.42017	-0.14983
C	1.406328	3.356411	-0.0871
O	2.619733	3.523932	-0.04787
O	-2.78319	3.239949	-0.23053
C	-6.77398	-0.87551	0.499698
C	6.623167	-3.20111	0.105362
H	1.262401	-3.61716	0.115938
H	-1.1418	-3.63912	0.110442

H	3.658751	0.52281	0.109362
H	6.125751	-0.3388	0.150349
H	-5.73384	-3.29405	-0.73278
H	-3.14775	-3.55285	-1.02027
H	0.930224	5.347467	-0.16333
H	-3.05426	2.300168	-0.21939
H	-7.0053	0.053639	-0.03616
H	-7.50967	-1.62846	0.198427
H	-6.91126	-0.68035	1.570533
H	7.502445	-2.54958	0.136075
H	6.700567	-3.83049	-0.79015
H	6.664022	-3.86453	0.978414

QPH_1:

C	0.701483	-2.50761	0.000399
C	-0.70141	-2.50763	0.000397
C	-1.47474	-1.34827	0.000218
C	-0.72747	-0.11432	0.000112
C	0.727476	-0.1143	0.000116
C	1.474775	-1.34823	0.00022
N	-1.39178	1.057588	1.9E-05
C	-0.70966	2.186812	-3.5E-05
C	0.709615	2.186829	-1.9E-05
N	1.391761	1.057621	3.73E-05
C	2.936464	-1.41209	0.000142
C	-2.93643	-1.41218	0.000148
C	3.895751	-0.41545	0.000592
C	5.23149	-0.90611	0.000384
C	5.327857	-2.27495	-0.00025
S	3.738566	-2.99138	-0.00059
S	-3.73846	-2.99151	-0.00047
C	-5.32778	-2.27514	-0.00018
C	-5.23147	-0.90629	0.000339
C	-3.89576	-0.41558	0.000516
C	-1.49022	3.464439	-9.3E-05
N	-0.6995	4.586743	-0.00022
N	0.699394	4.586759	-0.00015
C	1.49014	3.464474	-4.6E-05
O	2.711731	3.550755	5.5E-05
O	-2.71181	3.55069	-3.4E-05
H	1.192538	-3.47612	0.000591
H	-1.19244	-3.47615	0.000584
H	3.644854	0.635912	0.00102
H	6.101852	-0.25666	0.000687
H	-6.10186	-0.25688	0.000586

H	-3.6449	0.63579	0.000869
H	-1.14812	5.493885	-0.00018
H	1.147996	5.493912	-0.00014
C	-6.56282	-3.12605	-0.00053
H	-6.61384	-3.77307	-0.88541
H	-6.61383	-3.77381	0.883804
H	-7.45104	-2.48581	-0.00026
C	6.562932	-3.12581	-0.00066
H	6.613957	-3.77364	0.883622
H	6.61398	-3.77275	-0.88559
H	7.451118	-2.48552	-0.00032

QPMe:

C	-0.71001	-2.72601	-0.01757
C	0.694472	-2.7313	-0.00067
C	1.471144	-1.5685	0.010346
C	0.727559	-0.3331	0.004007
C	-0.7252	-0.32764	-0.00764
C	-1.47799	-1.5574	-0.02147
N	1.395809	0.850398	0.002031
C	0.717258	1.995356	0.000119
C	-0.69754	2.000601	0.010353
N	-1.38461	0.86077	0.001542
C	-2.93422	-1.60633	-0.03556
C	2.926975	-1.62838	0.024125
C	-3.88731	-0.60958	-0.01115
C	-5.24161	-1.07289	-0.03186
C	-5.39276	-2.4334	-0.07366
S	-3.77383	-3.24445	-0.08917
S	3.754332	-3.273	0.068173
C	5.379271	-2.47398	0.057336
C	5.238276	-1.11216	0.023466
C	3.887473	-0.63864	0.005502
C	1.487312	3.257841	-0.07923
N	0.728487	4.418603	-0.07001
N	-0.69071	4.423369	0.095051
C	-1.45817	3.268291	0.097349
O	-2.70306	3.318013	0.234999
O	2.732542	3.29908	-0.2166
H	-1.20958	-3.68801	-0.02506
H	1.186859	-3.69703	0.000909
H	-3.61752	0.436158	0.023667
H	-6.0899	-0.39739	-0.01541
H	6.09159	-0.44292	0.010934
H	3.625491	0.409265	-0.02318

C	6.62717	-3.29795	0.084756
H	6.686113	-3.92145	0.985996
H	6.695219	-3.9666	-0.78282
H	7.503128	-2.64033	0.072509
C	-6.64677	-3.24786	-0.10587
H	-6.71034	-3.86564	-1.01073
H	-6.71984	-3.92103	0.757791
H	-7.5178	-2.58381	-0.08978
C	1.349279	5.683937	-0.48879
H	1.287392	6.441425	0.295884
H	2.397697	5.459803	-0.68228
H	0.873913	6.054504	-1.40326
C	-1.3021	5.690757	0.521286
H	-0.82374	6.052606	1.437676
H	-1.23498	6.452263	-0.25906
H	-2.35207	5.473185	0.713909

FT-IR Characterization

Solid-state IR spectra were collected using the GladiATRTM attachment (Pike Technologies). All measurements were acquired with Perkin Elmer Spectrum software at 298 K.

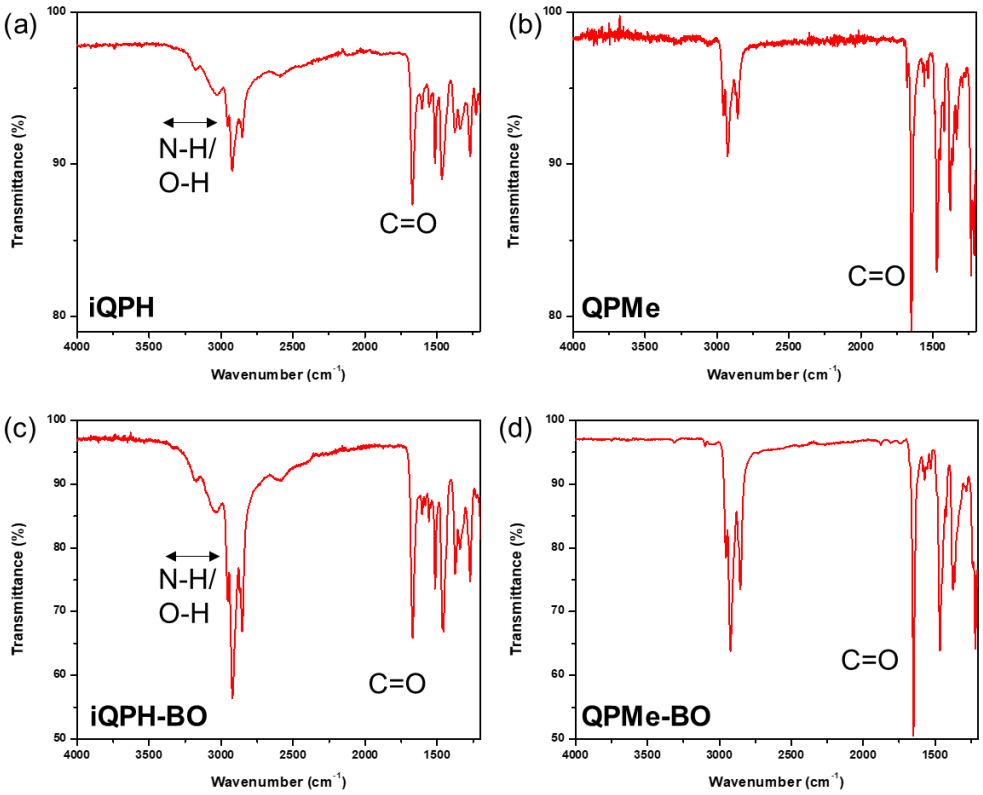

Fig. S21 Solid-state FT-IR spectra of (a) **iQPH**, (b) **QPMe**, (c) **iQPH-BO**, and (d) **QPMe-BO**.

The solid-state FT-IR spectra also provided structural information for the H-bonding capable molecules, **iQPH** and **iQPH-BO**, and comparator molecules, **QPMe** and **QPMe-BO** (Fig. S21). The broad peaks near 3300 and 3100 cm^{-1} observed in the spectra of **iQPH** and **iQPH-BO** are consistent with the stretching of the N-H and O-H bonds, giving further confirmation of the NH/OH tautomeric structures observed in NMR experiments. These two peaks are not observed in the spectra of **QPMe** and **QPMe-BO** because there are no N-H and O-H bonds in the H-bonding incapable molecules. The C=O stretches from the PH unit are at 1671 cm^{-1} for **iQPH** and **iQPH-BO**, and at 1650 cm^{-1} for **QPMe** and **QPMe-BO**. The lower energy of the C=O peak in **QPMe** and **QPMe-BO** relative to **iQPH** and **iQPH-BO** is suspected to be due to the electron-donating nature of the methyl units in the amide groups similar to what was observed in our previous work.[6] The stronger absorption of the C=O stretch in the H-bonding incapable molecules is related to the symmetric structures of the comparators, each possessing two C=O groups, while the C=O absorption is weaker for the H-bonding capable molecules because the asymmetric tautomeric forms possess only one C=O group.

Solution UV-vis Spectroscopy Studies

Variable concentration (at 298 K) and variable temperature UV-vis measurements were obtained on a Cary 100 Bio UV-Visible dual beam spectrophotometer controlled by Cary Win UV software and equipped with a Peltier 1 x 1 Cell Holder using capped 1 cm quartz cells. Spectrophotometric grade solvents were used for the absorption studies.

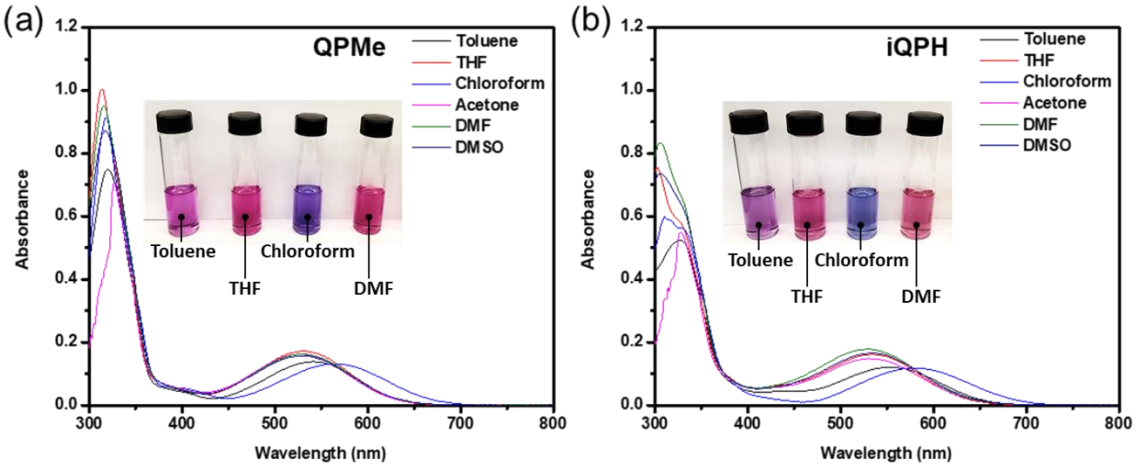

Fig. S22 Absorption spectra in various solvents at 20 μM (a) **QPMe** and (b) **iQPH**.

Table S5 Optical data of 20 μM **QPMe** and **iQPH** in different solvent and the DFT calculated $\lambda_{max,vis}$ in gas-phase.

	QPMe[a]	**iQPH**[a]
Toluene	540 nm	553 nm
THF	530 nm	533 nm
Chloroform	564 nm	574 nm
Acetone	527 nm	531 nm
DMF	529 nm	528 nm
DMSO	529 nm	532 nm
TD-DFT[b]	637 nm	662 nm

[a] Absorbance data from solutions (20 μM; 1 cm cell). [b] $\lambda_{max,vis}$ as the maximum absorption in the low-energy region calculated by TD-DFT at the B3LYP/6-31+G(d) level of theory in gas phase.

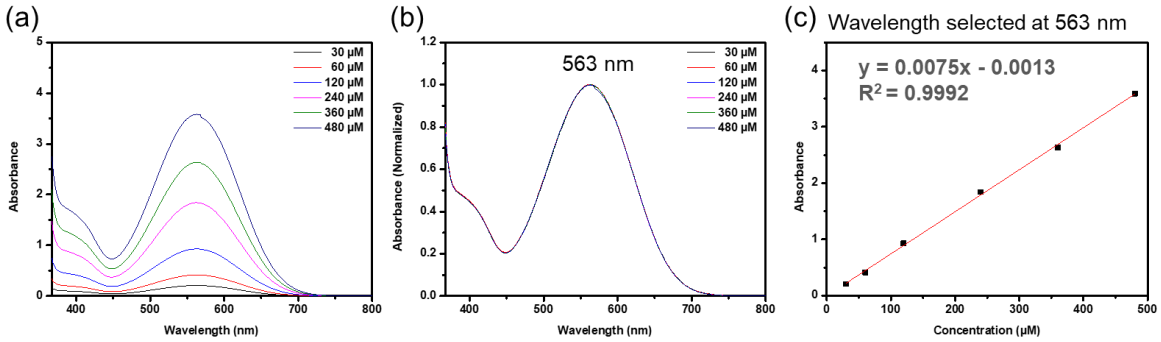

Fig. S23 Concentration-dependent UV-vis experiments of **QPMe** in chloroform. (a) Absorption spectrum, (b) normalized spectrum, and (c) Beer-Lambert plot.

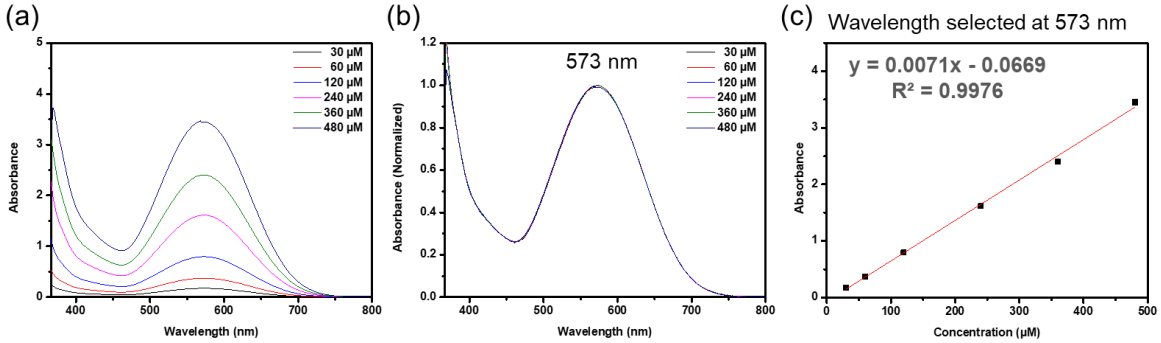

Fig. S24 Concentration-dependent UV-vis experiments of **iQPH** in chloroform. (a) Absorption spectrum, (b) normalized spectrum, and (c) Beer-Lambert plot.

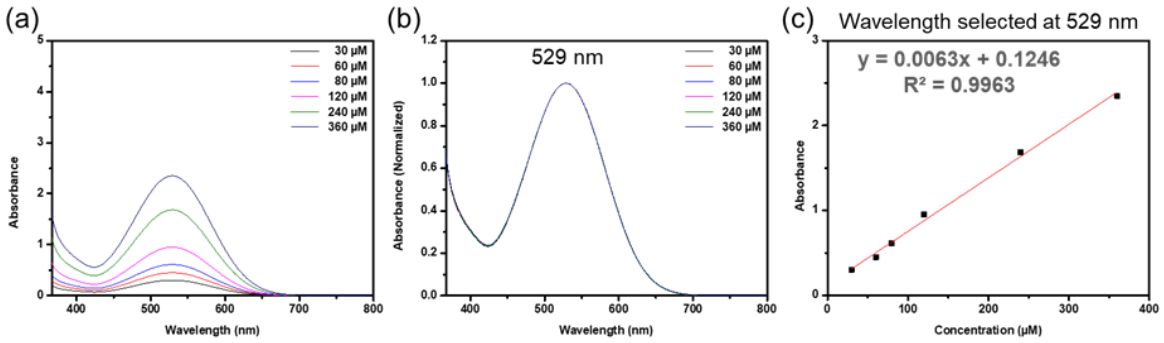

Fig. S25 Concentration-dependent UV-vis experiments of **QPMe** in DMSO. (a) Absorption spectrum, (b) normalized spectrum, and (c) Beer-Lambert plot.

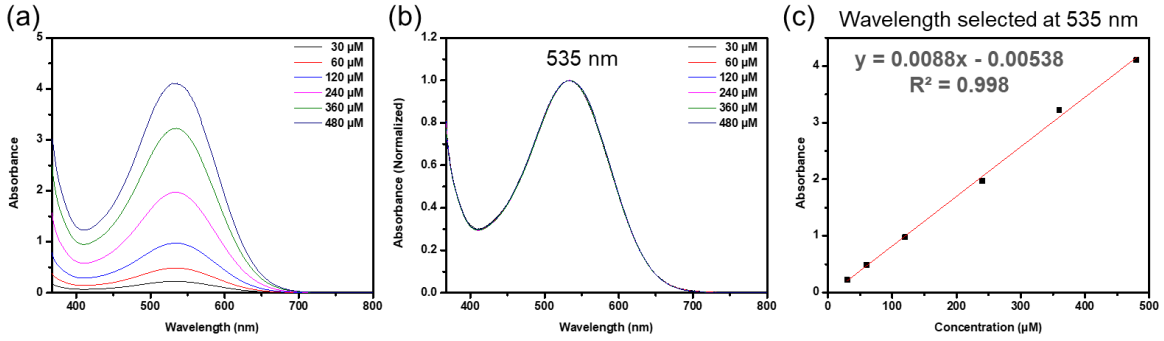

Fig. S26 Concentration-dependent UV-vis experiments of **iQPH** in DMSO. (a) Absorption spectrum, (b) normalized spectrum, and (c) Beer-Lambert plot.

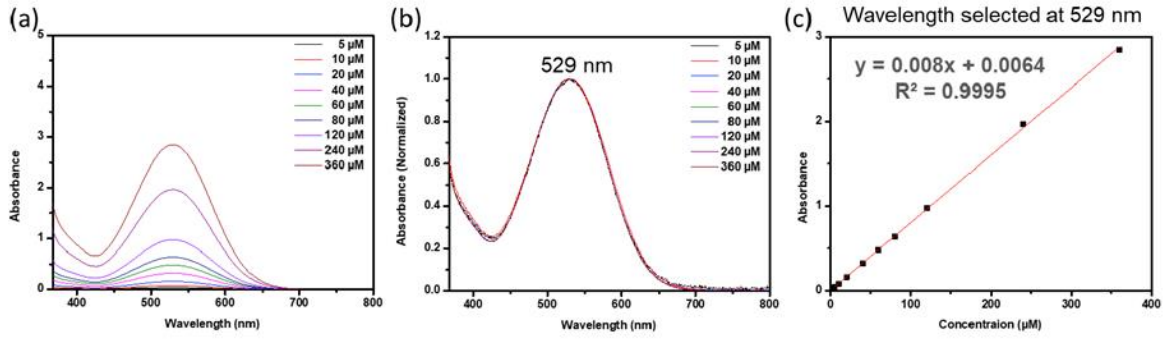

Fig. S27 Concentration-dependent UV-vis experiments of **QPMe** in DMF. (a) Absorption spectrum, (b) normalized spectrum, and (c) Beer-Lambert plot.

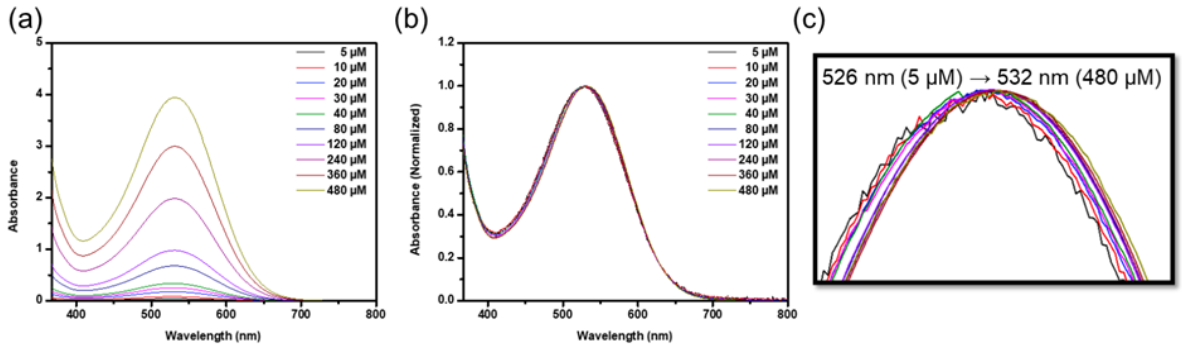

Fig. S28 Concentration-dependent UV-vis experiments of **iQPH** in DMF. (a) Absorption spectrum, (b) normalized spectrum, and (c) expanded normalized spectrum.

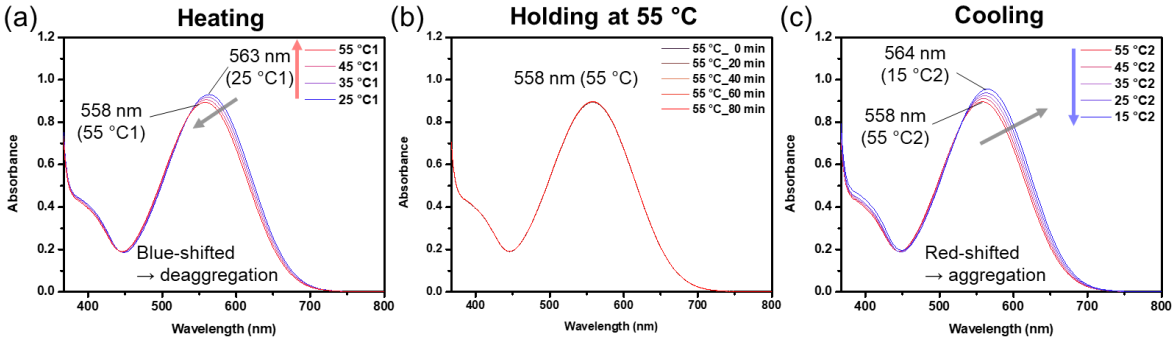

Fig. S29 Variable-temperature UV-vis of **QPMe** 120 μM in chloroform during (a) heating, (b) holding temperature at 55 °C, and (c) cooling.

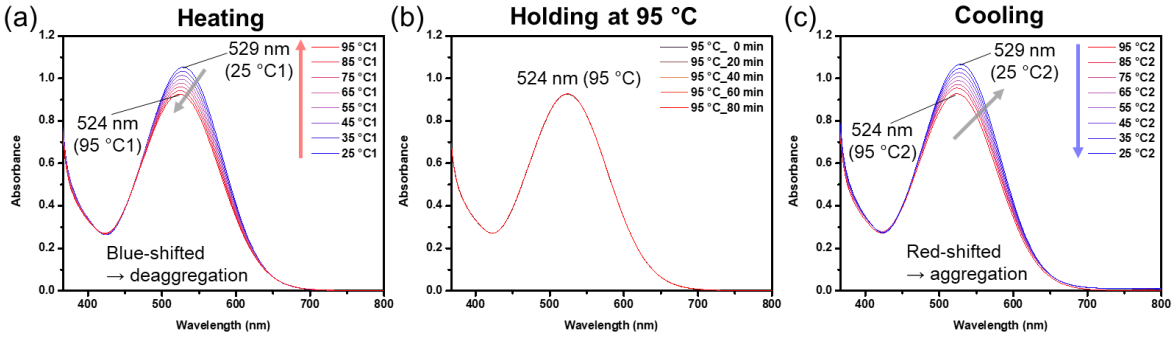

Fig. S30 Variable-temperature UV-vis of **QPMe** 120 μM in DMSO during (a) heating, (b) holding temperature at 55 °C, and (c) cooling.

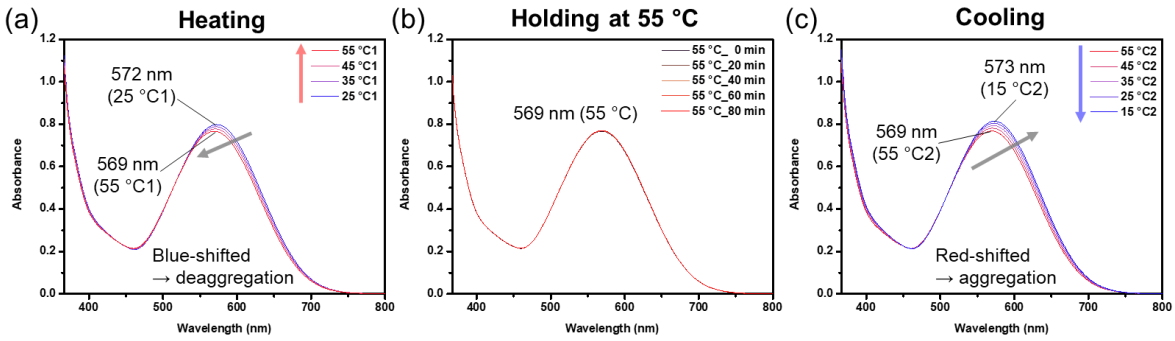

Fig. S31 Variable-temperature UV-vis of **iQPH** 120 μM in chloroform during (a) heating, (b) holding temperature at 55 °C, and (c) cooling.

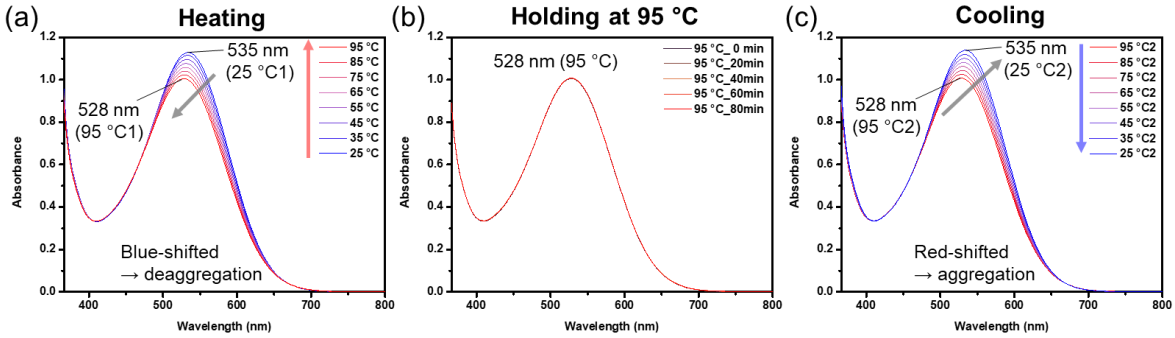

Fig. S32 Variable-temperature UV-vis of **iQPH** 120 μM in DMSO during (a) heating, (b) holding temperature at 55 °C, and (c) cooling.

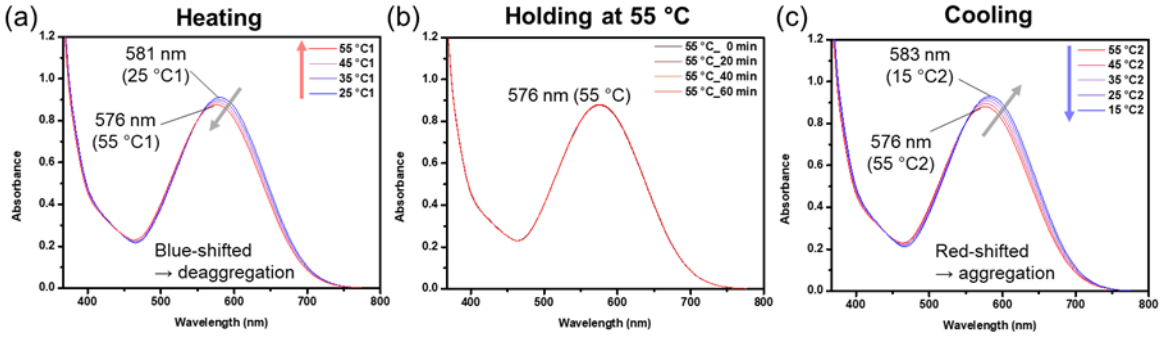

Fig. S33 Variable-temperature UV-vis of **iQPH-BO** 120 μM in chloroform during (a) heating, (b) holding temperature at 55 °C, and (c) cooling.

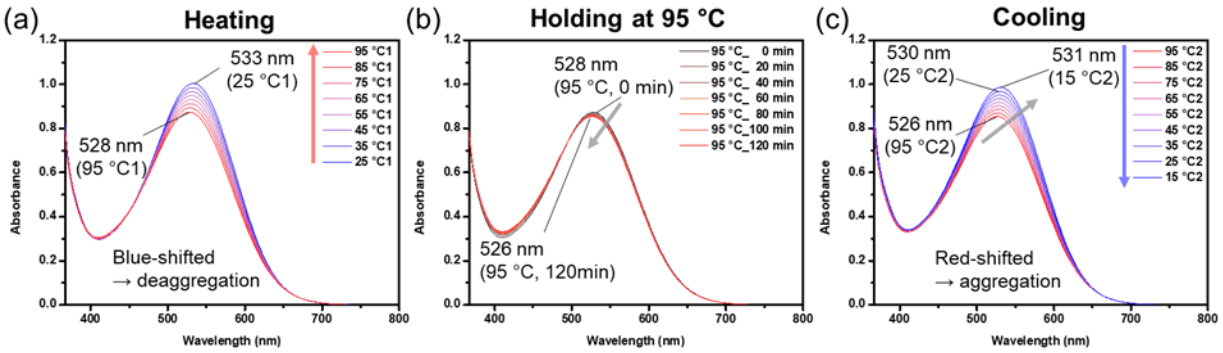

Fig. S34 Variable-temperature UV-vis of **iQPH-BO** 120 μM in DMF (a) during heating, (b) holding temperature at 95 °C, and (c) during cooling.

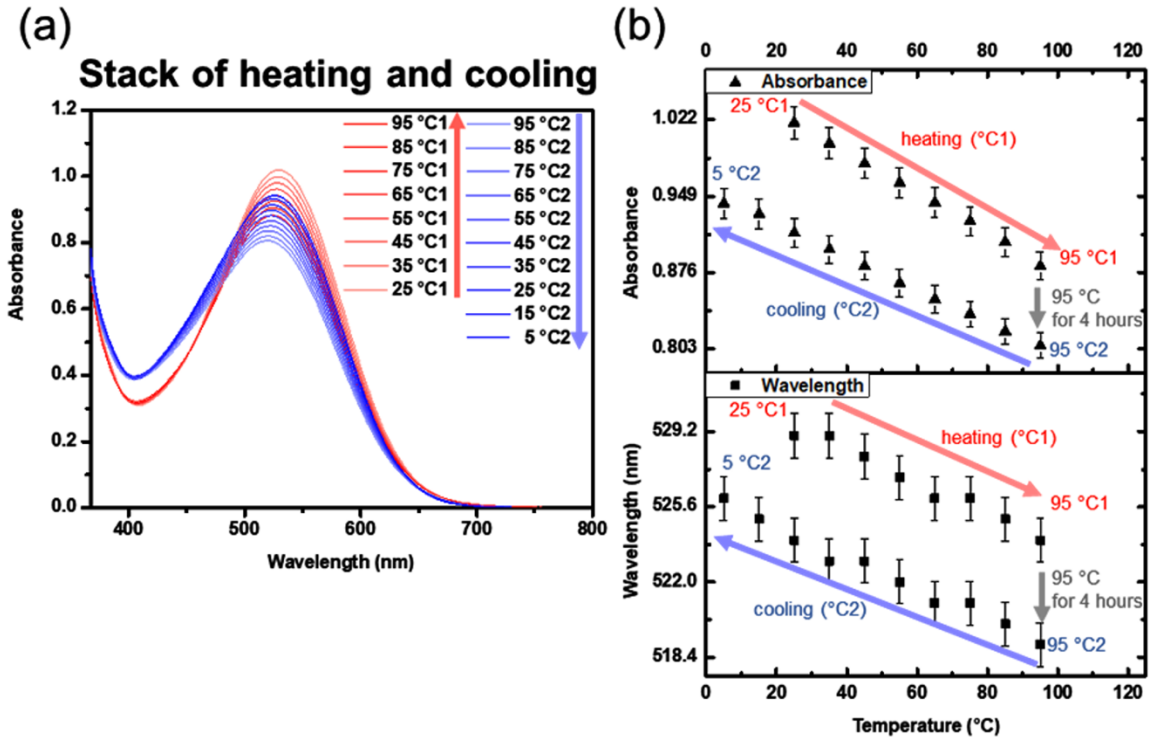

Fig. S35 (a) Stacked absorption spectra during heating and cooling of 120 μM **iQPH** in DMF, and (b) stacked plots of absorbance at $\lambda_{max,vis}$ and $\lambda_{max,vis}$ over various temperatures. Spectra were recorded three minutes after the desired temperature was achieved to allow the solution to reach equilibrium. The absorbance at 95 °C1 was the obtained during the first heating process and the absorbance at 95 °C2 was taken after holding temperature at 95 °C for 120 minutes.

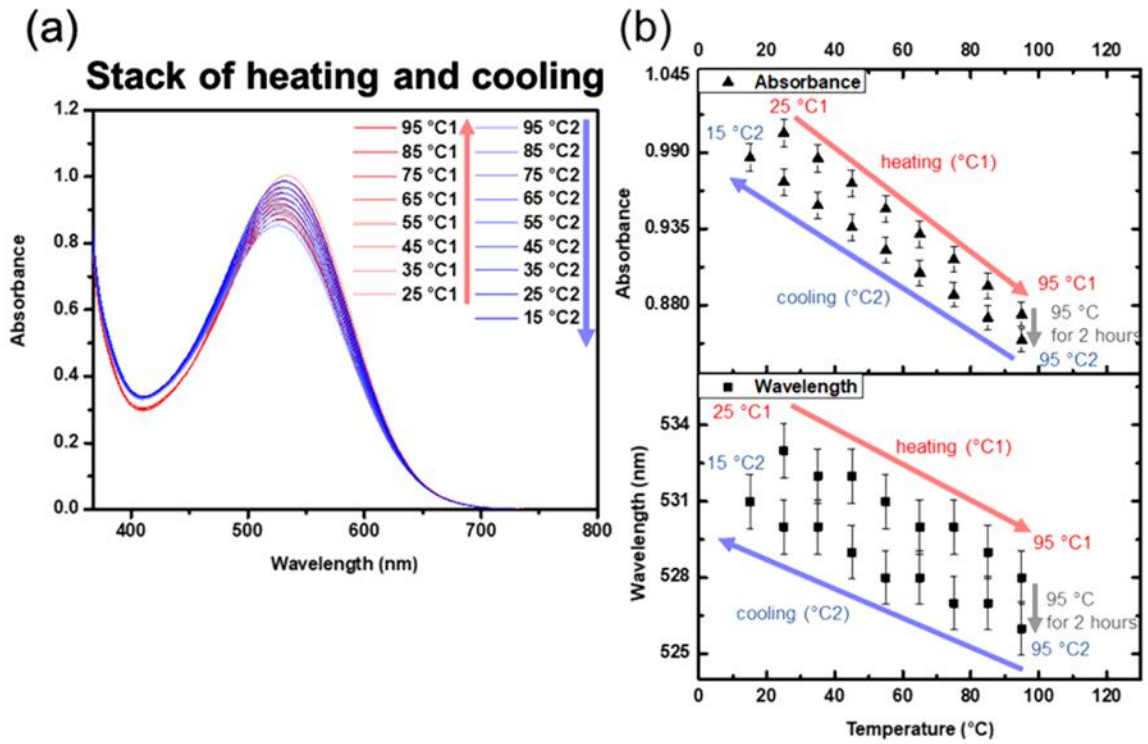

Fig. S36 (a) Stacked heating and cooling spectra of **iQPH-BO** 120 μM in DMF and (b) stacked plots of absorbance at $\lambda_{max,vis}$ and $\lambda_{max,vis}$ versus temperature. Spectra were recorded three minutes after the desired temperature was achieved to allow the solution to reach equilibrium. The absorbance at 95 °C1 was the obtained during the first heating process and the absorbance at 95 °C2 was taken after holding temperature at 95 °C for 120 minutes.

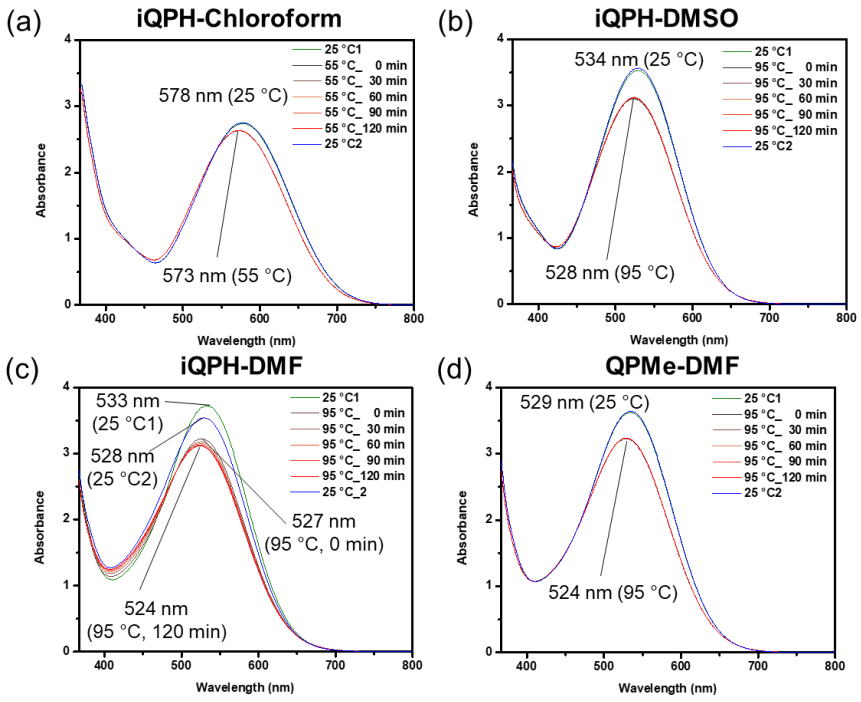

Fig. S37 VT-UV-vis absorption spectra of 450 μM **iQPH** in (a) chloroform, (b) DMSO, (c) DMF, and (d) 450 μM **QPMe** in DMF.

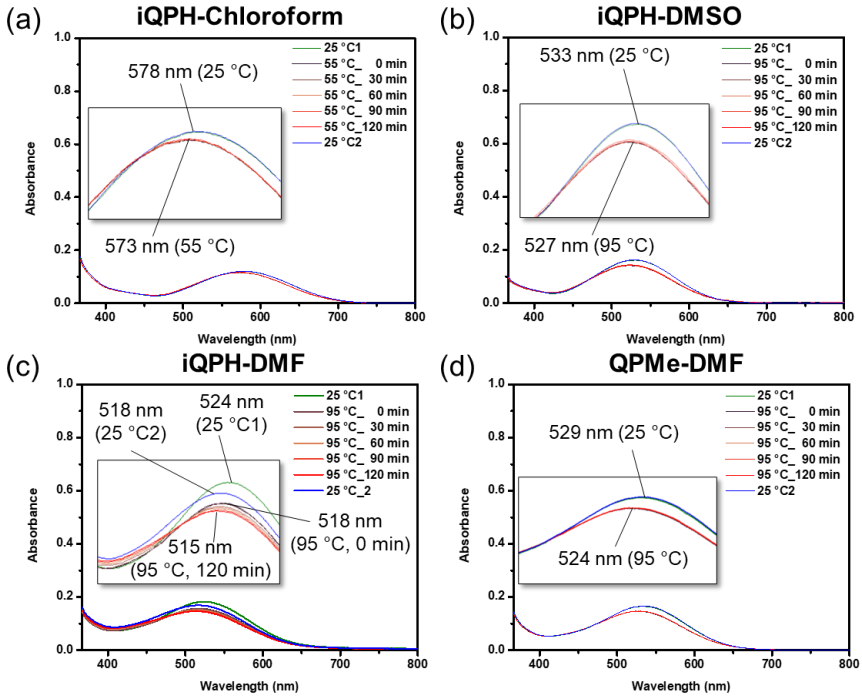

Fig. S38 VT-UV-vis absorption spectra of 20 μM **iQPH** in (a) chloroform, (b) DMSO, (c) DMF, and (d) 20 μM **QPMe** in DMF.

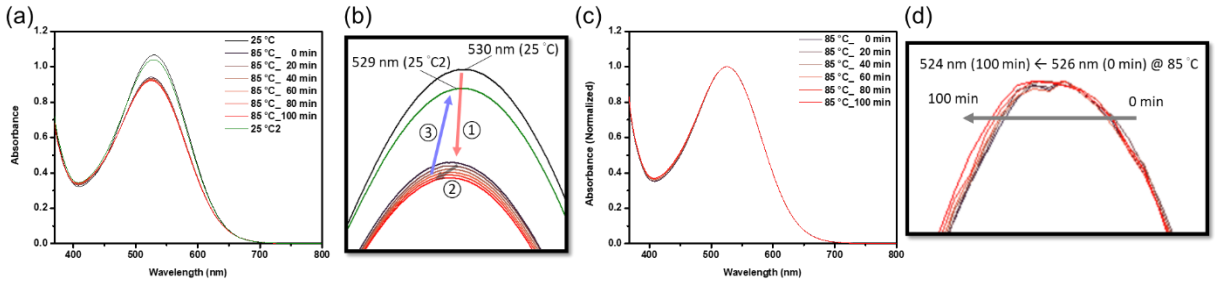

Fig. S39 (a) VT-UV-vis absorption spectrum of 120 μM **iQPH** in DMF, (b) expanded spectrum (① is heating from 25 °C to 85 °C, ② is holding temperature at 85 °C, and ③ is cooling from 85 °C_100 min to 25 °C2), (c) normalized VT-UV-vis absorption spectrum of 120 μM **iQPH** in DMF in the period of 85 °C, and (d) expanded normalized spectrum at 85 °C from 0 minutes to 100 minutes.

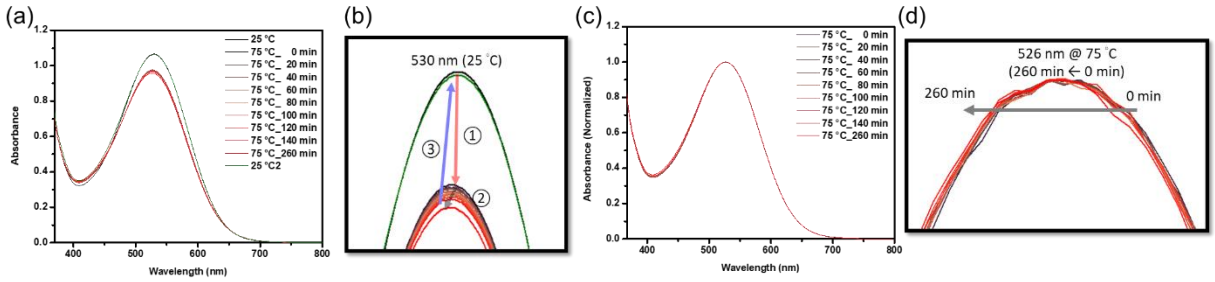

Fig. S40 (a) VT-UV-vis absorption spectrum of 120 μM **iQPH** in DMF, (b) expanded spectrum (① is heating from 25 °C to 75 °C, ② is holding temperature at 75 °C, and ③ is cooling from 75 °C_260 min to 25 °C2), (c) normalized VT-UV absorption spectrum of 120 μM **iQPH** in DMF in the period of 75 °C, and (d) expanded normalized spectrum at 75 °C from 0 minutes to 260 minutes.

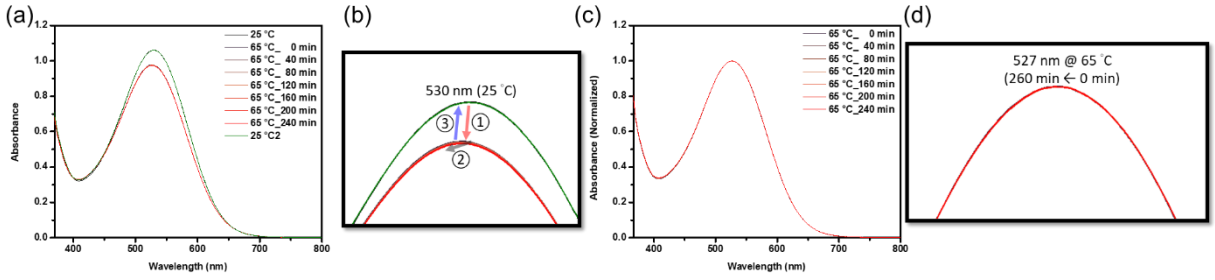

Fig. S41 (a) VT-UV-vis absorption spectrum of 120 μM **iQPH** in DMF, (b) expanded spectrum (① is heating from 25 °C to 65 °C, ② is holding temperature at 65 °C, and ③ is cooling from 65 °C_260 min to 25 °C2), (c) normalized VT-UV absorption spectrum of 120 μM **iQPH** in DMF in the period of 65 °C, and (d) expanded normalized spectrum at 65 °C from 0 minutes to 260 minutes.

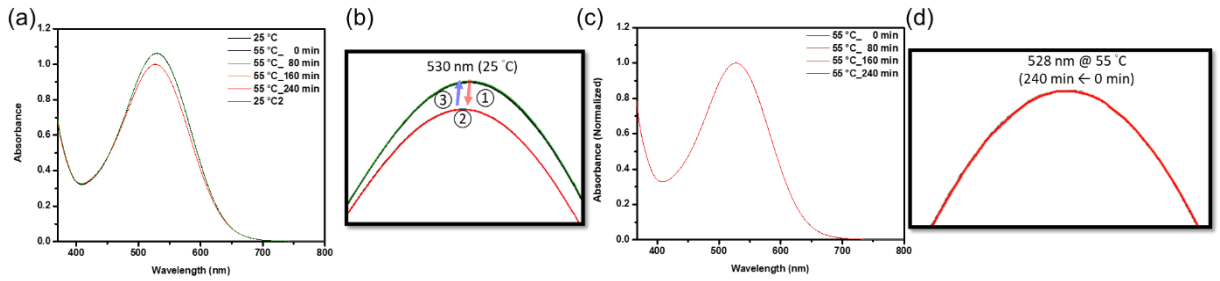

Fig. S42 (a) VT-UV-vis absorption spectrum of 120 μM **iQPH** in DMF, (b) expanded spectrum (① is heating from 25 °C to 55 °C, ② is holding temperature at 55 °C, and ③ is cooling from 55 °C_240 min to 25 °C2), (c) normalized VT-UV absorption spectrum of 120 μM **iQPH** in DMF in the period of 55 °C, and (d) expanded normalized spectrum at 55 °C from 0 minutes to 240 minutes.

During VT-UV-vis experiments, **iQPH** demonstrated unique behavior in DMF when holding the temperature constant and further dissociation from trimers was considered as a reason. Therefore, we investigated if there were any further changes in chemical shift in the NMR spectrum when holding at a high temperature. To simulate the same conditions as conducted for UV-vis experiments, the sample was prepared at 450 μM with DMF instead of deuterated DMF, and the ^{1}H NMR spectra was taken with solvent suppression technique in the range from 7.15 to 13.15 ppm. The temperature was directly increased from 25 to 130 °C, expecting to facilitate dissociation and the spectrum was recorded every 20 minutes over a 3-hour timeframe. Only the initial shielding was observed from 25 to 130 °C and no further changes were detected (Fig. S43). After 3 hours of heating, the peaks went back to original position when the sample was cooled back to 25 °C.

To give clearer view, the highest concentration of 7 mM **iQPH** sample was prepared with DMF-d_7. After recording the spectrum at 25 °C, the sample was heated to 95 °C directly and spectra were recorded every hour, then the sample was cooled back to 25 °C. However, the stacked spectrum looks like the stacked spectra with normal DMF (Fig. S44). Although the dissociation information was not found in the NMR experiment, we can confirm that the further blueshift detected by UV-vis was not caused by decomposition in DMF.

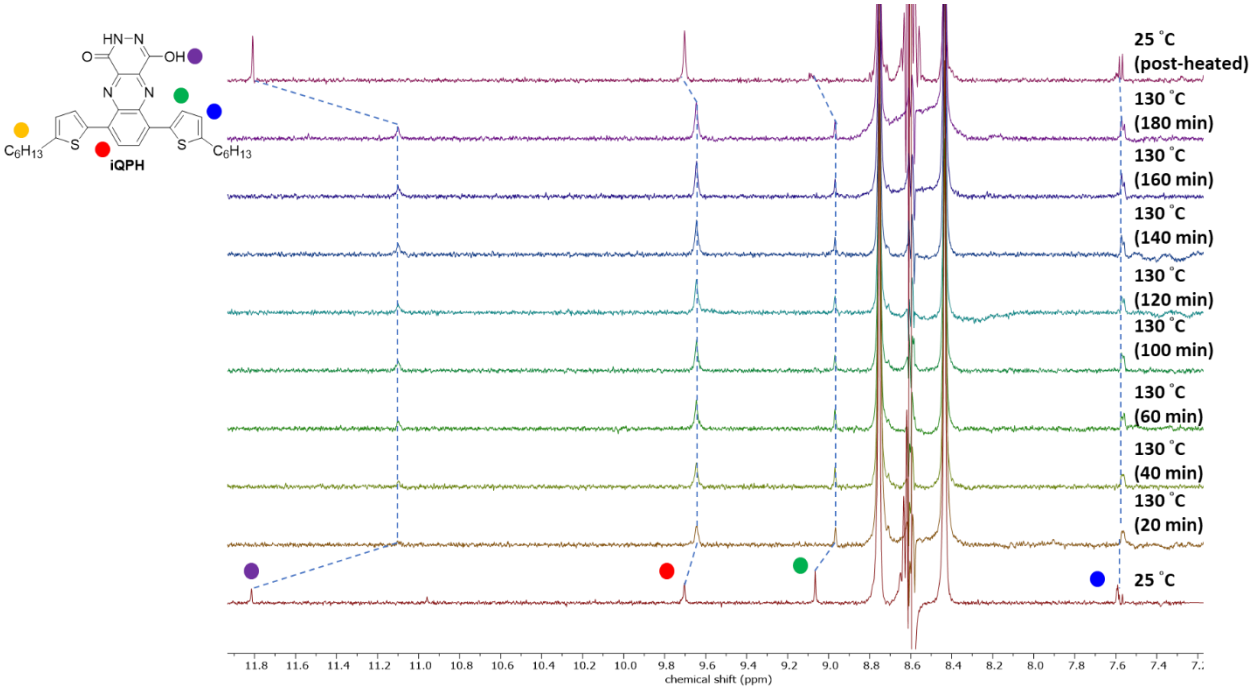

Fig. 43 Stacked ^{1}H NMR spectra of 450 μM **iQPH** in normal DMF at 25 °C, during heating at 130 °C, and at 25 °C after heating for 3 hours.

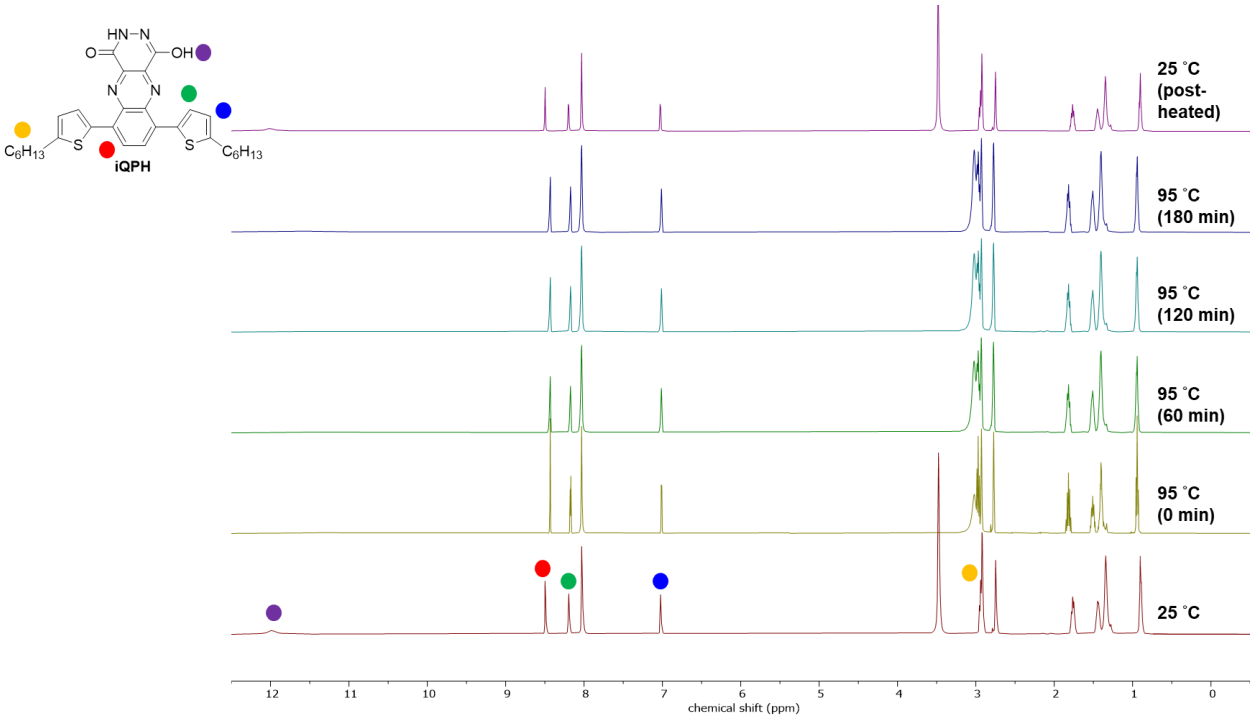

Fig. S44 Stacked ^{1}H NMR spectra of 7 mM **iQPH** in DMF-d_7 at 25 °C, during heating at 95 °C, and at 25 °C after heating for 3 hours.

VT-NMR Studies

From high to low temperatures, the positive value of Δδ means deshielding while negative value means shielding.

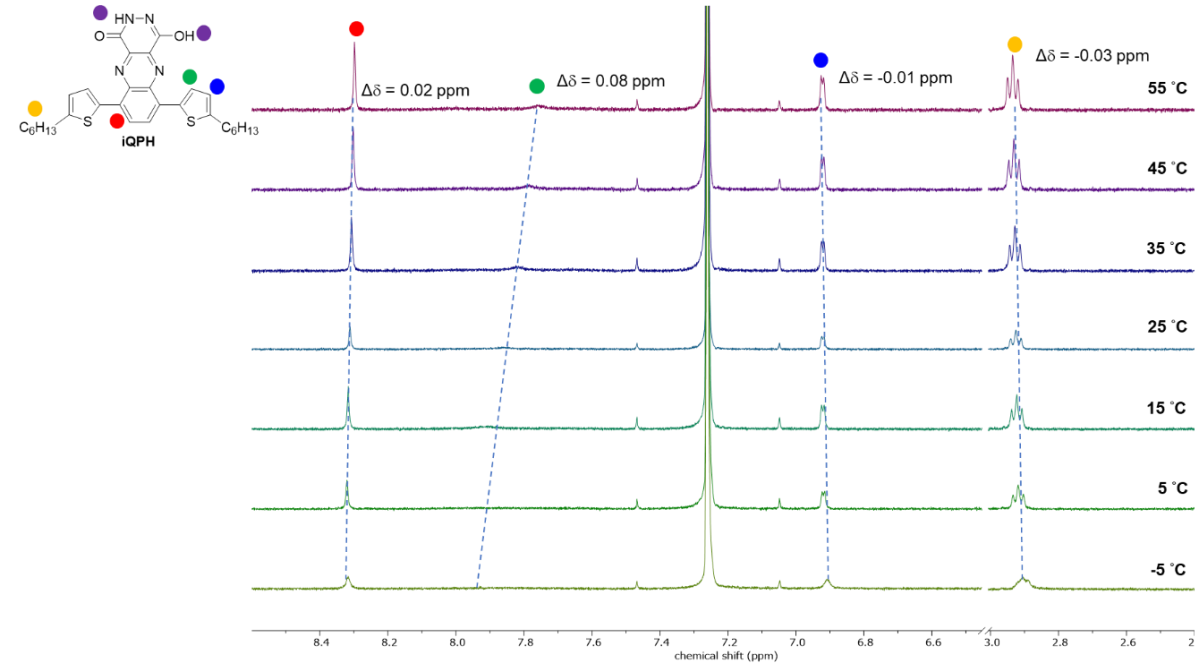

Fig. S45 VT ^{1}H NMR of **iQPH** (450 μM) in $CDCl_3$.

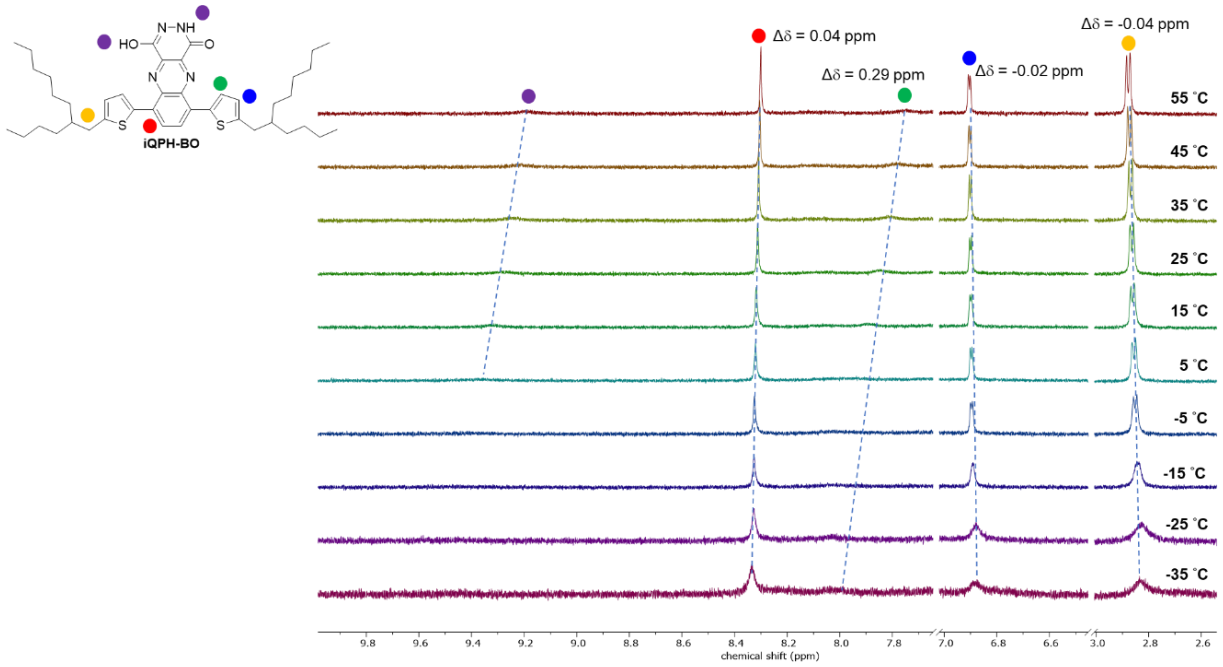

Fig. S46 VT ^{1}H NMR of **iQPH-BO** (450 μM) in $CDCl_3$.

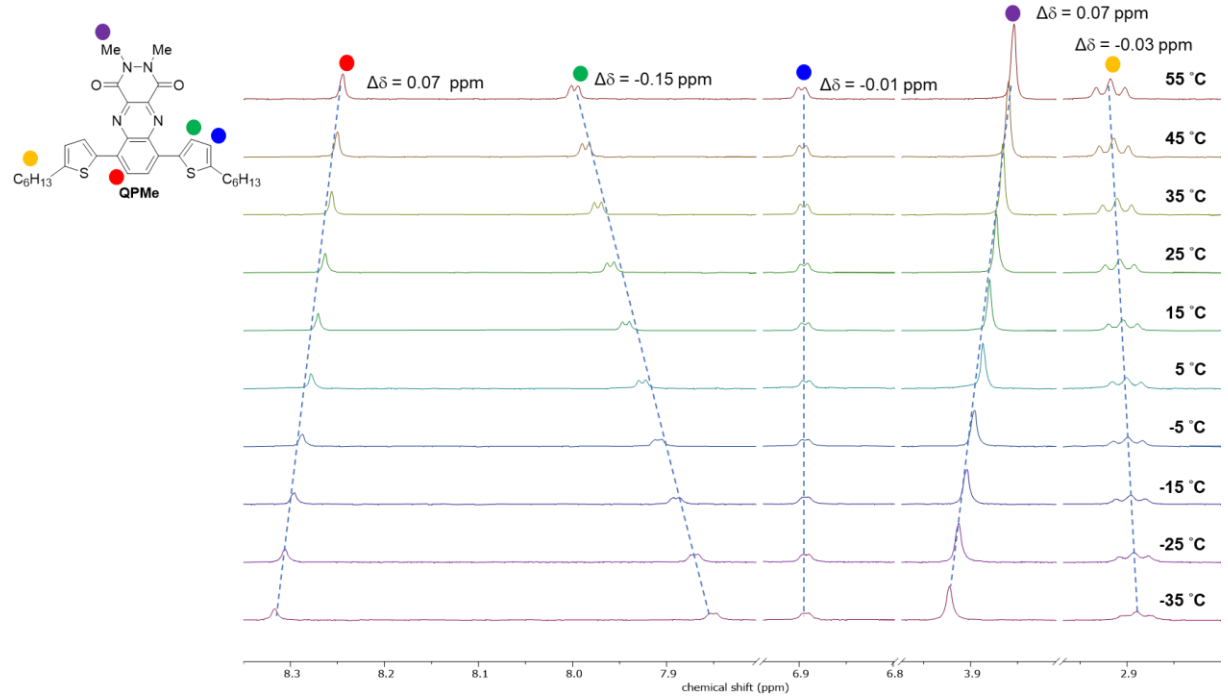

Fig. S47 VT ^{1}H NMR of **QPMe** (450 μM) in $CDCl_3$.

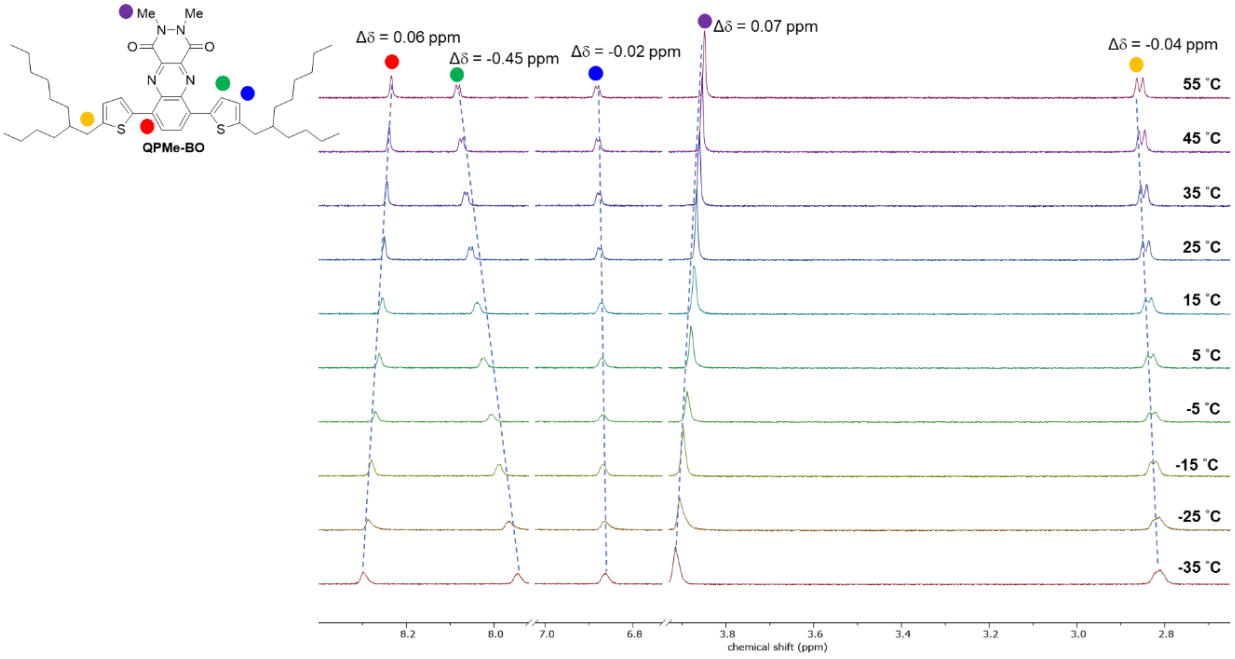

Fig. S48 VT ^{1}H NMR of **QPMe-BO** (450 μM) in $CDCl_3$.

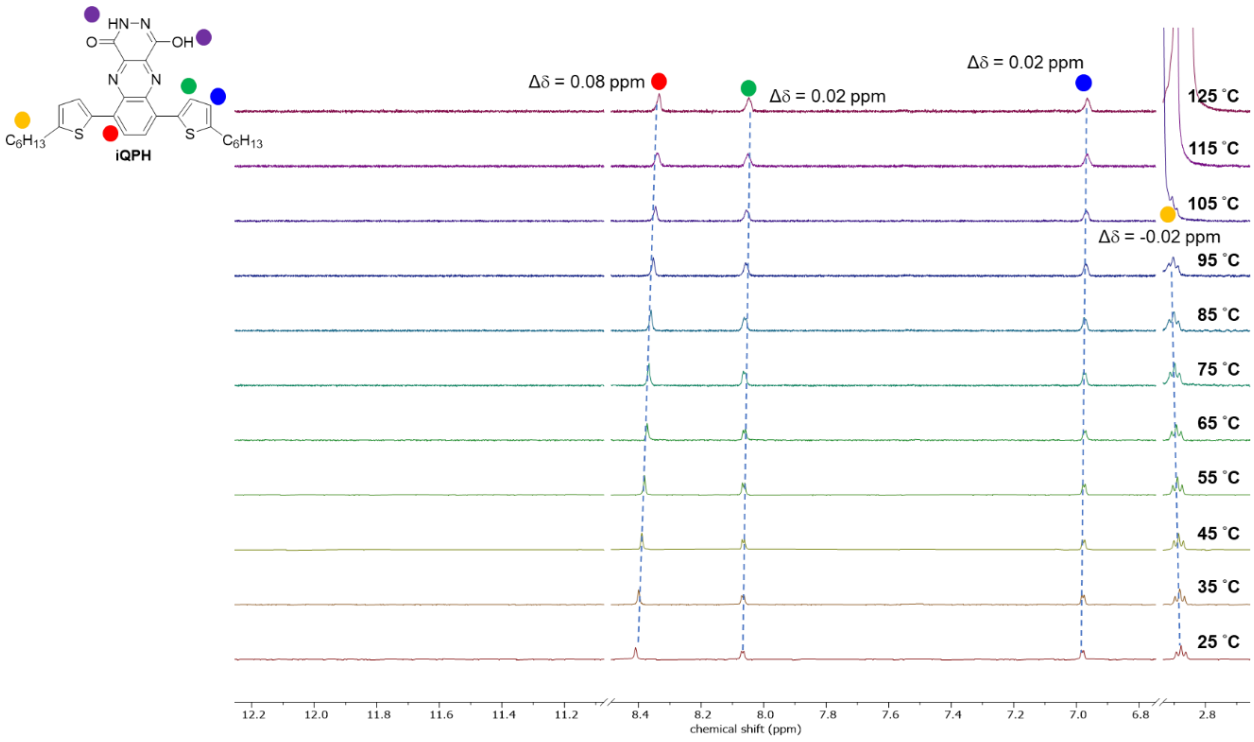

Fig. S49 VT ^{1}H NMR of **iQPH** (450 μM) in DMSO-d_6.

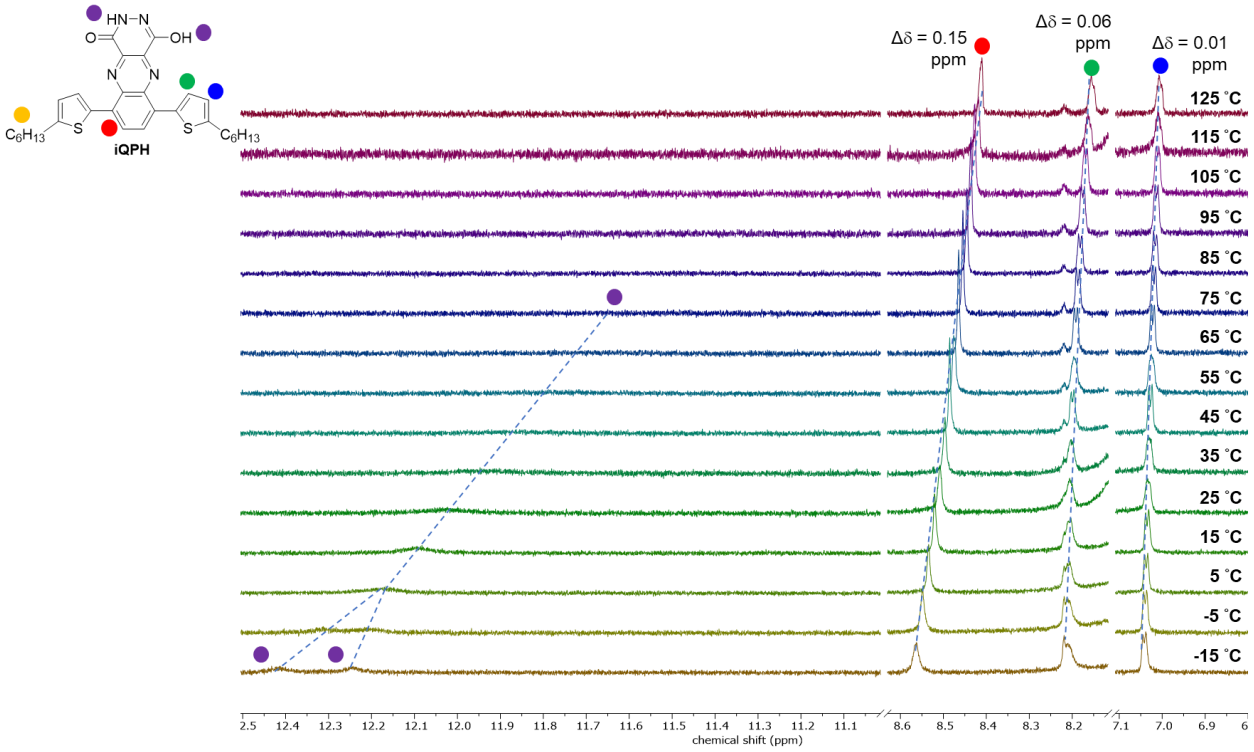

Fig. S50 VT ^{1}H NMR of **iQPH** (450 μM) in DMF-d_7.

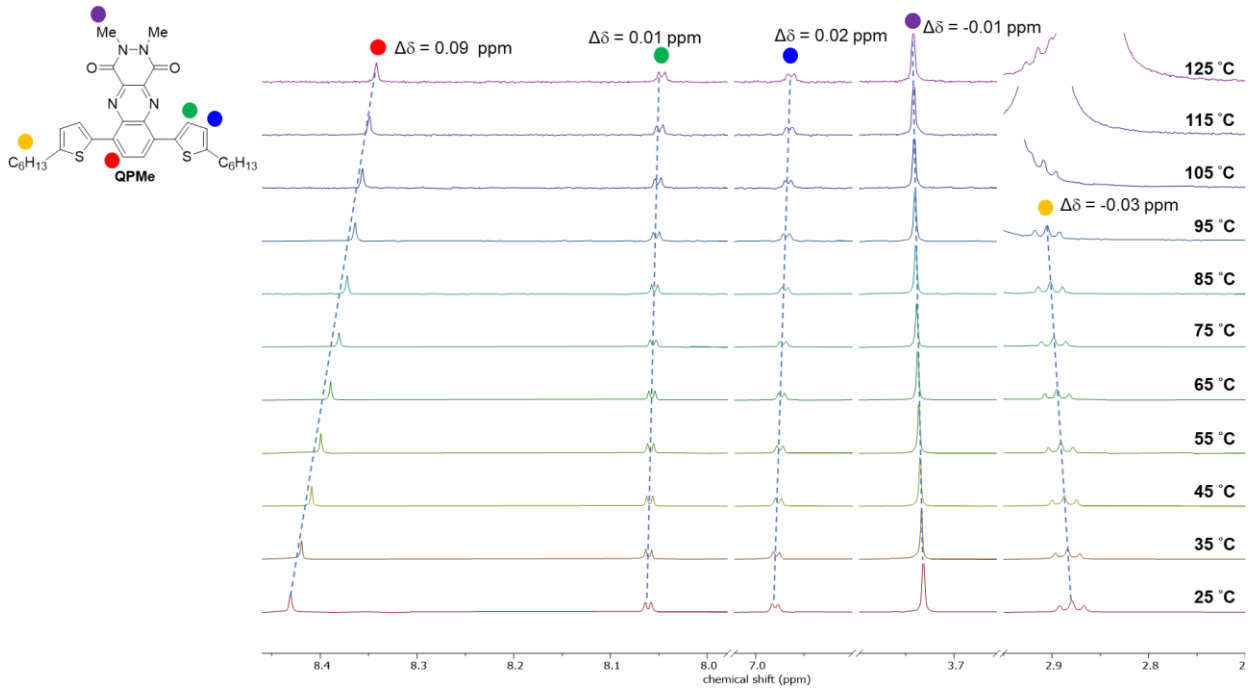

Fig. S51 VT ^{1}H NMR of **QPMe** (450 μM) in DMSO-d_6.

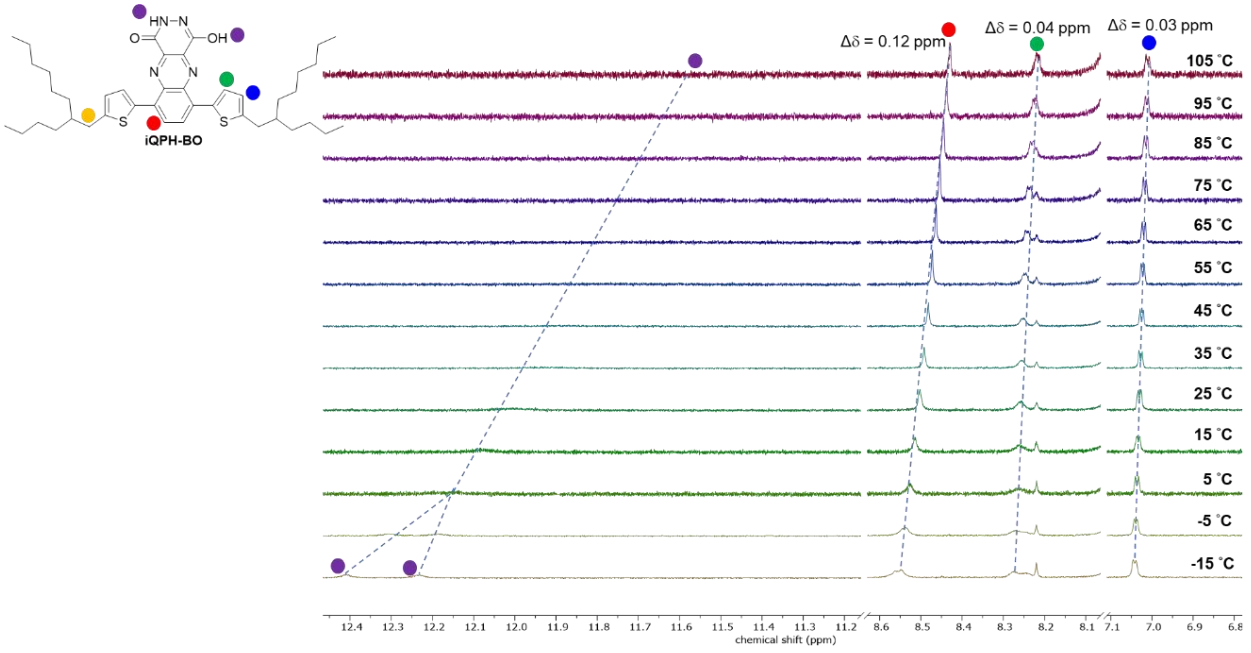

Fig. S52 VT ^{1}H NMR of **iQPH-BO** (450 μM) in DMF-d_7.

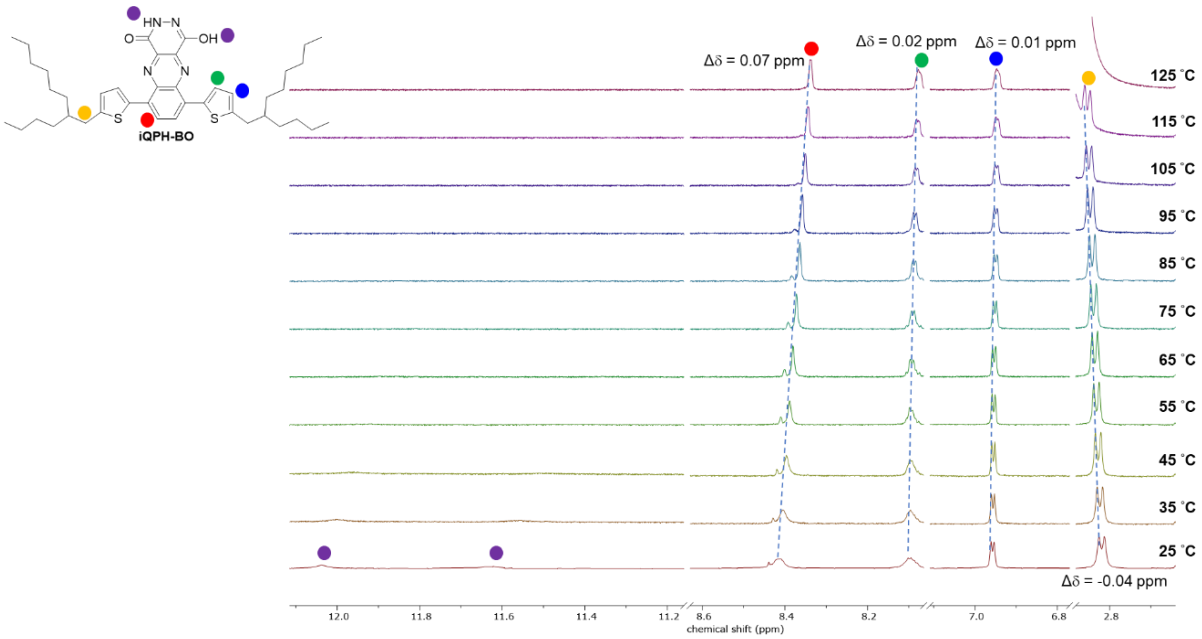

Fig. S53 VT ^{1}H NMR of **iQPH-BO** (450 μM) in DMSO-d_6.

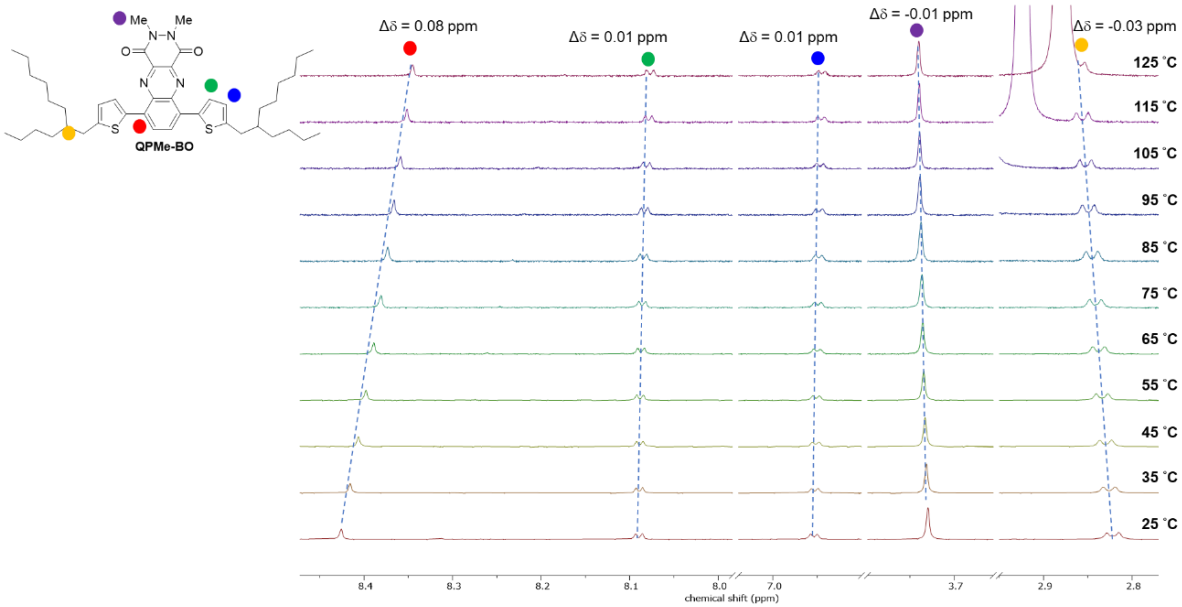

Fig. S54 VT ^{1}H NMR of **QPMe-BO** (450 μM) in DMSO-d_6.

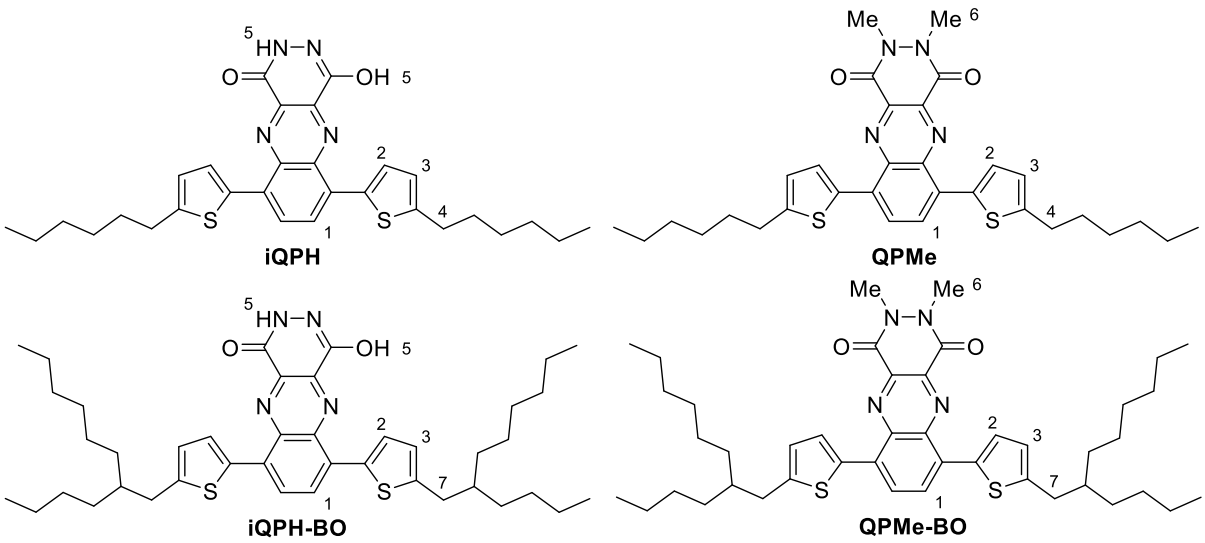

Fig. S55 Numbering system of **iQPH**, **iQPH-BO**, **QPMe**, and **QPMe-BO** for Table S6 and Table S7.

Table S6 Summary of the chemical shift changes for protons of interest in **iQPH** and **iQPH-BO** during VT experiments in different deuterated solvents.

	Range	H5 (NH/OH)	H1 (aromatic)	H2 (aromatic)	H3 (aromatic)	H4/H7 (aliphatic)
$CDCl_3$ (0.45 mM)						
iQPH	-5 – 55 °C	N/A	0.02	0.08	-0.01	-0.03
iQPH-BO	-35 – 55 °C	decoalesce	0.04	0.29	-0.02	-0.04
DMSO-d_6 (0.45 mM)						
iQPH	25 – 125 °C	N/A	0.08	0.02	0.02	-0.02[a]
iQPH-BO	25 – 125 °C	N/A	0.07	0.02	0.01	-0.04[b]
DMF-d_7 (0.45 mM)						
iQPH	15 – 125 °C	decoalesce	0.15	0.06	0.01	N/A
iQPH-BO	-35 – 115 °C	decoalesce	0.12	0.04	0.03	N/A

[a] Difference of chemical shift is from 105 to 75 °C because the solvent peak is too broad and weak in low temperature. [b] The difference of chemical shift is from 15 to -35 °C because the solvent peak overlaps with this peak. [c] N/A means the peaks are too broad or weak to be observed or are overlapped by the solvent peaks.

Table S7 Summary of the chemical shift changes in the protons of interest in **QPMe** and **QPMe-BO** during VT experiments in different deuterated solvents.

	Range	H1 (aromatic)	H2 (aromatic)	H3 (aromatic)	H6 (methyl)	H4/H7 (aliphatic)
$CDCl_3$ (0.45 mM)						
QPMe	-35 – 55 °C	0.07	-0.15	-0.01	0.07	-0.03
QPMe-BO	-35 – 55 °C	0.06	-0.45	-0.02	0.07	-0.04
DMSO-d_6 (0.45 mM)						
QPMe	25 – 125 °C	0.09	0.01	0.02	-0.01	-0.03
QPMe-BO	25 – 125 °C	0.08	0.01	0.01	-0.01	-0.03

Thermal Analysis

Thermogravimetric analysis (TGA) was performed on a TA Instruments Q5500. Samples (ca. 4 mg) were placed on a platinum pan and heated to 600 °C under 10 mL/min nitrogen flow at a variety of ramp rates and analyzed on Universal Analysis 2000 4.4A software. This technique was used to determine mass loss as a function of temperature. The thermal stabilities of quinoxaline-based compounds were assessed using TGA. The decomposition profiles are shown in Fig. S56, all the H-bonding capable and incapable compounds show good thermal stabilities with high decomposition temperatures (5% weight loss) above 350 °C.

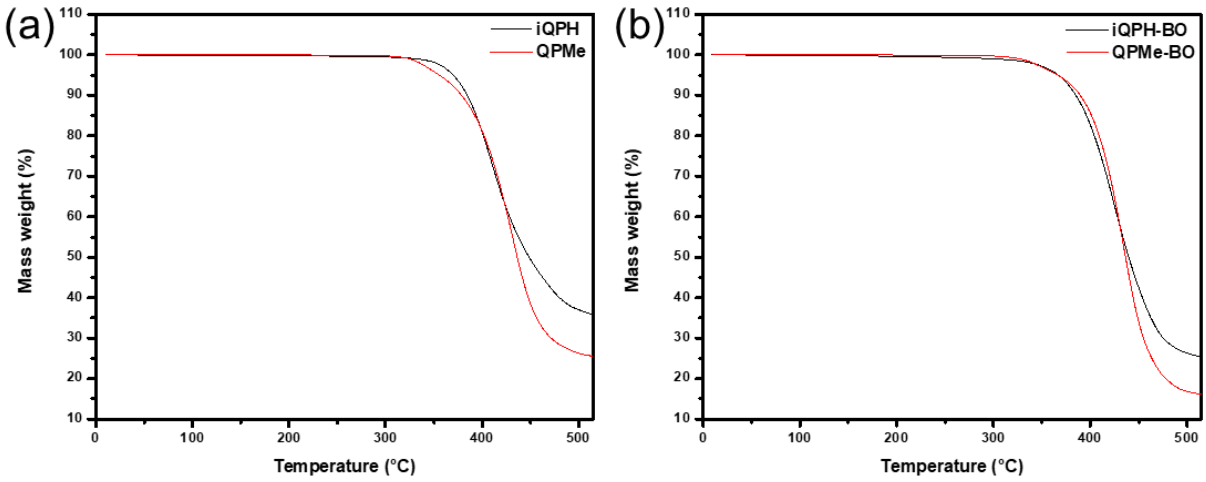

Fig. S56 (a) TGA of **iQPH** and **QPMe**, and (b) TGA of **iQPH-BO** and **QPMe-BO** under nitrogen atmosphere.

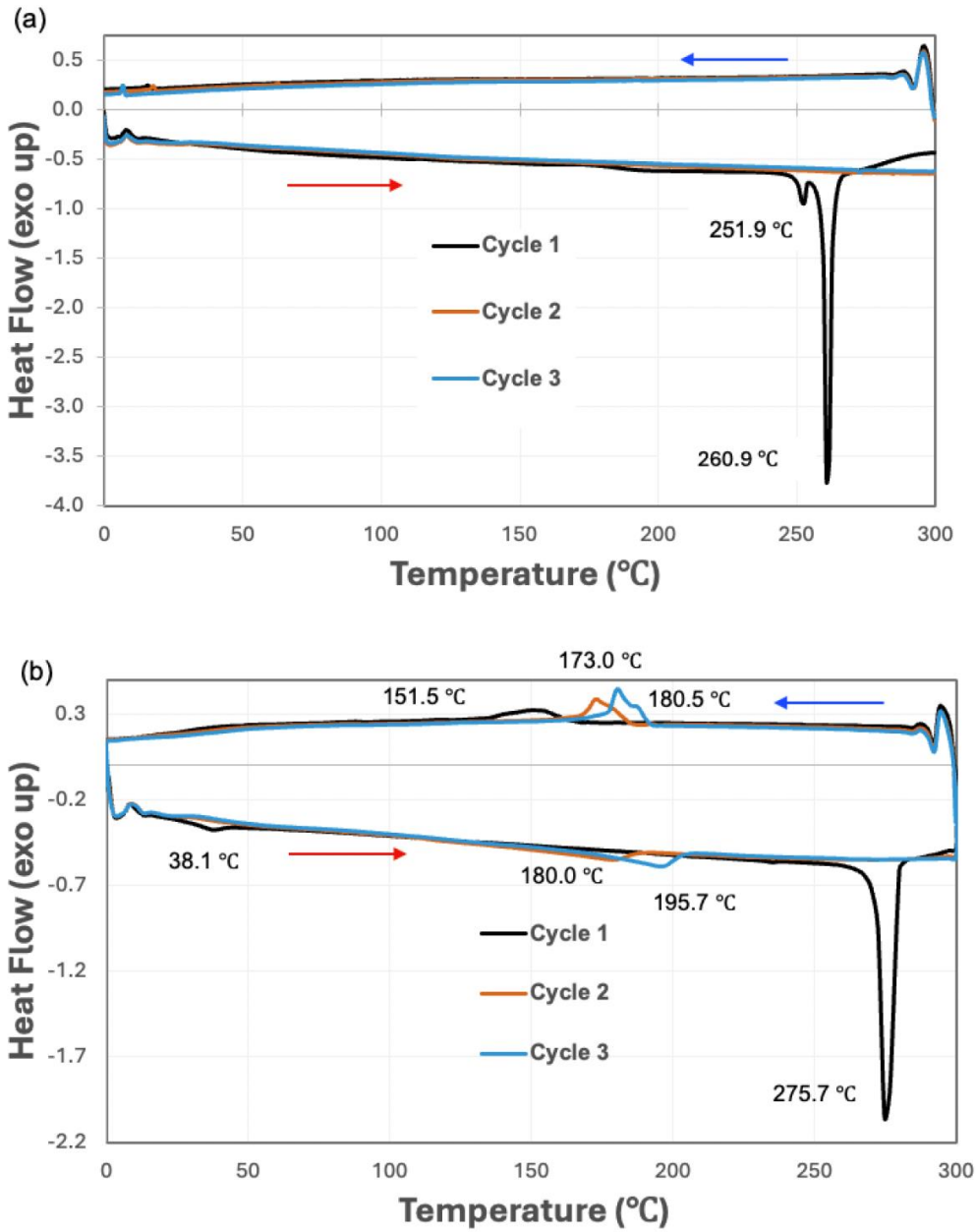

Fig. S57 Differential scanning calorimetry (DSC) data for (a) **iQPH** and (b) **QPMe**. Red arrows denote the heating direction and the blue arrows denote the cooling direction of the three cycles. 3.2 mg of each material was used and the temperature was cycled at 10°/min. The labeled temperatures correspond to major exothermic or endothermic events (crystallization and melting).

Electrochemical Analysis

Cyclic voltammetry experiments were performed in a custom gas-tight 3-electrode setup inside a N_2-filled dry box with a vitreous carbon working electrode (3 mm diameter, area = 0.071 cm^2), Ag|AgNO3

reference electrode (10 mM $AgNO_3$ in 100 mM Bu_4NPF_6 MeCN solution), and a Pt coil counter electrode with a Princeton Applied Research Versastat II potentiostat. Potentials were ultimately referenced using a ferrocene (Fc) pseudo-reference as an internal standard. The working electrode was polished using the BASi PK-4 electrode polishing kit prior to use and cycled in fresh electrolyte solution 10 times at 500 mV/s.

Table S8 Electrochemical data for **iQPH-BO** and **QPMe-BO**.

	$E_{ox\text{-}onset}$ (V)[a]	$E_{red\text{-}onset}$ (V)[a]	$\Delta E_{g\text{-}echem}$ (eV)[a]	E_{HOMO} (eV)[b]	E_{LUMO} (eV)[b]
iQPH-BO	0.605	-1.172	1.78	-5.71	-3.93
QPMe-BO	0.679	-1.341	2.02	-5.78	-3.76

[a] Oxidation ($E_{ox\text{-}onset}$) and reduction ($E_{red\text{-}onset}$) potentials are reported vs. Fc/Fc+. [b] HOMO and LUMO levels were calculated from $E_{ox\text{-}onset}$ and $E_{red\text{-}onset}$, respectively, considering that Fc/Fc^+ is 5.1 eV relative to vacuum.

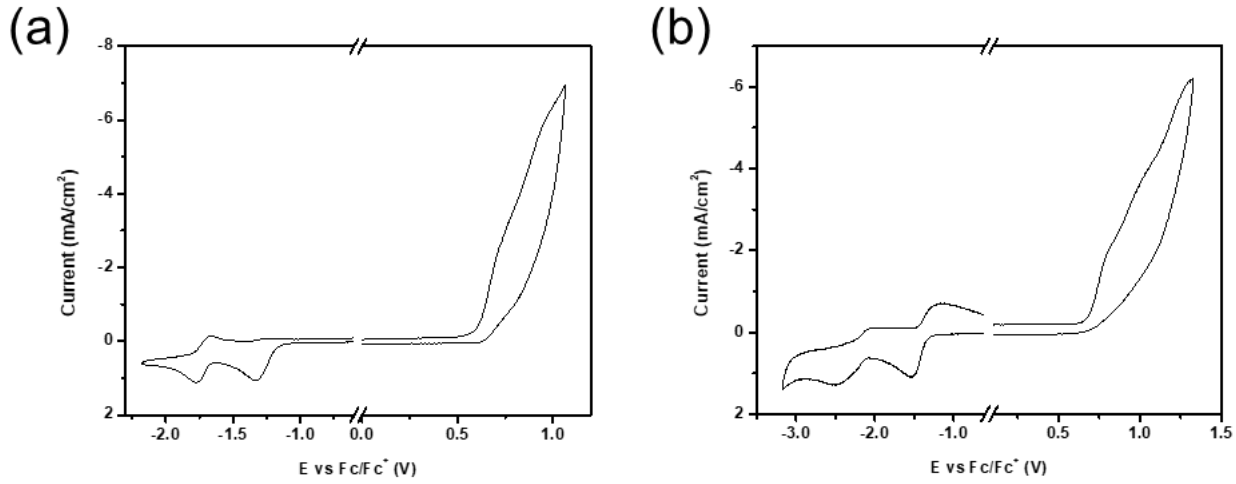

Fig. S58 CV scans of (a) **iQPH-BO** and (b) **QPMe-BO** in THF.

Table S9 Optical and electrochemical data for **iQPH-BO** and **QPMe-BO**.

	UV-vis (chloroform)			UV-vis (neat films)			CV (THF)			DFT calculation		
	$\lambda_{max,vis}$ [nm]	λ_{onset} [nm]	$E_{g,opt}$ [eV]	$\lambda_{max,vis}$ [nm]	λ_{onset} [nm]	$E_{g,opt}$ [eV]	HOMO [eV]	LUMO [eV]	$E_{g,echem}$ [eV]	HOMO [eV]	LUMO [eV]	$E_{g\text{-}calcd}$ [eV]
iQPH-BO	581	663	1.87	559	701	1.77	-5.71	-3.93	1.78	-5.48	-3.15	2.33
QPMe-BO	563	639	1.94	520	639	1.94	-5.78	-3.76	2.02	-5.42	-3.01	2.41

Single crystal X-ray structure

X-ray intensity data were collected at 100 K on a Bruker DUO diffractometer using MoKα radiation (l = 0.71073 Å) and an APEXII CCD area detector. Raw data frames were read by the program SAINT1 and integrated using 3D profiling algorithms. The resulting data were reduced to produce hkl reflections and their intensities and estimated standard deviations. The data were corrected for Lorentz and polarization effects and numerical absorption corrections were applied based on indexed and measured faces. The structure was solved and refined in SHELXTL2014, using full-matrix least-squares refinement. The non-H atoms were refined with anisotropic thermal parameters and all the H atoms were calculated in idealized positions and refined riding on their parent atoms. The molecule has its end thiophene disordered and refined in two parts. Their geometries are kept similar using several SADI commands. Their SOF were fixed at 0.82 and 0.18 in the final cycles of refinements. In the final cycle of refinement, 4153 reflections (of which 3443 are observed with $I > 2\sigma(I)$) were used to refine 217 parameters, and the resulting R1, wR2, and S (goodness of fit) were 5.19%, 10.03% and 1.084, respectively. The refinement was carried out by 23 minimizing the wR2 function using F2 rather than F values. R1 is calculated to provide a reference to the conventional R value but its function is not minimized.

Identification code	**iQPH**
Empirical formula	C_{33} H_{41} N_5 O_3 S_2
Formula weight	619.83 g/mol
Temperature	100(2) K
Wavelength	0.71073 Å
Crystal system	Monoclinic
Space group	C2/c
Unit cell dimensions	a = 33.974(8) Å; α= 90°, b = 5.0398(10) Å; β= 104.711(5)°, c = 38.358(9) Å, γ = 90°.
Volume	6352(2) $Å^3$
Z	8
Density (calculated)	1.296 g/cm^3
Absorption coefficient	0.210 mm^{-1}
F(000)	2640
Crystal size	0.384 x 0.196 x 0.118 mm^3
Theta range for data collection	1.853 to 27.499°.
Index ranges	$-44 \leq h \leq 44$, $-6 \leq k \leq 6$, $-49 \leq l \leq 49$
Reflections collected	93508
Independent reflections	7310 [R(int) = 0.0327]
Absorption correction	Multi-scan
Refinement method	Full-matrix least-squares on F2

Table S10 Atomic coordinates and equivalent isotropic displacement parameters for **iQPH**. U(eq) is defined as one third of the trace of the orthogonalized Uij tensor.

	x	y	z	U(eq)

S1	8108(1)	9827(1)	5780(1)	41(1)
S2	6385(1)-	1921(1)	5446(1)	38(1)
O1	7671(1)	3612(2)	7165(1)	44(1)
O2	6574(1)-	3213(2)	6386(1)	43(1)
O3	6304(1)	-6582(3)	6787(1)	57(1)
N1	7474(1)	4073(3)	6410(1)	37(1)
N2	6906(1)	403(3)	6020(1)	37(1)
N3	7237(1)	140(3)	7108(1)	40(1)
N4	6952(1)	-1676(3)	6927(1)	40(1)
N5	6347(1)	-8181(3)	7346(1)	49(1)
C1	7083(1)	2176(3)	5848(1)	36(1)
C2	6974(1)	2089(3)	5460(1)	37(1)
C3	7167(1)	3901(3)	5290(1)	39(1)
C4	7450(1)	5755(3)	5482(1)	39(1)
C5	7563(1)	5926(3)	5854(1)	36(1)
C6	7373(1)	4069(3)	6045(1)	36(1)
C7	7867(1)	7858(3)	6038(1)	37(1)
C8	8026(1)	8440(3)	6397(1)	39(1)
C9	8327(1)	10440(4)	6458(1)	43(1)
C10	8413(1)	11379(3)	6152(1)	40(1)
C11	8716(1)	13431(4)	6107(1)	44(1)
C12	8992(1)	14424(4)	6461(1)	48(1)
C13	9307(1)	16405(4)	6401(1)	59(1)
C14	9586(3)	17381(19)	6775(3)	58(2)
C15	9947(3)	19010(20)	6732(4)	91(2)
C16	10203(3)	20080(30)	7083(5)	137(5)
C14'	9613(7)	17490(40)	6656(7)	67(4)
C15'	9892(4)	19450(30)	6565(8)	75(5)
C16'	10227(4)	20500(30)	6882(10)	112(9)
C17	6676(1)	207(3)	5256(1)	37(1)
C18	6570(1)	-109(3)	4886(1)	41(1)
C19	6258(1)	-1991(3)	4759(1)	41(1)
C20	6124(1)	-3142(3)	5032(1)	39(1)
C21	5804(1)	-5219(3)	5013(1)	41(1)
C22	5548(1)	-5885(4)	4635(1)	44(1)
C23	5217(1)	-7891(4)	4650(1)	43(1)
C24	4927(1)	-8578(4)	4286(1)	50(1)
C25	4601(1)	-10554(4)	4322(1)	53(1)
C26	4294(1)	-11200(5)	3967(1)	68(1)
C27	7302(1)	2264(3)	6572(1)	37(1)
C28	7015(1)	424(3)	6379(1)	36(1)
C29	7422(1)	2119(3)	6972(1)	38(1)
C30	6845(1)	-1527(3)	6578(1)	39(1)
C31	6448(1)	-6497(6)	7109(1)	45(1)
C32	6029(1)	-10161(6)	7201(1)	55(1)
C33	6511(1)	-7983(7)	7720(1)	53(1)
C31'	6230(2)	-8348(11)	7014(2)	49(1)
C32'	6283(2)	-10342(14)	7598(2)	59(2)
C33'	6672(2)	-6254(12)	7548(2)	53(1)

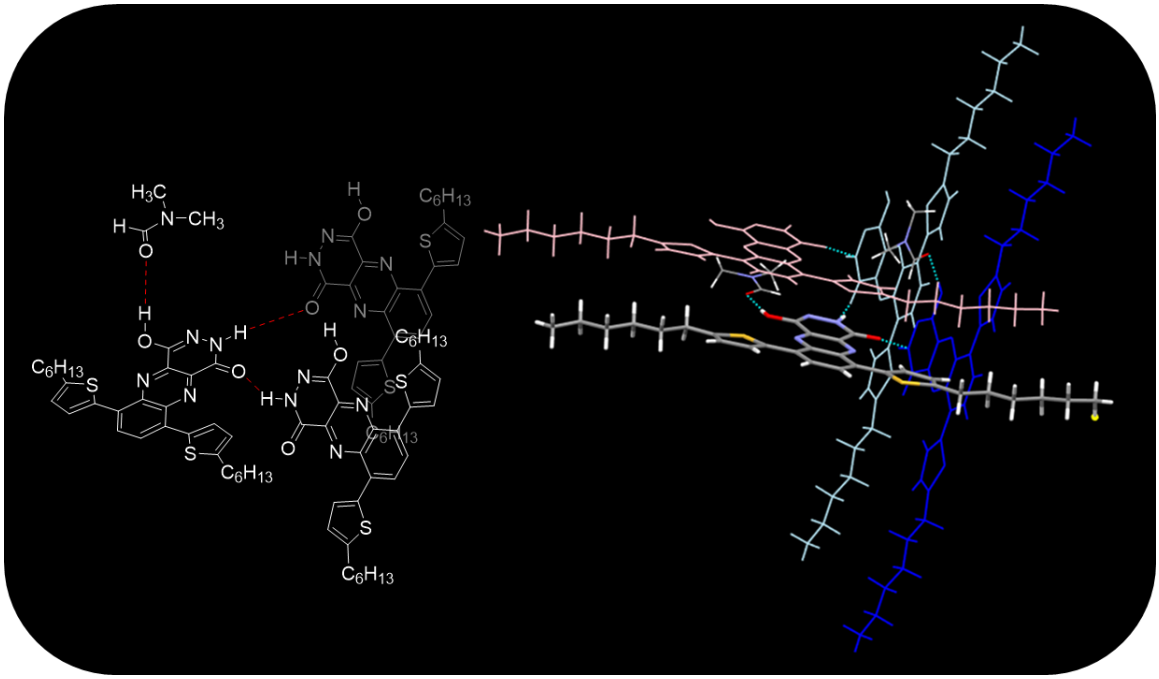

Fig. S59 X-ray structure analysis of H-bonding interactions between **iQPH** molecules and DMF.

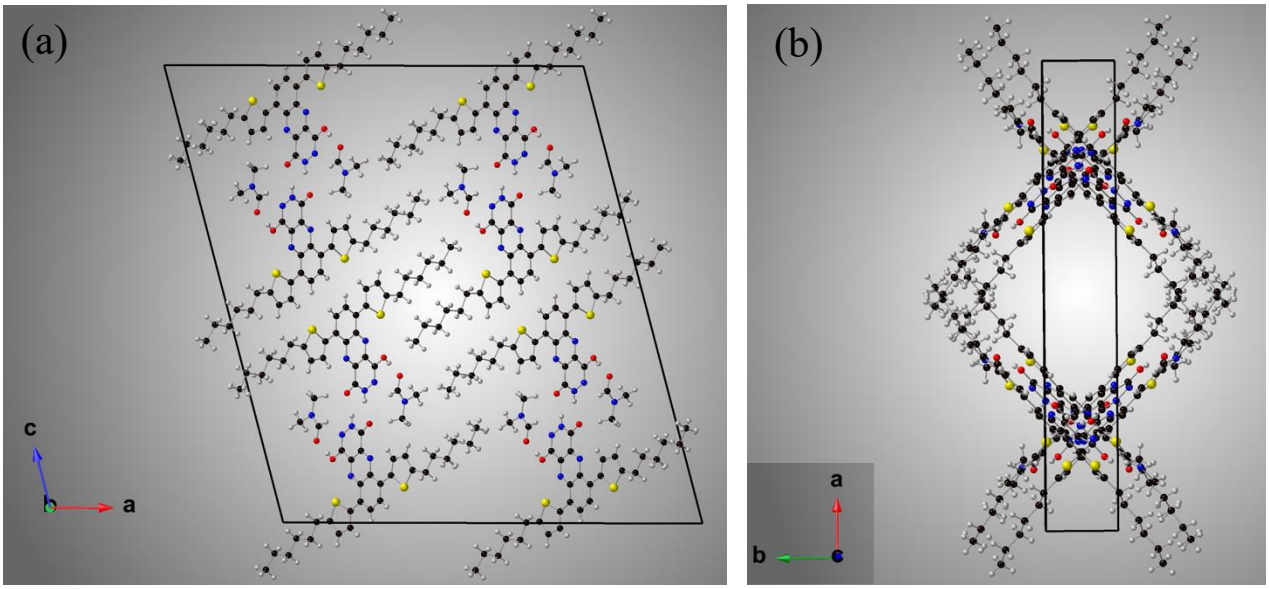

Fig. S60 Views of the **iQPH**-DMF unit cell. (a) Views along the (010) and (b) the (001).

UV-vis Spectra with H-bonding Competitive Solvent

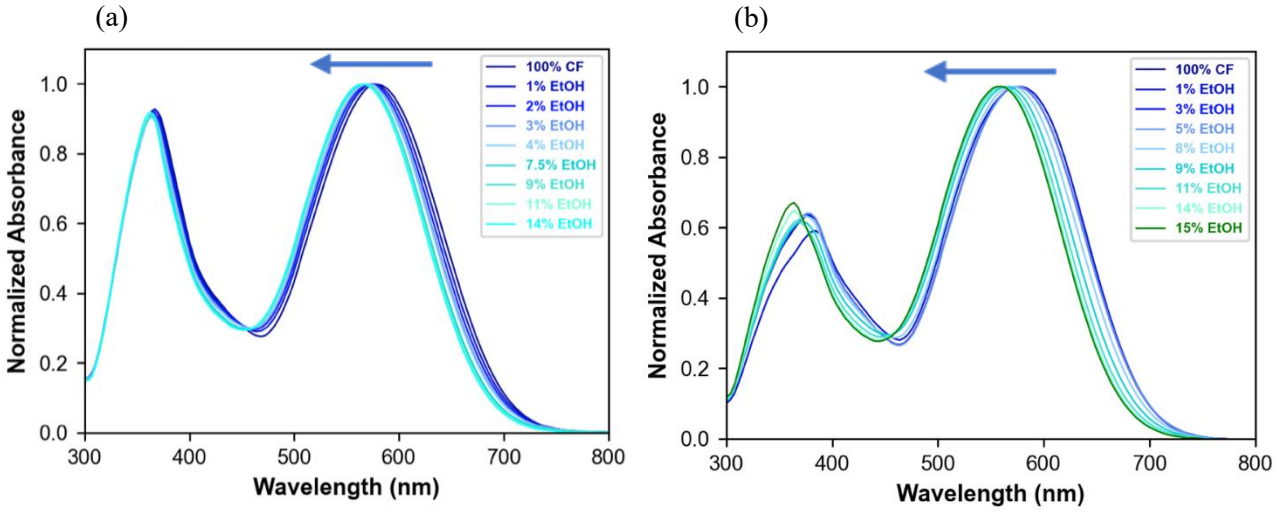

Fig. S61 UV-vis absorbance spectra of (a) **iQPH-BO** and (b) **iQPH** in chloroform with increasing volume percentage of ethanol (EtOH).

Wavelength-Dependent Photoluminescence Spectroscopy

Photoluminescence spectra was measured with a Jasco FP-6500 spectrofluorometer with entrance and exit slits set to 5 nm resolution and scan rate equal to 1000 nm/min.

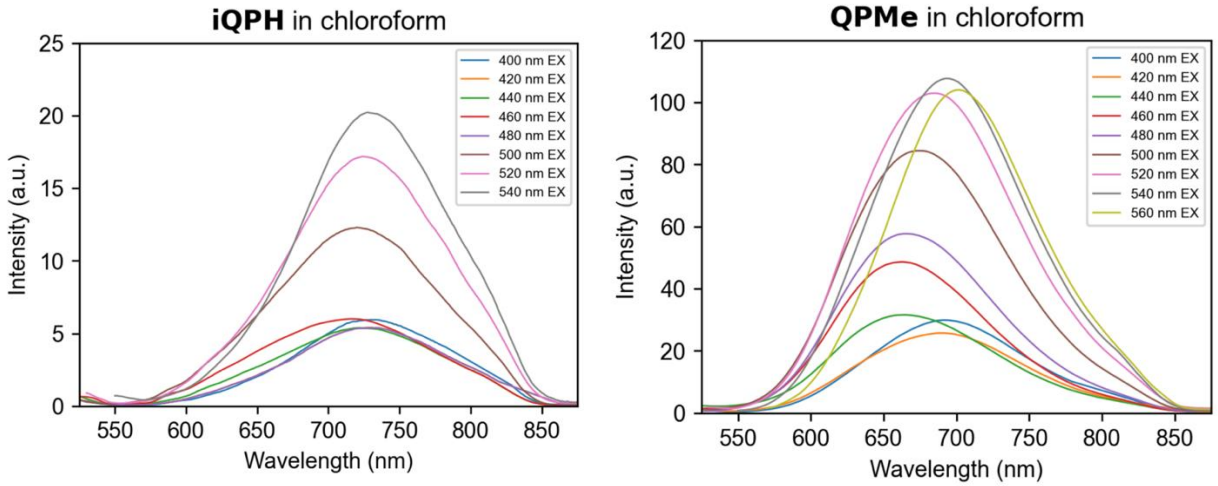

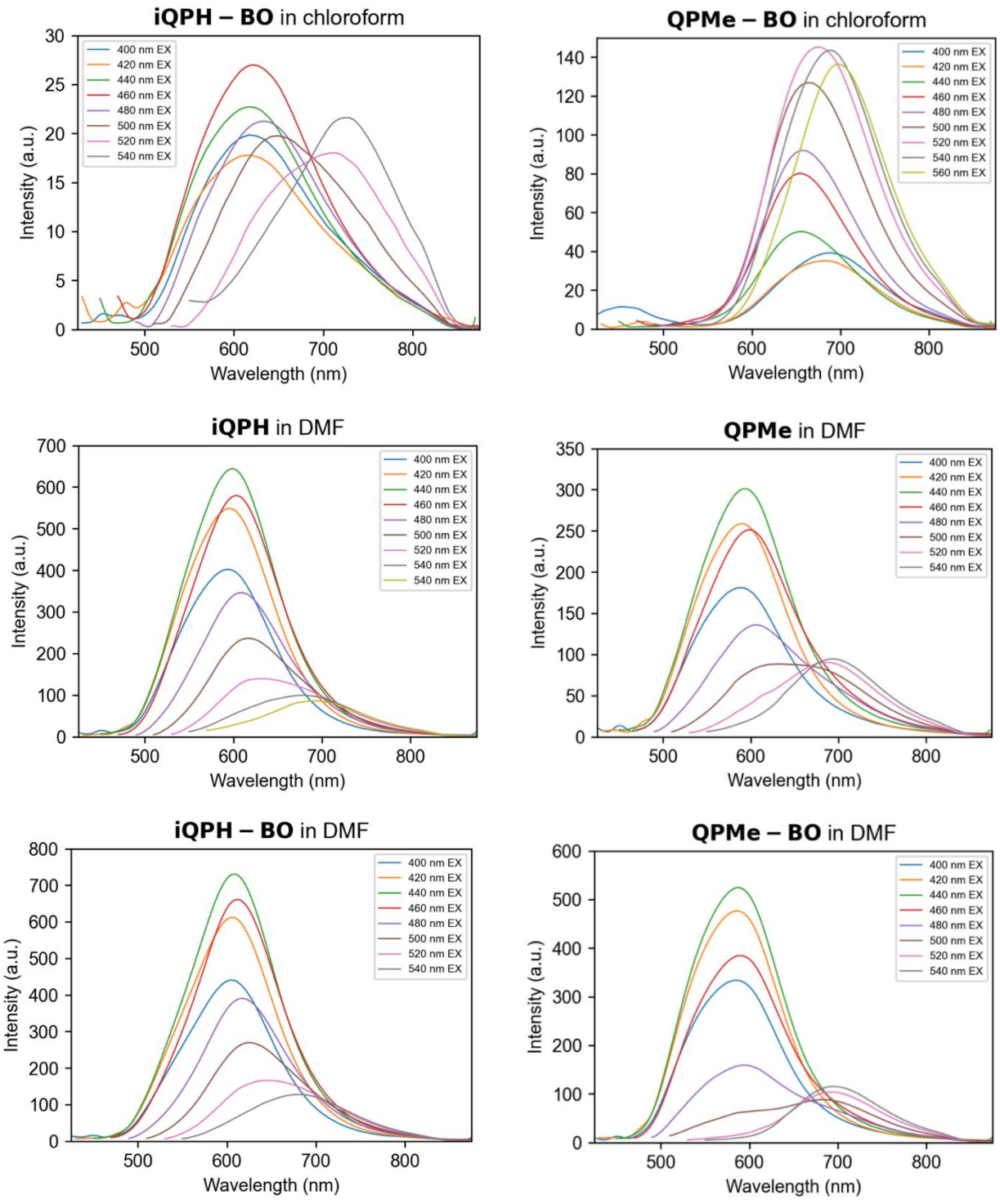

Fig. S62 Raw PL intensity of **iQPH**, **iQPH-BO**, **QPMe**, and **QPMe-BO** in chloroform and DMF at different excitation wavelengths.

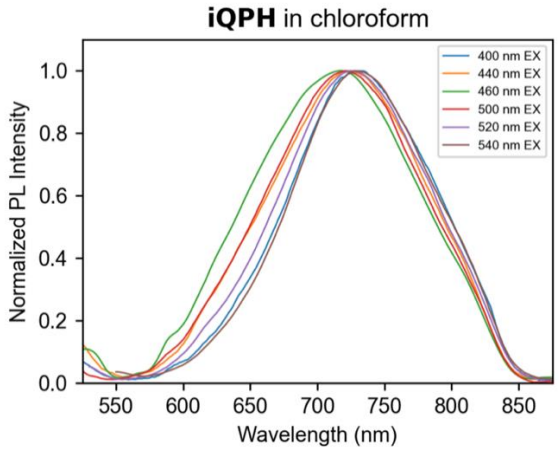
iQPH in chloroform
Normalized PL Intensity
Wavelength (nm)
400 nm EX
440 nm EX
460 nm EX
500 nm EX
520 nm EX
540 nm EX

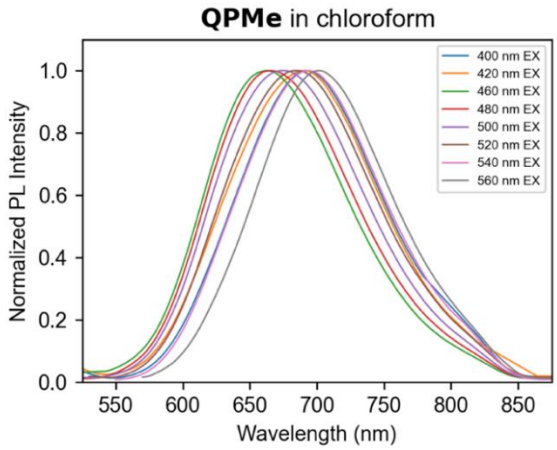
QPMe in chloroform
Normalized PL Intensity
Wavelength (nm)
400 nm EX
420 nm EX
460 nm EX
480 nm EX
500 nm EX
520 nm EX
540 nm EX
560 nm EX

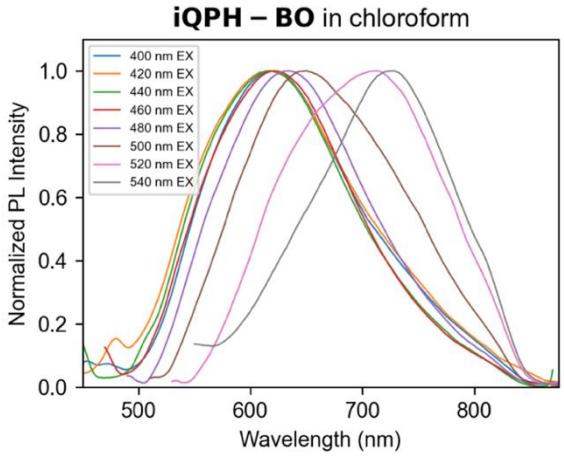
iQPH – BO in chloroform
Normalized PL Intensity
Wavelength (nm)
400 nm EX
420 nm EX
440 nm EX
460 nm EX
480 nm EX
500 nm EX
520 nm EX
540 nm EX

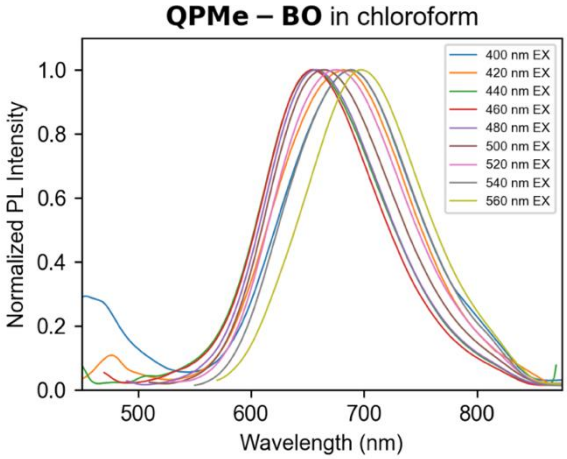
QPMe – BO in chloroform
Normalized PL Intensity
Wavelength (nm)
400 nm EX
420 nm EX
440 nm EX
460 nm EX
480 nm EX
500 nm EX
520 nm EX
540 nm EX
560 nm EX

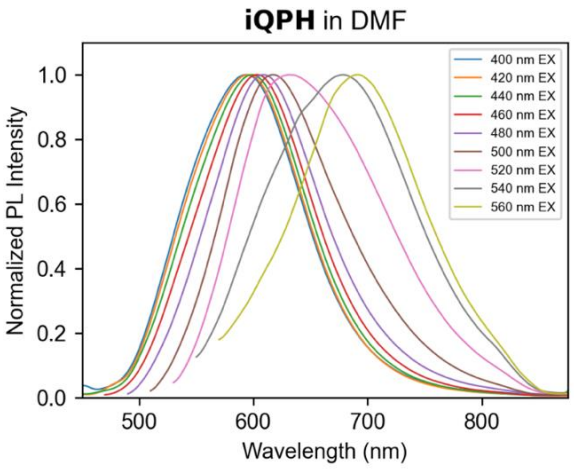
iQPH in DMF
Normalized PL Intensity
Wavelength (nm)
400 nm EX
420 nm EX
440 nm EX
460 nm EX
480 nm EX
500 nm EX
520 nm EX
540 nm EX
560 nm EX

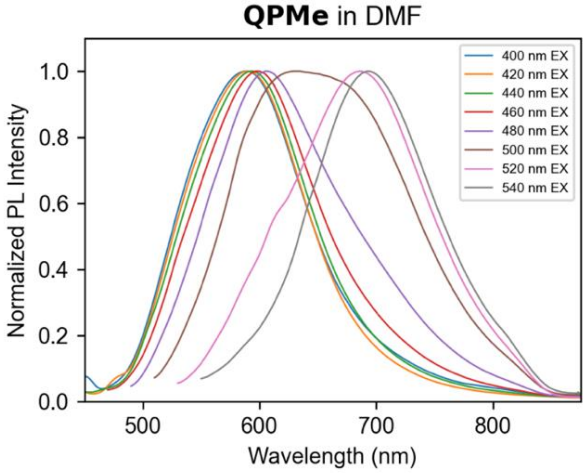
QPMe in DMF
Normalized PL Intensity
Wavelength (nm)
400 nm EX
420 nm EX
440 nm EX
460 nm EX
480 nm EX
500 nm EX
520 nm EX
540 nm EX

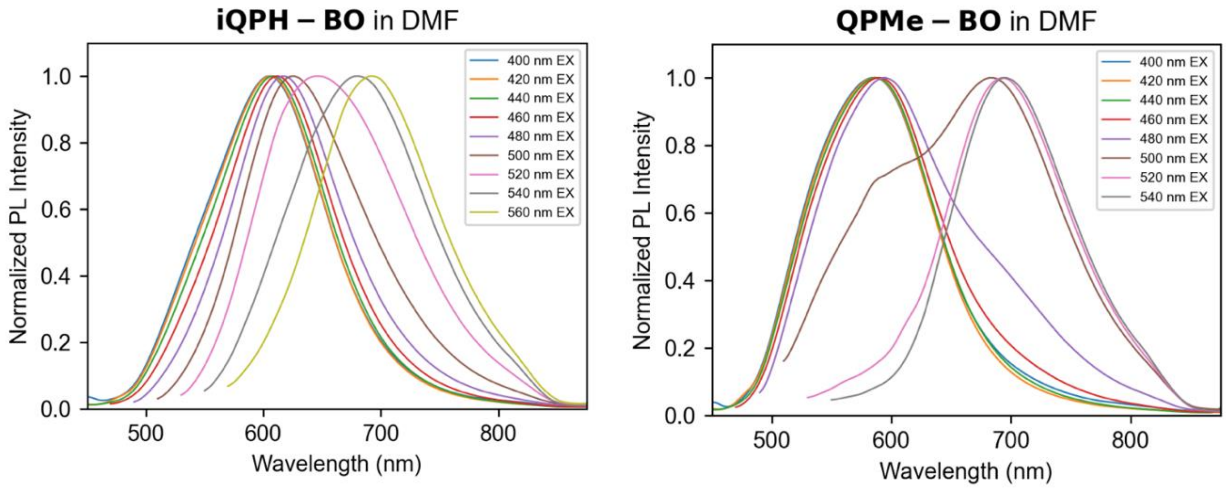

Fig. S63 Normalized PL intensity of **iQPH**, **iQPH-BO**, **QPMe**, and **QPMe-BO** in chloroform and DMF at different excitation wavelengths.

Thin-Film Fabrication

Thin films were fabricated inside a glovebox with a nitrogen environment, using a spin coating process. The investigated compounds (**iQPH-BO** and **QPMe-BO**) were taken in their powder form and dissolved in chlorobenzene and/or chloroform with concentrations of 10-20 mg/mL. They were dynamically casted with a spin speed of 600 rpm for 45 s on glass substrates. Thermal annealing experiments were carried out for some samples by placing them on a hot plate held at 90 °C-200 °C for specified intervals.

Thin-Film Optical Absorption

A 100 W quartz tungsten halogen lamp was used in conjunction with a Cornerstone 260 1/4 m monochromator (Newport 74100) to generate monochromatic light. The incident light was chopped at 480 Hz and recorded with a Newport 818-UV photodetector connected to a current amplifier (Keithley 428) and lock-in amplifier (Stanford Research Systems SR830 DSP). Transmittance and reflectance of thin film samples were measured simultaneously, which were used to calculate the thin-film absorbance. Monochromator slit widths were adjusted to enable 3 nm resolution in spectral measurements.

Grazing-Incidence Wide-Angle X-ray Scattering

All diffraction studies were performed on a Malvern Panalytical's X'Pert Pro MRD system employing the Bragg-Brentano diffraction geometry using a Cu Ka X-ray source. A parabolic mirror forming a quasi-parallel beam was used in conjunction with a 1/2° divergent slit and a 15 mm beam-width mask to inhibit beam spill. Diffraction beam optics consisted of a point detector, a 0.27° parallel plate

collimator, and a 0.1 mm width receiving slit to improve resolution for low 2θ angles. A proportional Xe point detector was used to measure diffracted intensity.

Atomic Force Microscopy

Atomic force microscopy (AFM) was carried out using a Dimension 3100 AFM operated in the tapping mode at 325 kHz. An aluminum coated silicon tip (Umasch HQ:NSC15/AL BS) was utilized for imaging.

Table S11 X-ray diffraction θ-2θ data summary for (a) as-spun **iQPH-BO** films, (b) thermally annealed **iQPH-BO** films, (c) as-spun **QPMe-BO** films, and (d) thermally annealed **QPMe-BO** films obtained through Gaussian peak fitting.

iQPH-BO as-spun

(a)

Peak #	Position (2θ°)	d-spacing (nm)	FWHM (2θ°)
1	1.63	5.42	0.42
2	2.10	4.20	0.21
3	4.06	2.17	0.33
4	21.94	0.40	1.43
5	22.70	0.39	0.55

iQPH-BO annealed

(b)

Peak #	Position (2θ°)	d-spacing (nm)	FWHM (2θ°)
1	1.64	5.38	0.40
2	2.10	4.20	0.21
3	4.05	2.18	0.34
4	21.93	0.40	1.48
5	22.70	0.39	0.55

QPMe-BO as-spun

(c)

Peak #	Position (2θ°)	d-spacing (nm)	FWHM (2θ°)
1	1.65	5.35	0.36
2	2.09	4.21	0.21
3	3.58	2.46	0.35
4	21.90	0.41	1.04
5	22.43	0.40	0.56

QPMe-BO annealed

(d)

Peak #	Position (2θ°)	d-spacing (nm)	FWHM (2θ°)
1	1.65	5.34	0.38
2	2.09	4.22	0.21
3	3.63	2.43	0.35
4	21.55	0.41	1.29
5	22.17	0.40	0.78

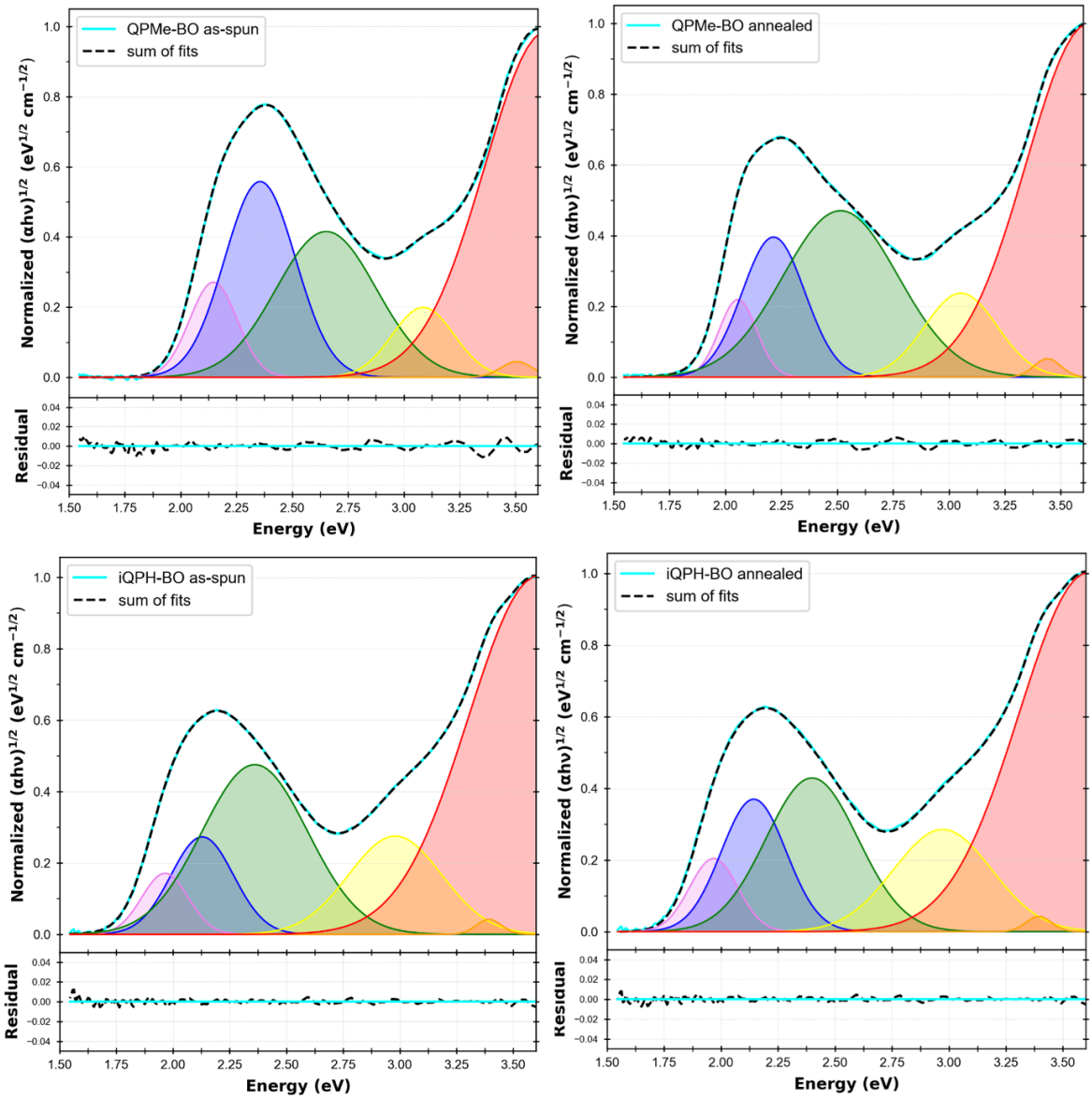

Fig. S64 Gaussian fits to the absorption spectra of (a) as-spun **QPMe-BO** films, (b) annealed **QPMe-BO** films, (c) as-spun **iQPH-BO** films, and (d) annealed **iQPH-BO** films.

^{1}H and ^{13}C NMR Spectra

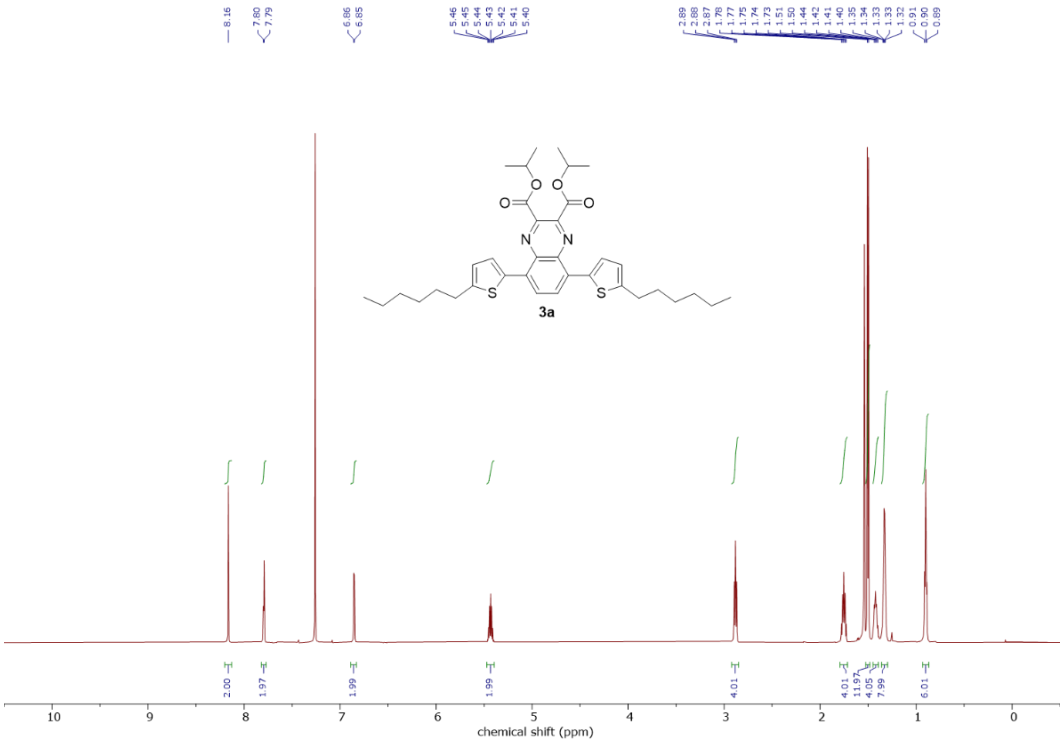

Fig. S65 ^{1}H NMR spectrum of **3a** in $CDCl_3$.

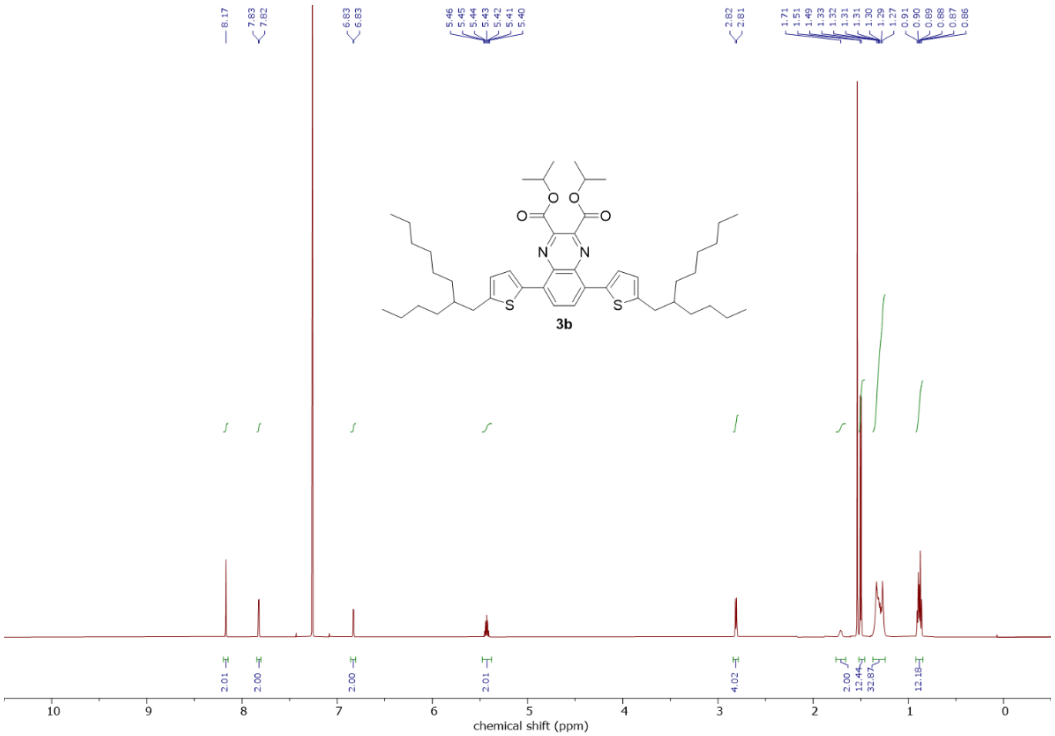

Fig. S66 ^{1}H NMR spectrum of **3b** in $CDCl_3$.

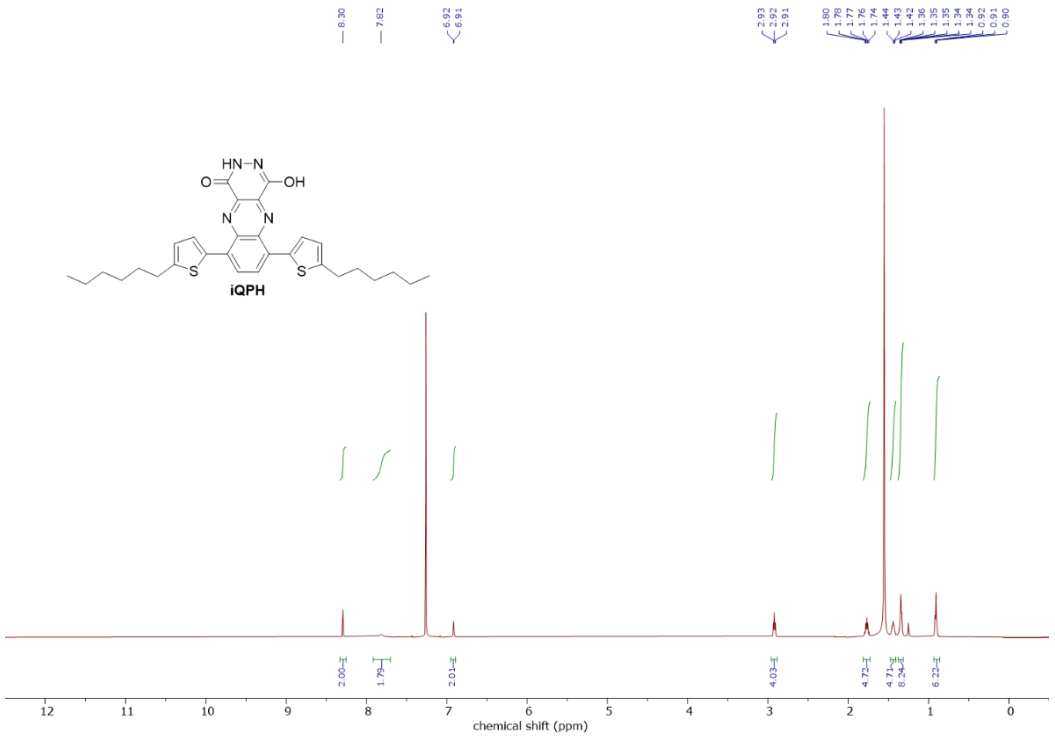

Fig. S67 ^{1}H NMR spectrum of **iQPH** in $CDCl_3$.

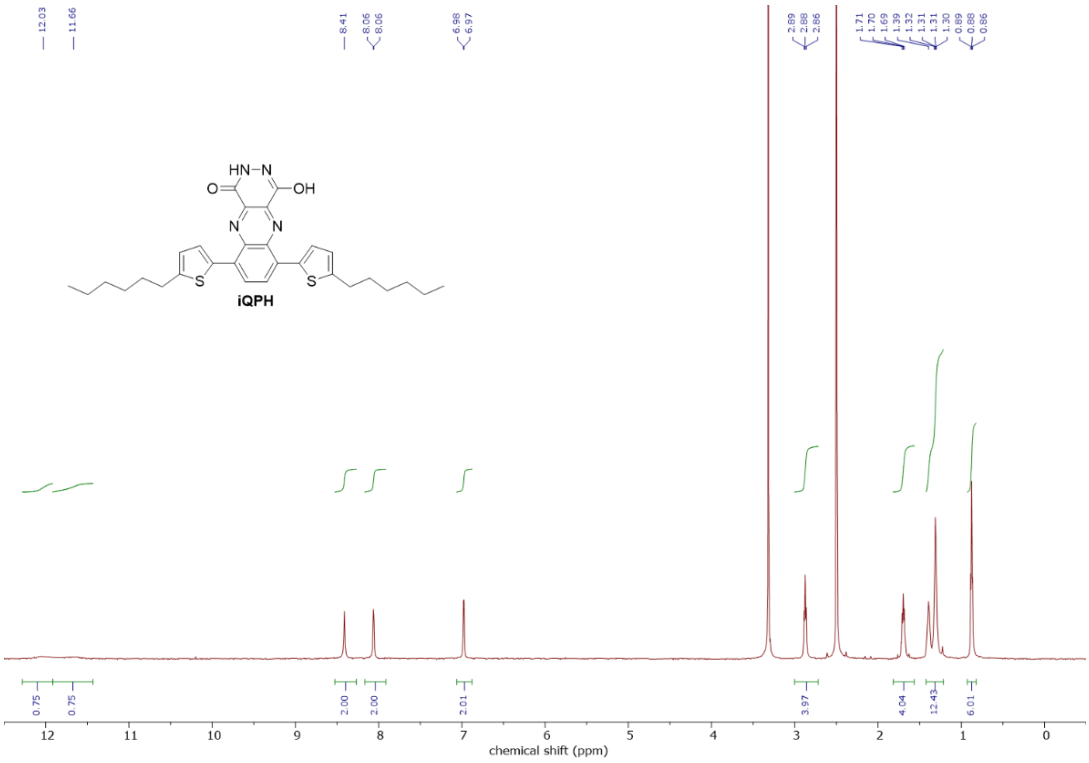

Fig. S68 ^{1}H NMR spectrum of **iQPH** in DMSO-d_6.

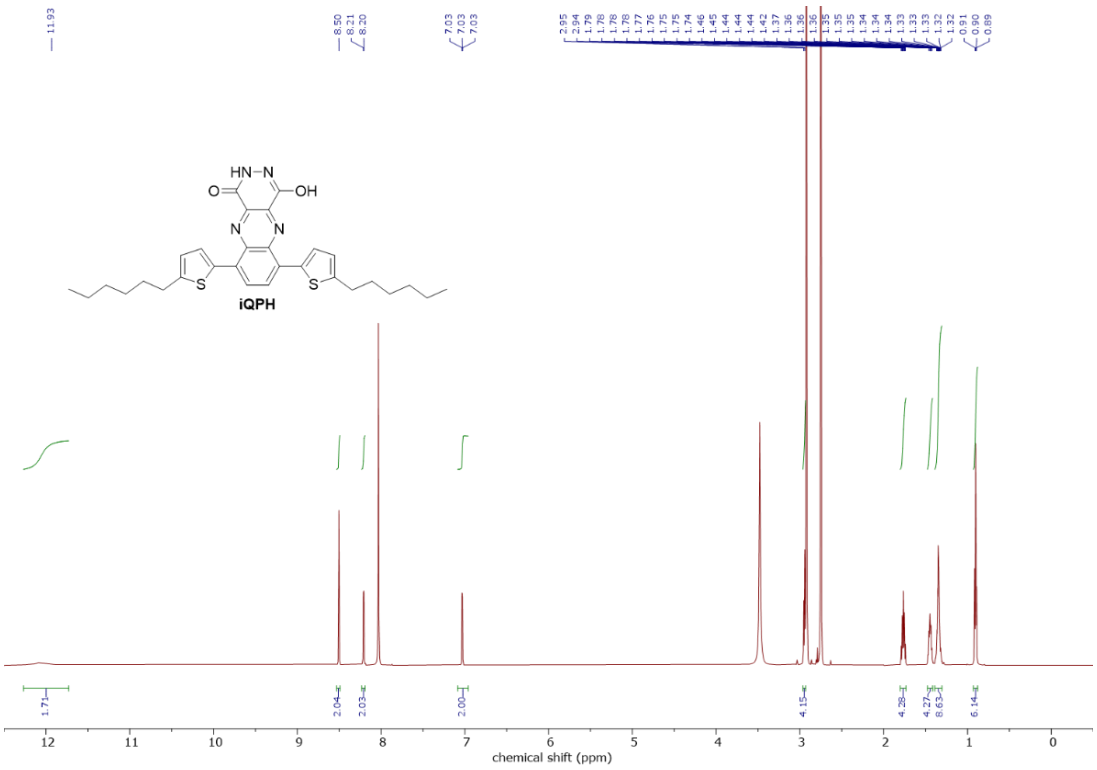

Fig. S69 ^{1}H NMR spectrum of **iQPH** in DMF-d_7.

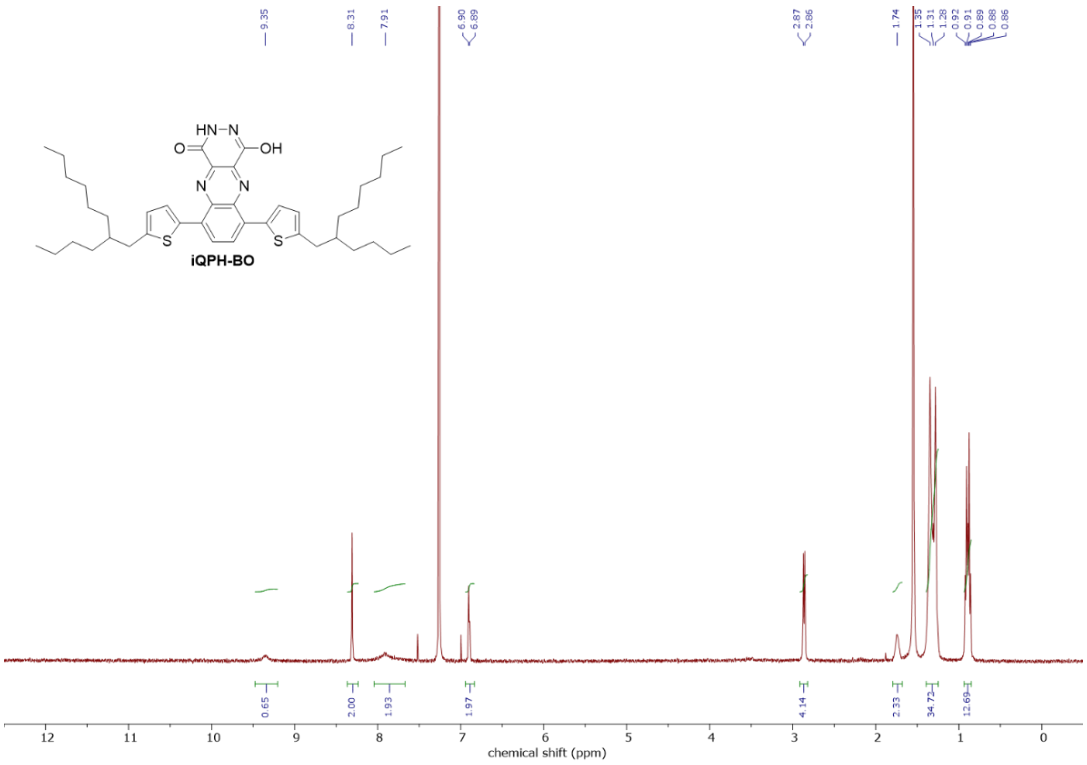

Fig. S70 ^{1}H NMR spectrum of **iQPH-BO** in $CDCl_3$.

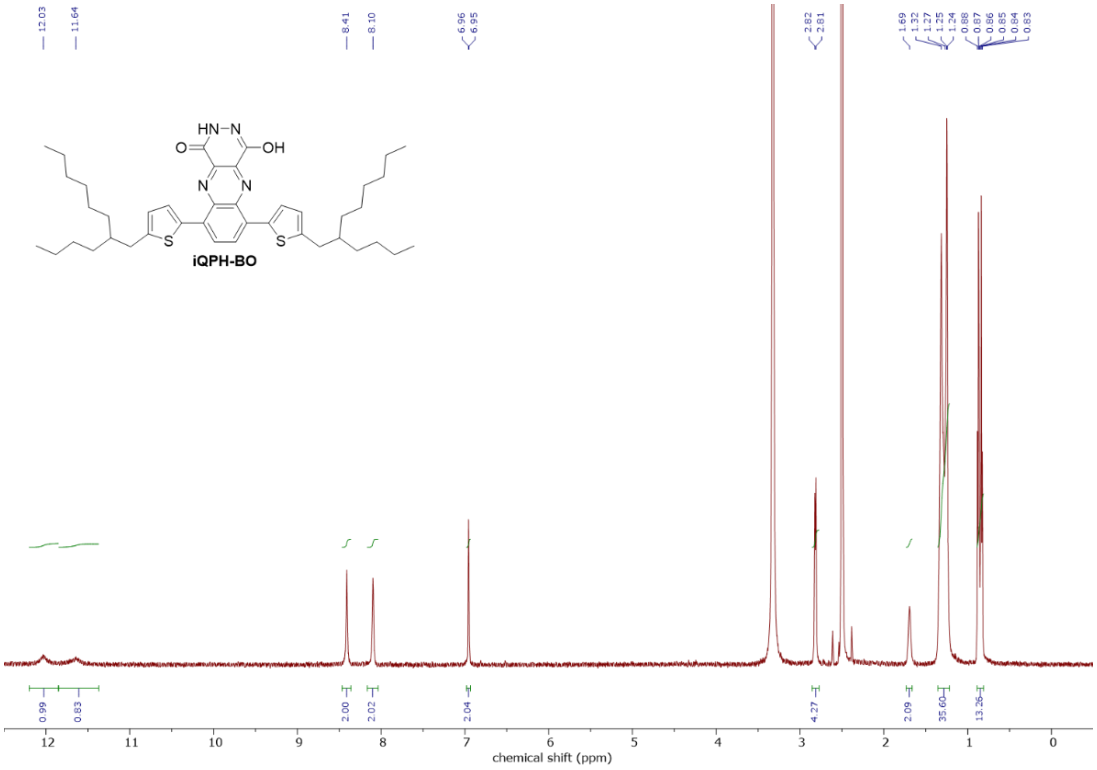

Fig. S71 ^{1}H NMR spectrum of **iQPH-BO** in DMSO-d_6.

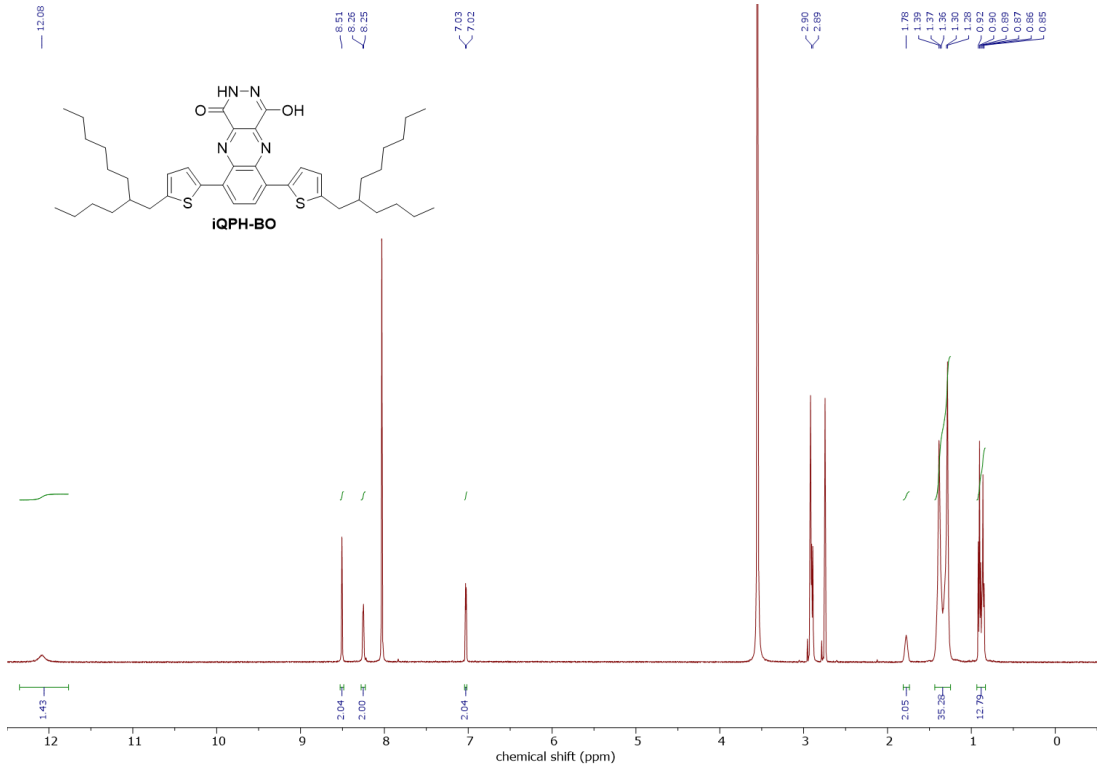

Fig. S72 ^{1}H NMR spectrum of **iQPH-BO** in DMF-d_7.

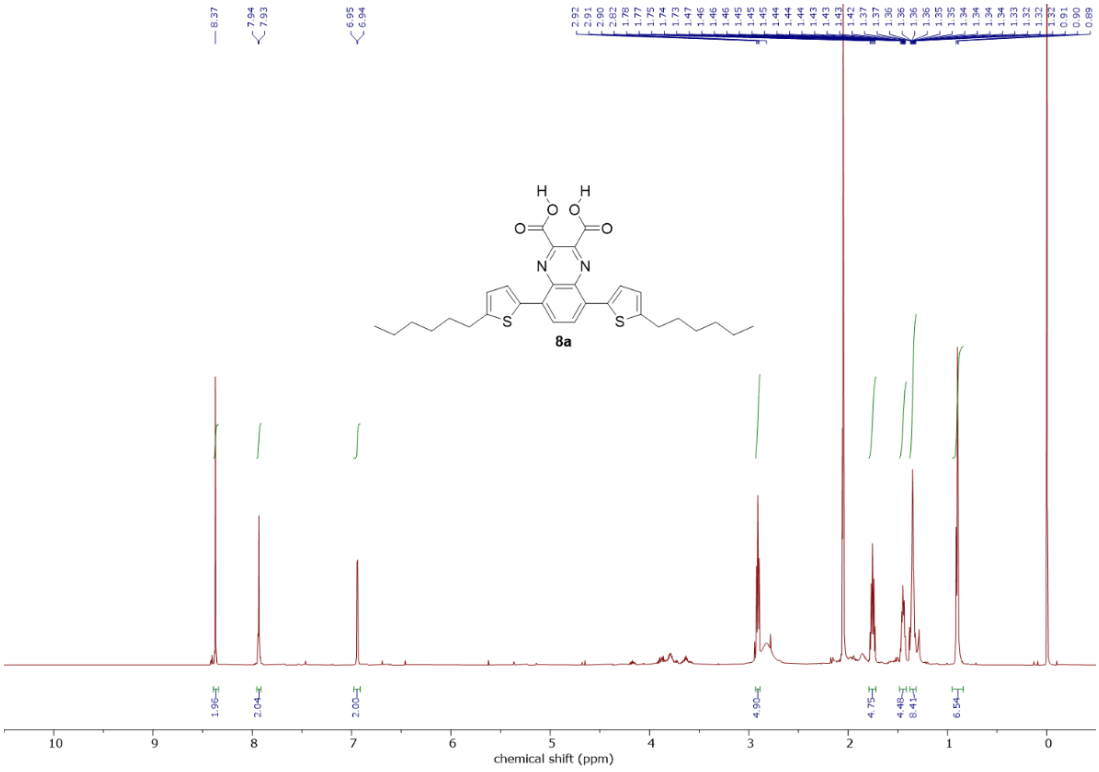

Fig. S73 ^{1}H NMR spectrum of **8a** in $CDCl_3$.

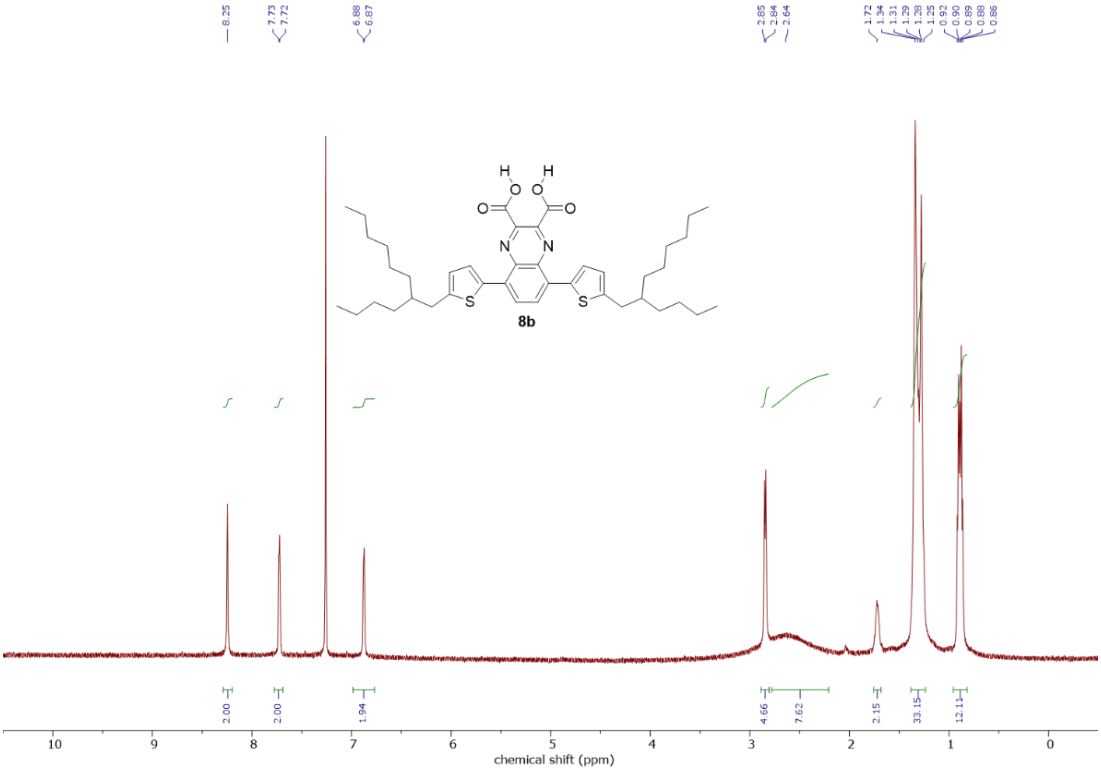

Fig. S74 ^{1}H NMR spectrum of **8b** in $CDCl_3$.

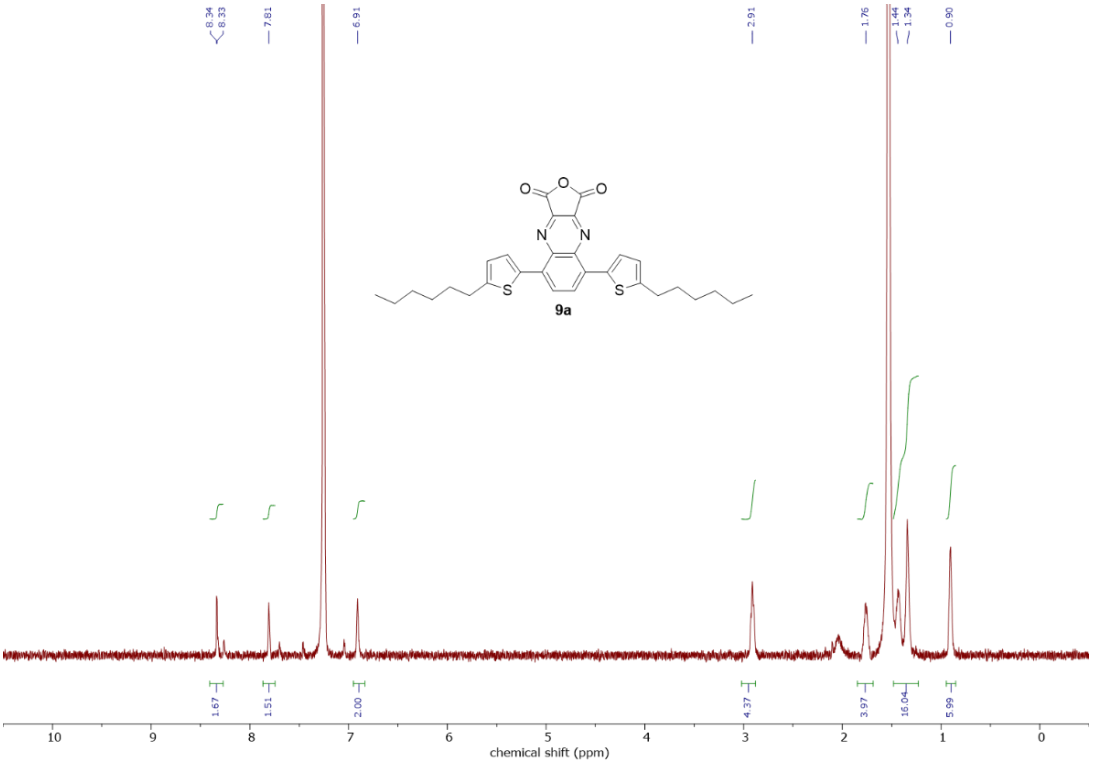

Fig. S75 ^{1}H NMR spectrum of **9a** in $CDCl_3$.

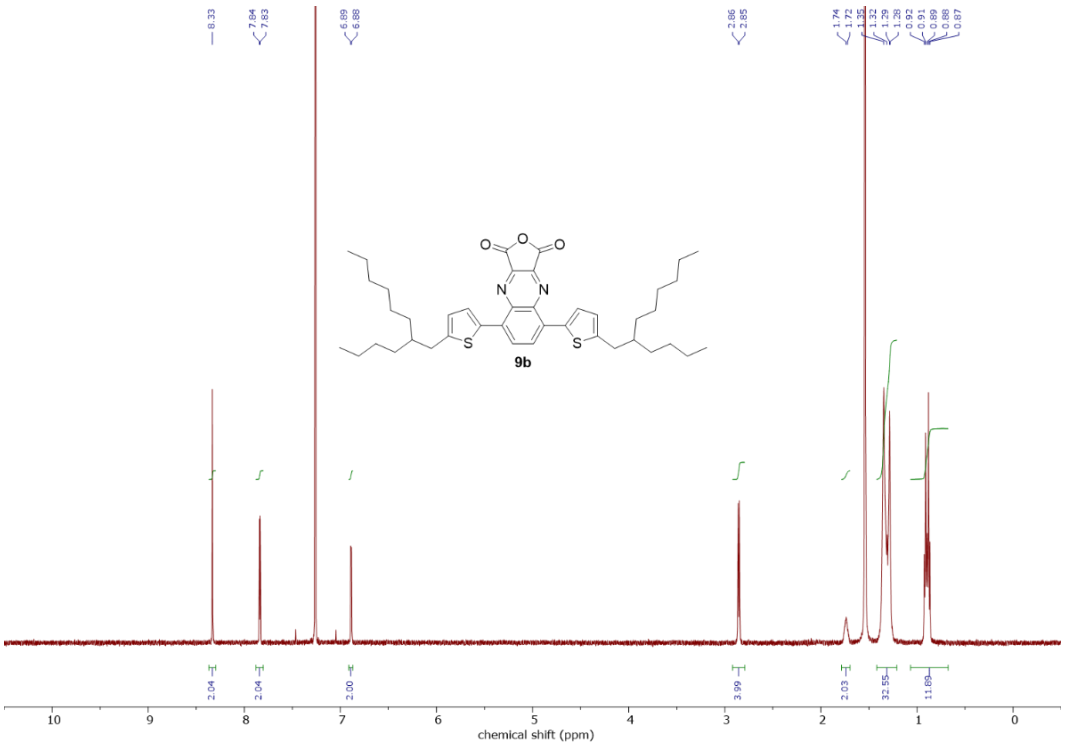

Fig. S76 ^{1}H NMR spectrum of **9b** in $CDCl_3$.

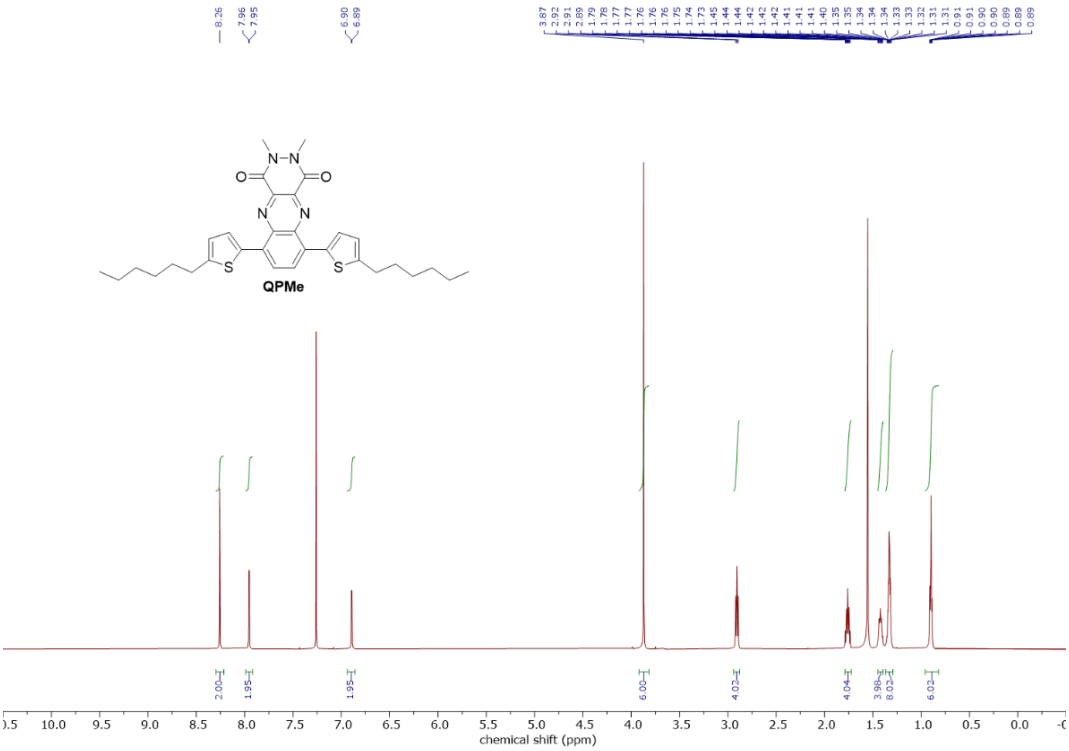

Fig. S77 ^{1}H NMR spectrum of **QPMe** in $CDCl_3$.

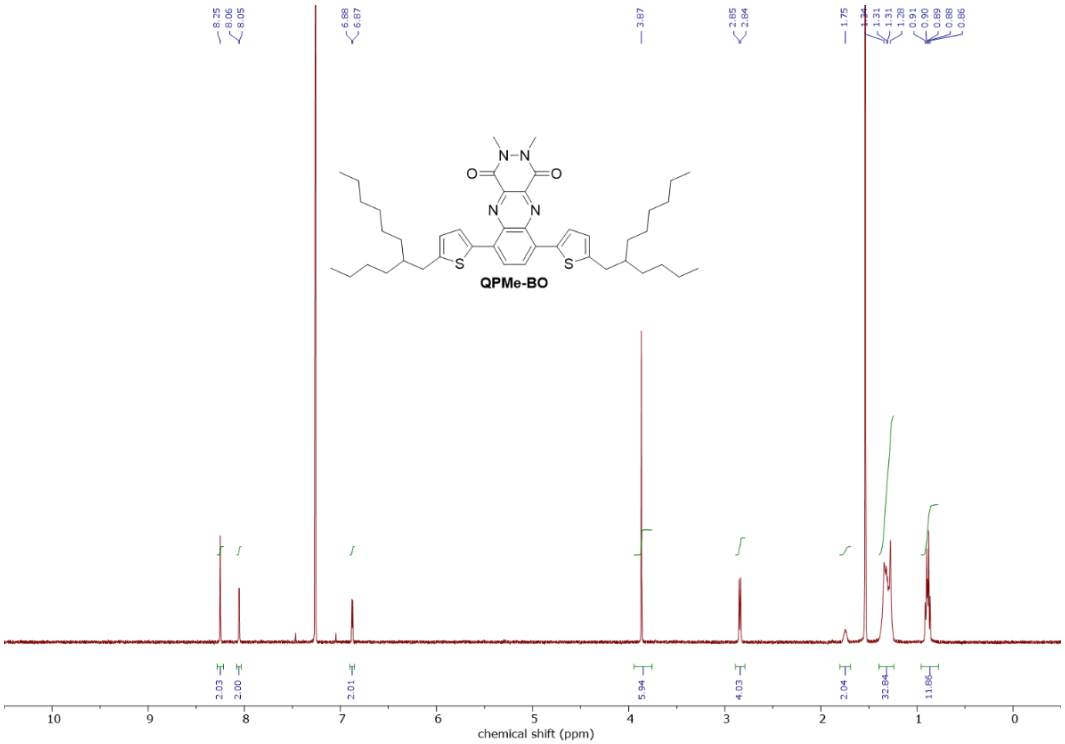

Fig. S78 ^{1}H NMR spectrum of **QPMe-BO** in $CDCl_3$.

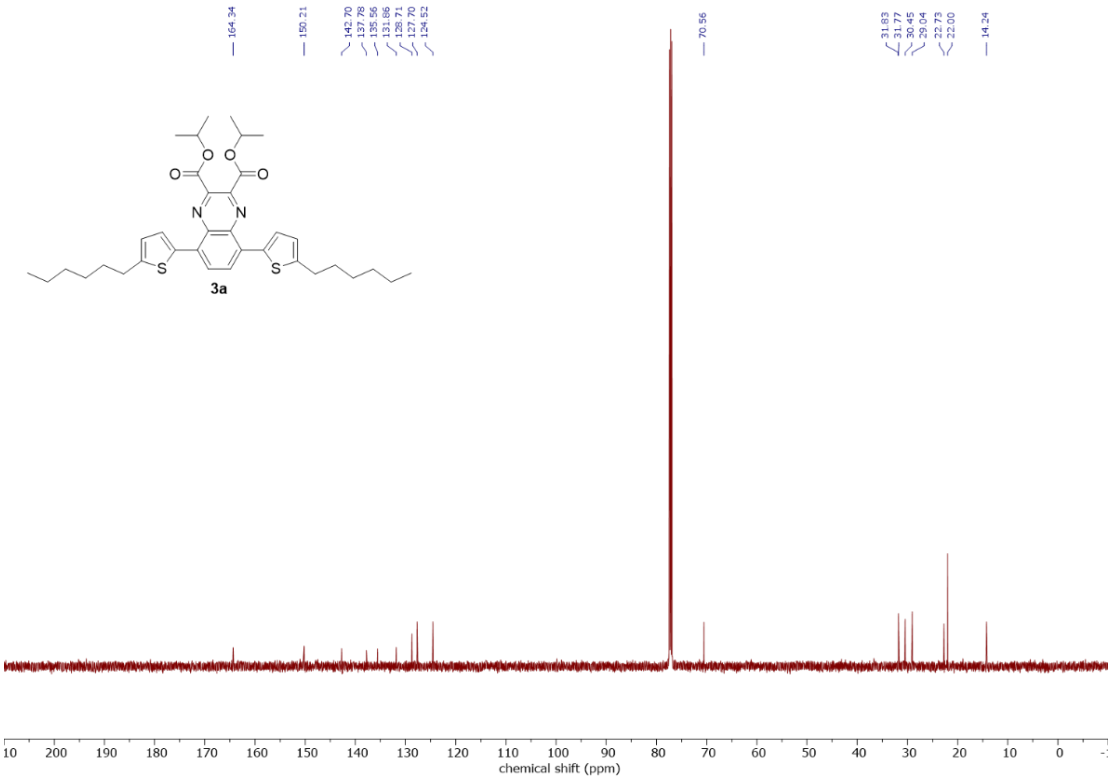

Fig. S79 ^{13}C NMR spectrum of **3a** in $CDCl_3$.

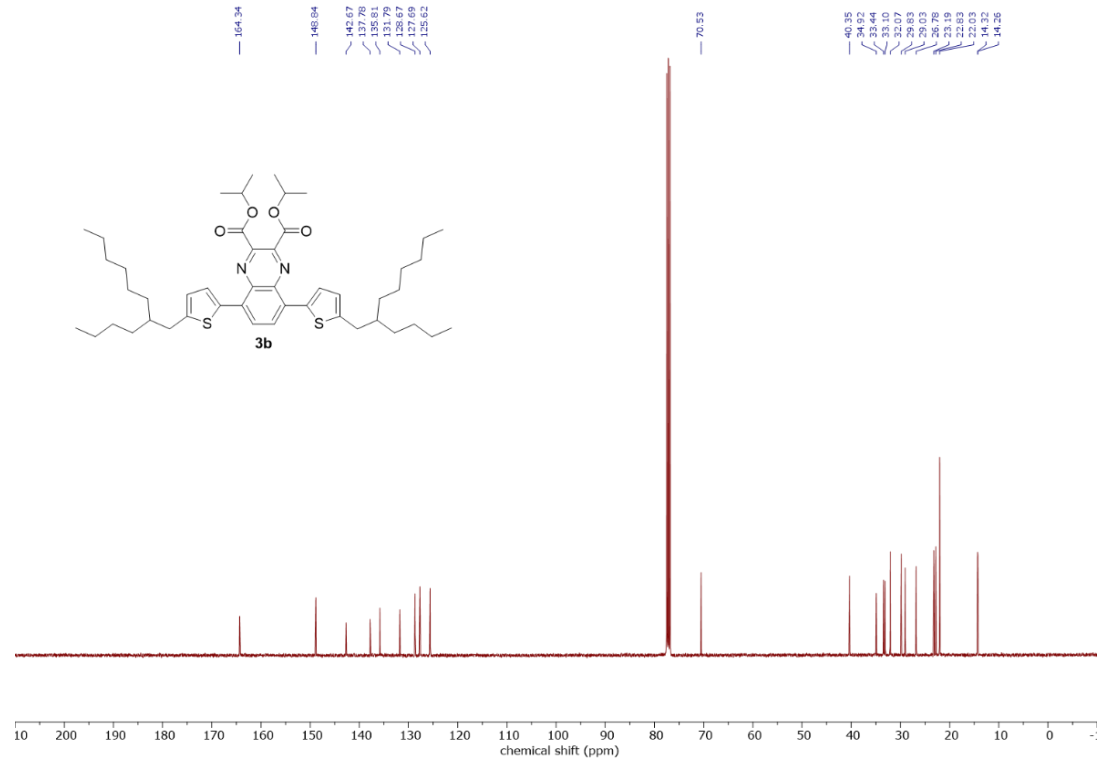

Fig. S80 ^{13}C NMR spectrum of **3b** in $CDCl_3$.

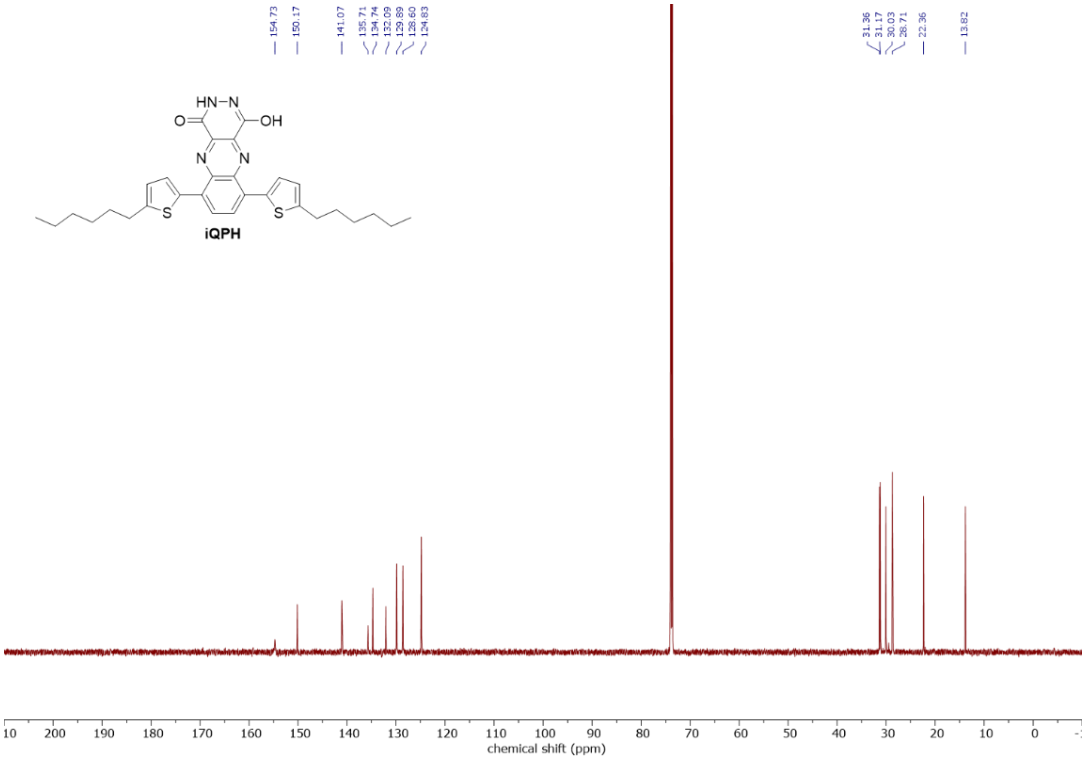

Fig. S81 ^{13}C NMR spectrum of **iQPH** in TCE-d_2 at 80 °C.

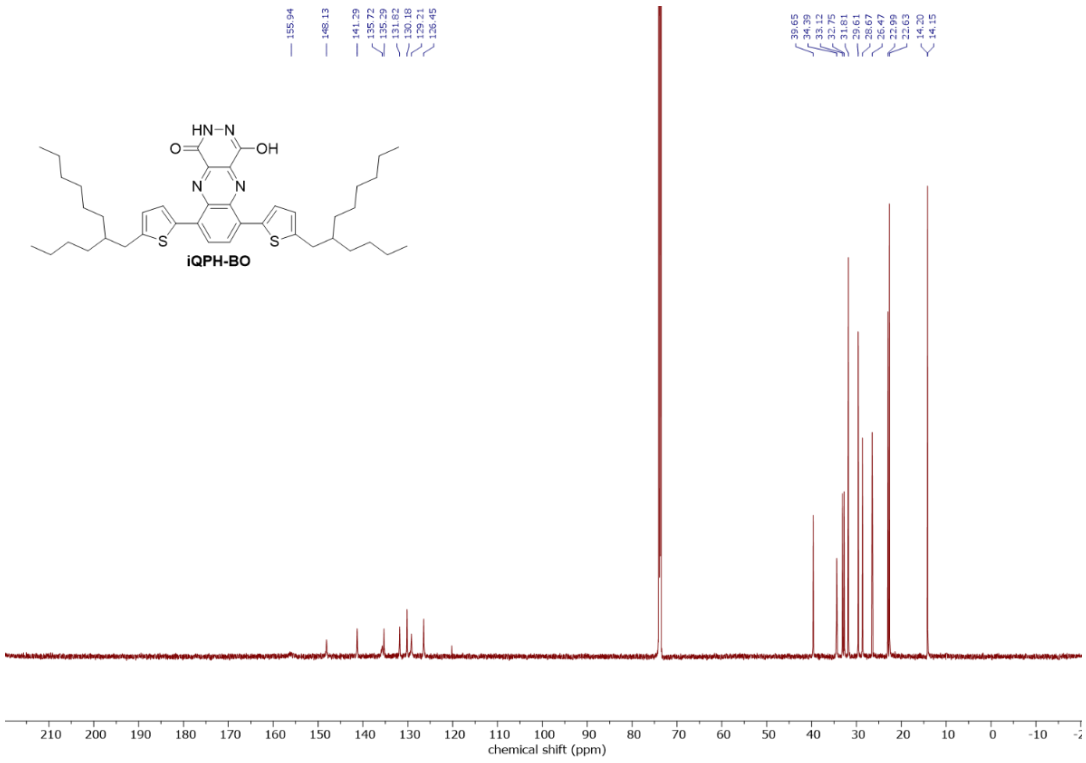

Fig. S82 ^{13}C NMR spectrum of **iQPH-BO** in TCE-d_2.

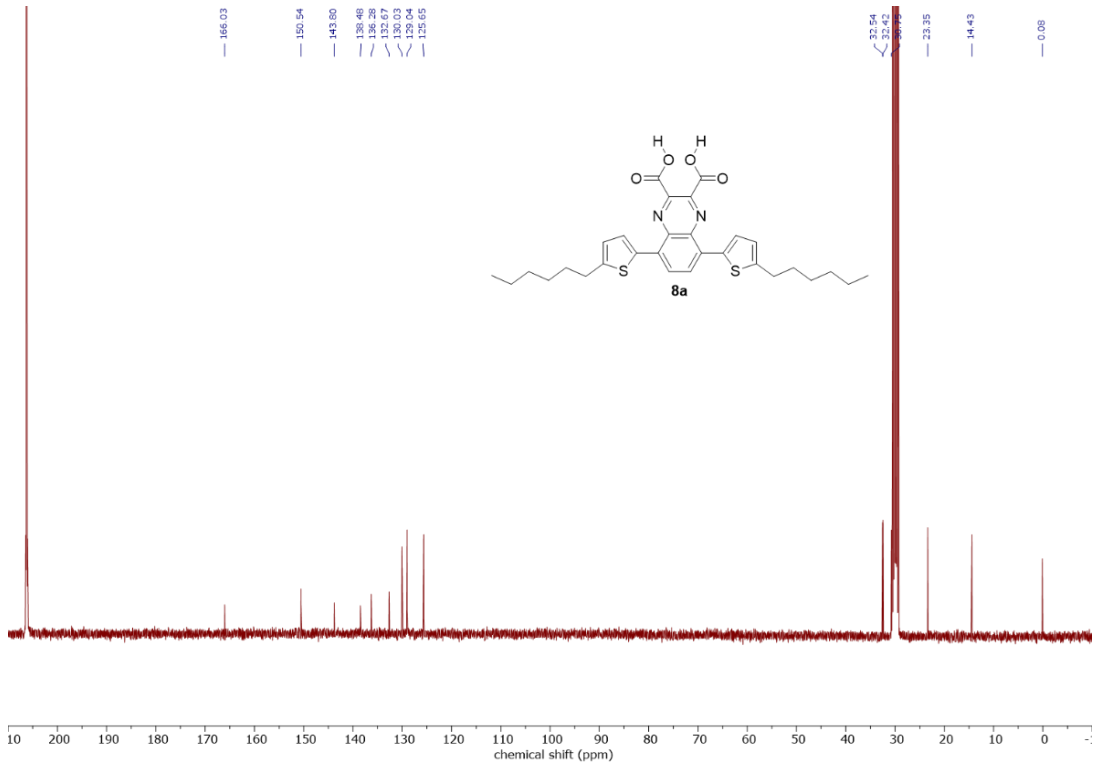

Fig. S83 ^{13}C NMR spectrum of **8a** in Acetone-d_6.

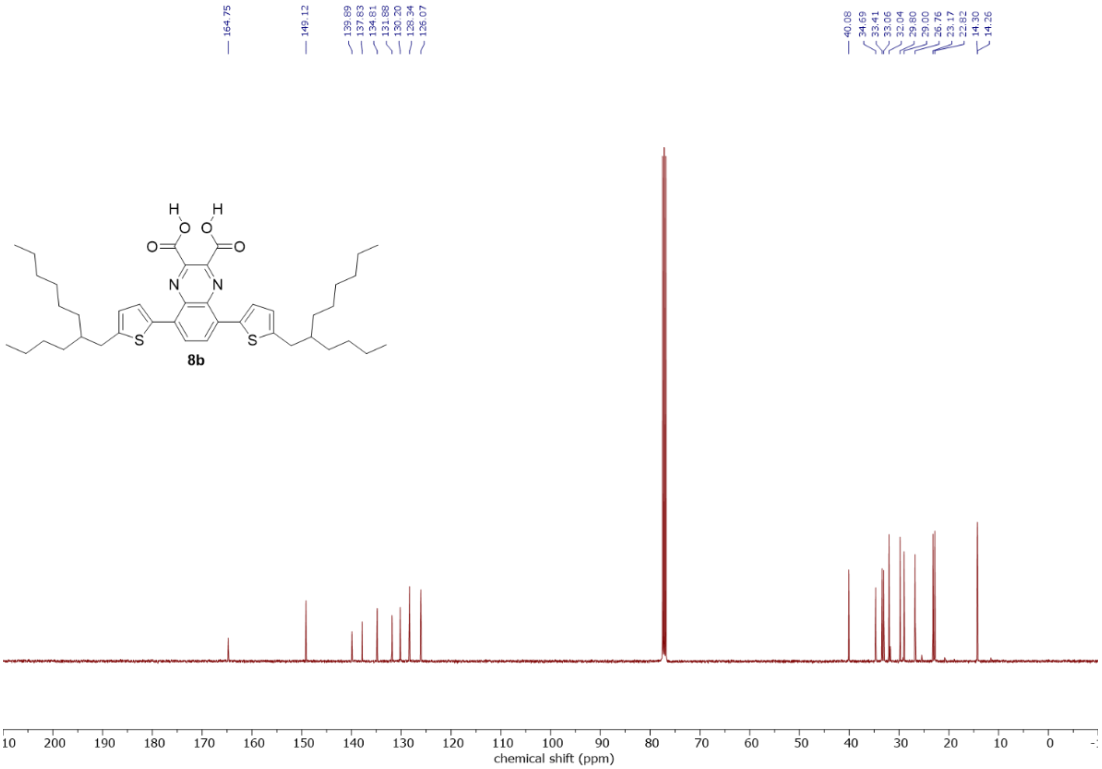

Fig. S84 ^{13}C NMR spectrum of **8b** in $CDCl_3$.

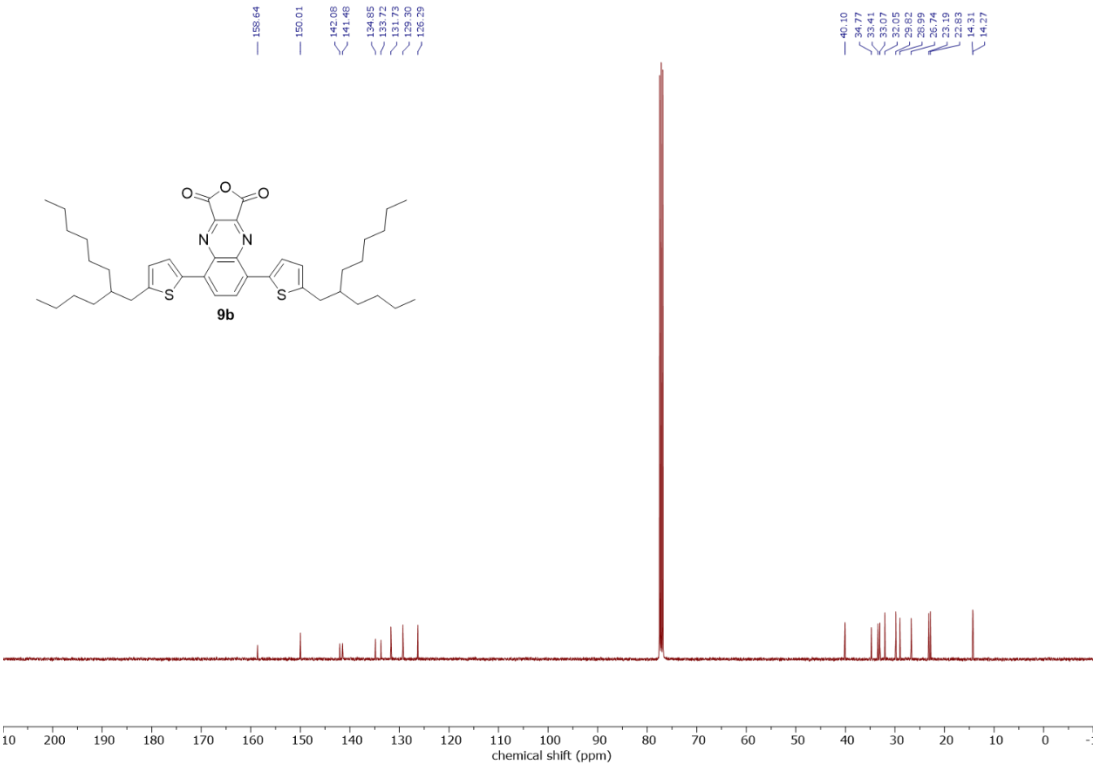

Fig. S85 ^{13}C NMR spectrum of **9b** in $CDCl_3$.

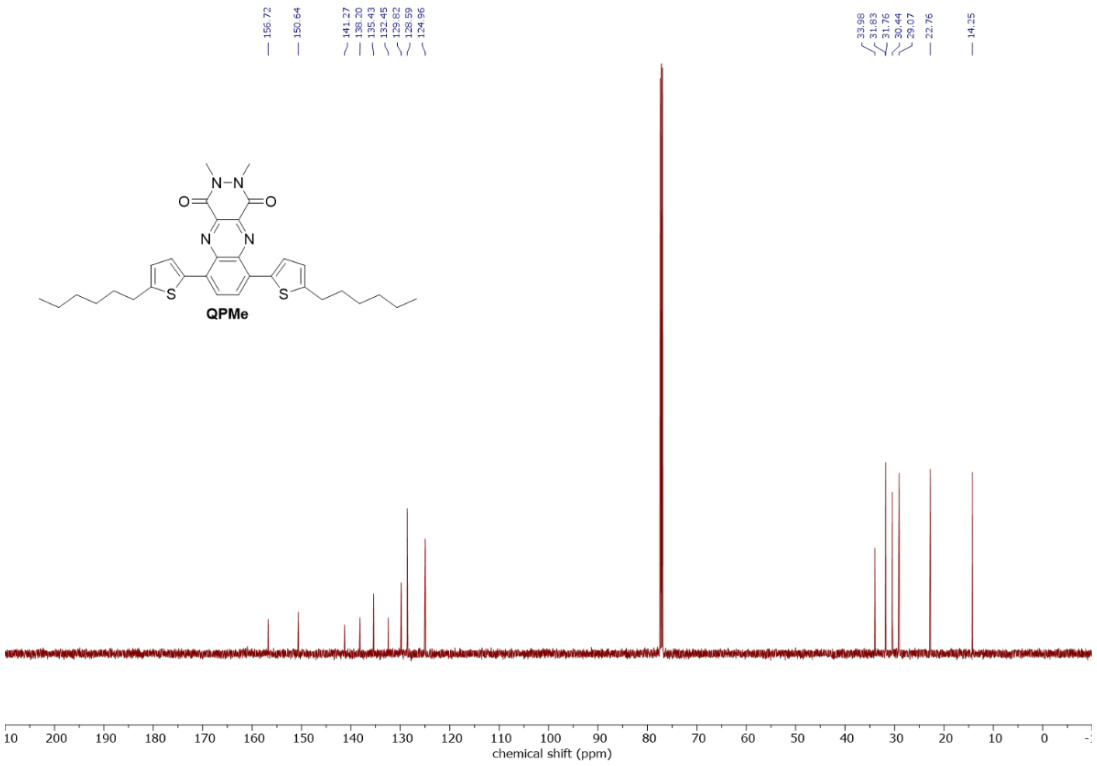

Fig. S86 ^{13}C NMR spectrum of **QPMe** in $CDCl_3$.

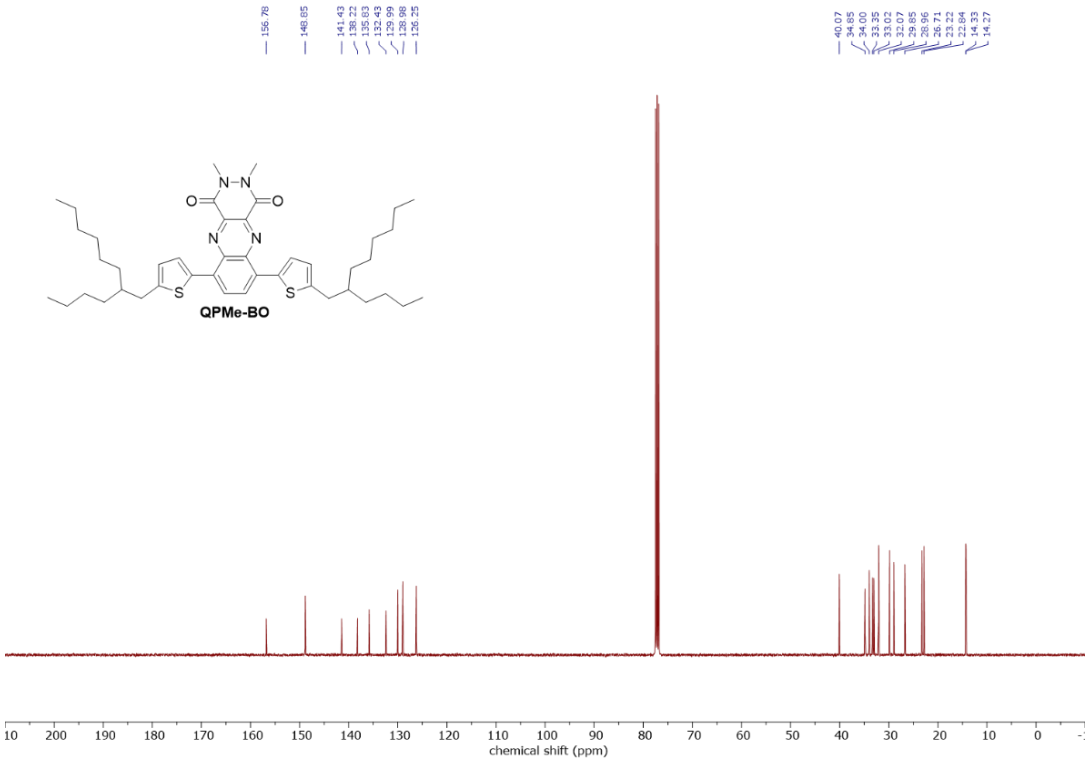

Fig. S87 ^{13}C NMR spectrum of **QPMe-BO** in $CDCl_3$.

References

(1) F. He, W. Wang, W. Chen, T. Xu, S. B. Darling, J. Strzalka, Y. Liu and L. Yu, *J. Am. Chem. Soc.*, 2011, **133**, 3284–3287.

(2) P. Gawrys, T. Marszalek, E. Bartnik, M. Kucinska, J. Ulanski and M. Zagorska, *Org. Lett.*, 2011, **13**, 6090–6093.

(3) T. Hasegawa, M. Ashizawa, S. Kawauchi, H. Masunaga, N. Ohta and H. Matsumoto, *RSC Adv.*, 2019, **9**, 10807–10813.

(4) L.-K. Wang, J.-J. Zhou, Y.-B. Lan, S.-Y. Ding, W. Yu and W. Wang, *Angew Chem Int Ed Engl*, 2019, **58**, 9443–9447.

(5) J. P. Heiskanen, P. Vivo, N. M. Saari, T. I. Hukka, T. Kastinen, K. Kaunisto, H. J. Lemmetyinen and O. E. O. Hormi, *J Org Chem*, 2016, **81**, 1535–1546.

(6) N. T. Shewmon, D. L. Watkins, J. F. Galindo, R. B. Zerdan, J. Chen, J. Keum, A. E. Roitberg, J. Xue and R. K. Castellano, *Advanced Functional Materials*, 2015, **25**, 5166–5177.